University of Rhode Island

DigitalCommons@URI

2009

Feed-Forwad Hypertensis Compensation for Active Clamping Systems on Wood Machining Centers

Erik Allen Anderson
University of Rhode Island

Follow this and additional works at: https://digitalcommons.uri.edu/theses

Recommended Citation

FEED-FORWARD HYSTERESIS COMPENSATION FOR ACTIVE

CLAMPING SYSTEMS ON WOOD MACHINING CENTERS

BY

ERIK ALLEN ANDERSON

A THESIS SUBMITTED IN PARTIAL FULFILLMENT OF THE

REQUIREMENTS FOR THE DEGREE OF

MASTER OF SCIENCE

IN

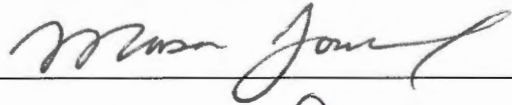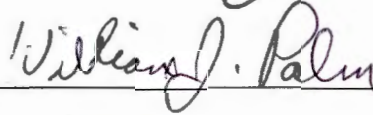MECHANICAL ENGINEERING AND APPLIED MECHANICS

UNIVERSITY OF RHODE ISLAND

2009

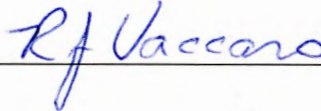MASTER OF SCIENCE THESIS

OF

ERIK ALLEN ANDERSON

APPROVED:

Thesis Committee:

Major Professor

William J. Palm

R J Vaccaro

DEAN OF THE GRADUATE SCHOOL

UNIVERSITY OF RHODE ISLAND

2009

ABSTRACT

The modeling and compensation of hysteresis in piezoelectrically driven systems is very important for positioning and vibration compensation applications. A vacuum clamping system for a stationary wood machining center is integrated with a piezoelectric actuator for the purpose of vibration control. This actuator is used to reduce workpiece vibrations through an X-filtered LMS algorithm. The clamping system has an inherent hysteresis effect between input voltage and the output position of the vacuum plate. This hysteresis effect is modeled with two main techniques: the Bouc-Wen and the Classical Preisach models.

The parameters for the Bouc-Wen model were identified using the Optimization Toolbox in Matlab. The parameters were identified from hysteresis curves from the unloaded actuator as well as the loaded actuator. The unloaded actuator parameters were more suitable for feed-forward compensation. Compensation based on these parameters was implemented experimentally, and an average outer loop hysteresis reduction of 30% was observed for input rates of 10, 100, 500, 1000 and 1500 V/s.

The Classical Preisach technique was used to model descending hysteresis curves in the 0 to 10 V input range. The compensation of this model was split into parallel and series inverse implementations. The parallel inverse could reduce outer loop hysteresis by 66% and the series inverse could reduce by 80%. The Classical Preisach model was used to model hysteresis in the offset 4 to 8 V range. The series inverse control used for this case could achieve a reduction in outer loop hysteresis of 77%.

The offset inverse series compensation was used in conjunction with the X-filtered LMS algorithm to test its effectiveness. The hysteresis compensated system could reduce acceleration output amplitude to 10% its original value twice as

quickly as the uncompensated system. However, the compensated system could not reduce the amplitude any further, while the uncompensated system could reduce the amplitude down to 3% of its original value.

ACKNOWLEDGMENTS

TABLE OF CONTENTS

LIST OF TABLES

LIST OF FIGURES

CHAPTER 1

Introduction

1.1 Background

The demand for high performance positioning and vibration control systems has driven research and engineering efforts in the development of new actuator concepts. The idea for applying *smart materials* to actuator design has become more commonplace over the past two decades. Recent interest in this field can be attributed to developments in the design of actuators made from smart materials, the introduction of inexpensive, yet powerful digital signal processors and further advancements in control system theory and their application to these smart actuators.

Smart materials, also known as *adaptronics* [5], form the basis for active sensing and actuation in conventionally inactive structures. Adaptronics can take on many different forms, including shape memory alloys, magnetostrictive materials and electrorheological (ER) and magnetorheological (MR) fluids. However, piezoelectric (or piezoceramic) materials have been most often used for precision positioning vibration suppression in the micro and nanometer ranges. Piezoelectric materials have the property of generating an electric potential in response to an applied mechanical stress. This process is also reversible, where a voltage applied to the material causes mechanical stress within the material. This stress can be used to impart a force and / or a displacement when integrated with an inactive structure.

Piezoelectric materials require very high voltages (up to 1000 V) using high voltage amplifiers (100x) in order to achieve displacements in the micrometer range. However, certain piezoelectric materials achieve open loop step input settling times in the millisecond range, or even faster when in closed loop. The piezoelectric

1

actuator's high stiffness, fast settling times, excellent frequency response and fine resolution make it ideal for precise positioning and vibration control applications. The primary disadvantages of piezoelectric actuators are that they exhibit position drift over time and hysteresis nonlinearity when comparing system input voltage to position output. When left uncompensated, these nonlinearities negatively affect the performance of piezoelectric actuators and thereby limit their application.

Hysteresis is a nonlinear phenomenon encountered in many areas of science and engineering. It generally refers to a condition where the system's output is not only dependent on the current system input, but also on the system's input history (hysteresis with nonlocal memory). Figure 1.1 illustrates the typical hysteresis effect in an input-output diagram, where the loading and subsequent unloading of a system leads to differing output signal *paths*.
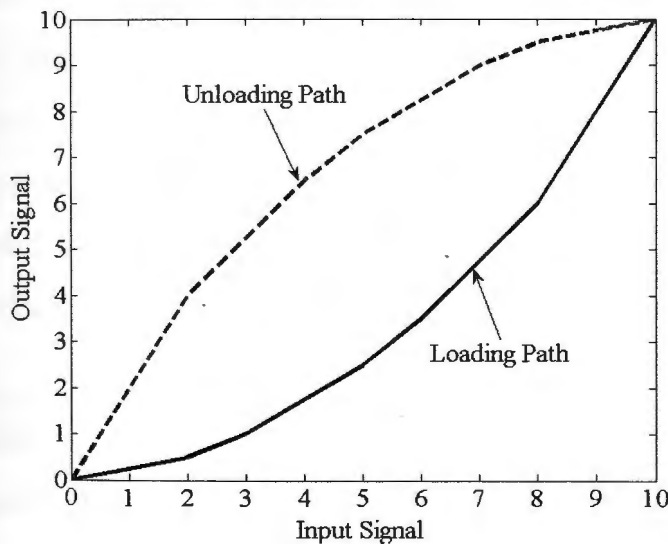
Figure 1.1. Hysteresis Due to Differing Loading and Unloading Paths

Hysteresis is sometimes seen as a positive effect in engineered systems. For example, a thermostat uses the principle of hysteresis for room temperature control. Hysteresis however is typically interpreted as having a negative effect on the control

of position and vibration. When this effect is not properly modeled, the system under open-loop control exhibits unpredictable output to a varying input. Systems with rate-independent hysteresis properties behave as though they have a phase lag which is dependent on the input signal's amplitude rather than input frequency. When the system is under closed-loop control, the system may become unstable when phase margins are insufficient. For these reasons, it is important to apply hysteresis modeling and compensation techniques to controller design in order to achieve the desired dynamic system response.

There exists many methods for the compensation of systems exhibiting hysteresis in piezoelectric actuators. For example, [6] details the use of charge amplifiers instead of voltage amplifiers to drive piezoelectric actuators for vibration control. A significant reduction in output hysteresis may be observed when a piezoelectric actuator is driven in this manner. Since the system under consideration (see Section 2.1) is driven by a voltage amplifier and does not include a sensor for position feedback, this thesis will concentrate on feed-forward hysteresis compensation methods using voltage as a control signal. These methods generally either invert or subtract out the hysteresis model for the determination of a suitable control signal which linearizes the system response.

1.2 Literature Review of Hysteresis Modeling and Feed-Forward Compensation

Many papers have been written over the past two decades regarding the modeling and feed-forward compensation of piezoelectric actuators. This literature review only covers key techniques and provides some application examples.

The application of the Preisach modeling techniques has been documented in [2], [7], [1] and [8]. This method is based on the summation of hysteretic relay operators with gain outputs. The values of the *on* and *off* switching values and

the gain would need to be identified to describe system hysteresis. However, in the above mentioned implementations, this identification step has been circumvented and the resulting Preisach model is based directly on experimentally measured data - i.e. the model's output value for any given input is directly extrapolated from experimentally measured hysteresis loop values.

The Prandtl-Ishlinskii model was likewise used in [9], [10] and [11] for piezo-electric hysteresis modeling and control. This model is very similar to the Preisach model, in that it is a summation of hysteresis *play* and *stop* operators instead of relay operators. This model has in fact been recognized as a particular subclass of the Preisach operator [10], and therefore is expected to behave similarly to the Preisach model.

Hysteresis modeling has also been achieved by curve fitting ascending and descending hysteresis curves such as in [12] and [13]. In the first paper, curve fitting was applied only to the experimentally determined major ascending and descending hysteresis loops. The authors then used a general formula to estimate hysteresis for a given inner loop based on data from the major loop and the voltage input direction switching value. In the second paper, the authors applied curve fitting to several hysteresis loops with given minimum and maximum voltage direction switching values.

The model proposed in [14] and [15] is completely based on physical principles. This model describes the static and dynamic behavior of the actuator with a "lumped-parameter energy-based representation." This electromechanical model utilizes the generalized Maxwell resistive capacitor for representing hysteresis. Mechanically, this can be interpreted as a parallel connection of massless linear springs with unique stiffnesses, representing pure energy-storage, coupled with blocks subject to unique Coulomb breakaway friction forces, which repre-

4

sent rate-independent dissipation. This model is similar to both the Preisach and Prandtl-Ishlinskii models in it represents hysteresis in discrete elements.

Rate-independent hysteresis can also be described through the use of a first order differential equation. The Bouc-Wen hysteresis model was utilized in [16], [17], [18], [19], [20] and [21]. The Duhem model was utilized by Adriaens et al. in [22] and [23] to describe and compensate for hysteresis. Both these techniques provide for a relatively simple description of hysteresis without needing a large amount of data in a lookup table as in Preisach. They also allow for the direct determination of analytical response when including the calculated hysteresis into the total system's force balance equation. However, they are generally only applicable in the case of symmetric hysteresis, where the ascending and descending curves have roughly the same shape. Both these models use hysteresis loop shape parameters which are identified from experimental data.

1.3 Thesis Objectives

The primary goal of this thesis is to develop feed-forward hysteresis compensation for a piezoelectrically driven active clamping assembly. This system will be introduced later in Section 2.1. Hysteresis compensation would eventually be used to improve the vibration canceling performance of an filtered-X LMS algorithm which has been developed by another researcher.

A suitable hysteresis model must be developed which corresponds to experimentally measured data. This hysteresis model would then be adapted to provide an open-loop control voltage which would *cancel out* the hysteresis, thereby effectively linearizing the system response. The effectiveness of this hysteresis compensation is experimentally verified on two identical active clamps. After the assembly's hysteresis reduction has been proven, the compensation will be coupled with the filtered-X LMS algorithm to validate performance improvements in

vibration cancellation using one assembly.

The frequency of the vibration disturbance originating from the wood machine tool is about 300 Hz. This frequency is the primary modal frequency which needs to be canceled by the LMS algorithm. For this thesis, the operating bandwidth of the feed-forward control system has been limited to 300 Hz. This suggests that rate dependency could potentially play a role in modeling system hysteresis. Although such a rate-dependent hysteresis model can potentially yield better modeling over a wider range of input signal frequencies, the author assumes for this thesis that hysteresis rate-dependency plays a minor role in the overall modeling of the system. Instead, the assumption is made that the overall nonlinear system response to a given input is dependent on a certain combination of linear dynamic and rate-independent hysteretic responses.

For this thesis, Bouc-Wen and the Classical Preisach models have been selected for the modeling and compensation of hysteresis. The author has the impression that Bouc-Wen is one of the most commonly published analytical models and Preisach is one of the most commonly published discrete numerical models applied to a given system's hysteresis behavior. The author believes that these very different models are versatile in their application to hysteretic systems. The author wishes to contrast the modeling and control results from the relatively uncomplicated, but not very exact Bouc-Wen model to those from the elaborate, but very accurate Preisach model.

There is no specified level of assembly output hysteresis reduction that the hysteresis compensator needs to attain. It is desired that the rate-independent hysteresis is reduced as much as possible across the operating bandwidth of the system. It is also desired that the hysteresis compensator improves, rather than degrades the vibration canceling performance of the filtered-X LMS algorithm with

the active clamp assembly.

1.3.1 Bouc-Wen Background

The so-called *Bouc-Wen Hysteresis Model* was first developed by Bouc [24] and then later modified by Wen [25], [26] for the development of a differentially smooth hysteretic model for inelastic structures. The model has been successfully applied to other systems which also exhibit hysteretic properties. One of the first applications used for the modeling and control of hysteresis in piezoelectric actuators could be found in [16] and shortly thereafter in [17]. The author will utilize a simple identification method to determine this model's parameters based on the experimentally obtained major hysteresis loop.

1.3.2 Preisach Background

The Preisach model was originally developed by Ferenc Preisach for the mathematical description of hysteresis in ferromagnetic materials [27]. The Preisach model was originally interpreted as a physical model of hysteresis. In reality, it is a phenomenological model, meaning the hysteresis is modeled mathematically based on observed phenomena, but not directly derived from physical theory. This model was initially applied for use in piezoelectric actuator modeling and control in [2], [7] and [1]. Variants have since been developed, which include the modification of the Preisach hysteresis model for input signal rate dependency [28], [29], [30] and [31].

The author found an article [32] applying the rate dependent Preisach hysteresis model concepts from above to control piezoelectric hysteresis in a frequency bandwidth of up to 400 Hz. However, it appears that this method requires preprocessing of the entire reference position signal (calculating reference input sequence, full memory sequence and reduced memory sequence - see [32] for description) be-

fore applying feed-forward control to the system. There is, however, no prior knowledge concerning the reference signal for the given system in this thesis. This requirement for prior reference signal knowledge thereby significantly limits the practical application of this method, and therefore will not be pursued any further in this thesis.

The author will focus on the Classical Preisach implementation of the hysteresis model, as well as a so-called offset version of the Classical model, where the hysteresis effect is modeled only over a set input voltage range. This model relaxes the requirement for the input signal to be always cycled between a maximum and zero volts. Both models require experimental identification data in the form of *first order descending hysteresis curves.*

1.4 Thesis Outline

This thesis is made up of five separate chapters. Chapter 1 has introduced hysteresis modeling and feed-forward compensation including a literature review. Chapter 2 will explore the characterization of the active clamp assembly under various conditions. Chapter 3 will introduce the Bouc-Wen hysteresis modeling concept and provide modeling results. Chapter 3 also explores hysteresis compensation based on the Bouc-Wen model, including experimental results. Chapter 4 introduces the Classical Preisach technique for modeling hysteresis and provides modeling results for performance validation. This chapter also introduces the concept of an offset Classical Preisach model, where the model's outer hysteresis loop lies between a given input voltage minimum and maximum. Like in Chapter 3, Chapter 4 explores hysteresis compensation methods based on the Classical Preisach model and includes experimental results for performance validation. In chapter 5, concluding remarks will be made regarding the experimental results, and suggestions for further research and plant design changes will be made.

CHAPTER 2

Characterization of the Plant

2.1 Design of the Active Clamping System

The Institut für Werkzeugmaschinen und Fertigungstechnik (Institute for Machine Tools and Production Technology) at the Technische Universität Braunschweig (TU-Braunschweig) has developed a novel system for workpiece clamping and workpiece vibration control on a wood machining tool. The complete system comprises of four identical vacuum clamping assemblies (assemblies A, B, C and D) used for the fixation of wooden plate shaped workpieces during machining. However, this clamping action promotes work piece vibration, and since flat, plate shaped workpieces have a high tendency for acoustic radiation, this may lead to quality problems and elevated levels of noise during machining. Each vacuum clamping system has therefore been modified to include a piezoelectric actuator which is used to raise and lower the clamping surface. A Filtered-X LMS (Least Mean Square) control algorithm has been developed to counteract workpiece vibration by means of superposition [33], [3]. A picture of the stationary wood machining tool and the four active clamps is shown in Figure 2.1.

All of the active clamps are outfitted with piezoelectric actuators and amplifiers from Physik Instrumente GmbH & Co. KG. They are outfitted with actuator model P-216.80 with a nominal, unloaded maximum displacement of 120 μm. None of these actuators are outfitted with a strain gage sensor nor do the actuator amplifiers have a position controller for hysteresis compensation. This means that each assembly's position output / voltage input relation exhibits hysteretic properties. Each actuator is driven by amplifier model E-481.00 which has an output/input gain of 100x. Web links to PDF's of data sheets for P-216 and E-481 may be found in [34] and [35] respectively.
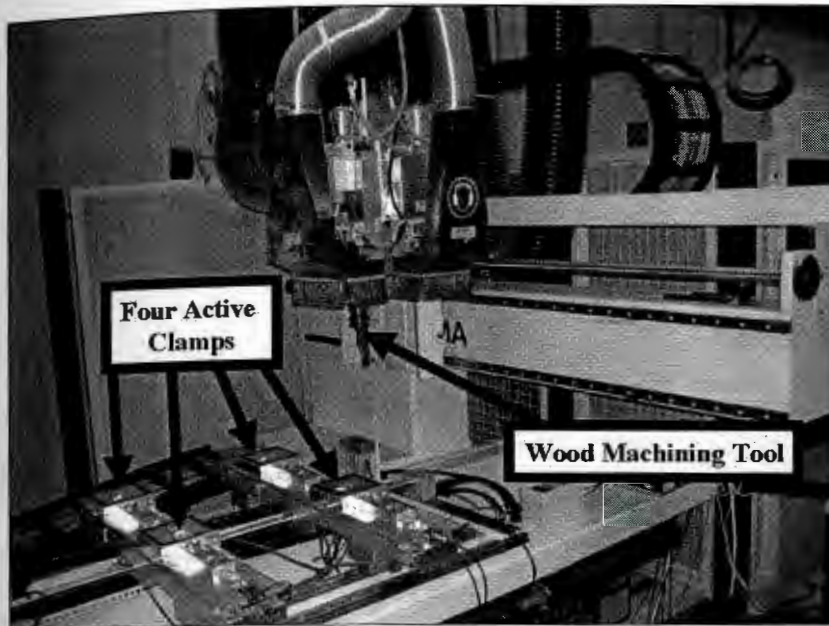
Figure 2.1. Stationary Wood Machining Tool with Active Clamp Assembly

The amplifiers are, in turn, driven by a real-time digital signal processing system from dSPACE GmbH. On the hardware side, this system is made up of the DS1006 processor board [36], the DS2004 A/D board [37] and the DS2102 D/A board [38]. On the software side, the experiment is designed using The Mathworks' Simulink package with automatic C-code generation and hardware linking managed by TargetLink [39]. Direct experiment interface and instrumentation is managed through ControlDesk [40].

IMPORTANT: All future references to voltage inputs in this thesis will be with respect to the dSPACE system's D/A output (0-10 V) and not to the output of the piezoelectric amplifier.

As seen in the SolidWorks generated cutaway side view of the assembly in Figure 2.2, the active clamp assembly is made up of several components. This graphic illustrates the function of each component. The piezoelectric actuator generates a force, which is transferred through the horizontal wedge. With increasing voltage,

this horizontal wedge moves to the right. This wedge has sliding frictional contact with the vertical wedge and pushes this part upward. While the vertical wedge moves upward, the washer attached to this wedge also moves upward. This motion compresses the spring which is located between the wedge and housing, creating a downward force onto the vertical wedge. The suction plate is actuated through the direct connection with the vertical wedge.
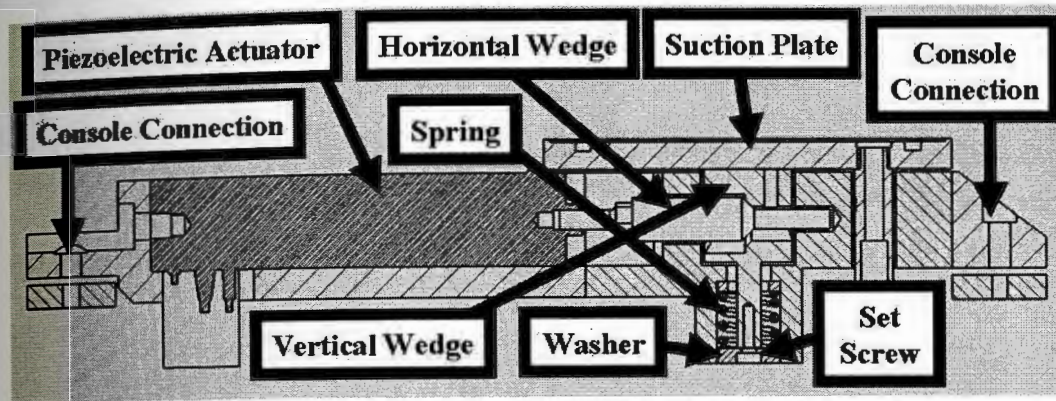
Figure 2.2. SolidWorks Generated Side Cutaway View Assembly

The active clamp assembly is mounted to the wood machining center's console by two screw connections. The tightening torque on each of these screws affects the relationship between input voltage and suction plate output position. These screw connections must be "tuned" properly before testing to ensure correct system behavior. This tuning process involves inputting a 300 Hz sinusoid signal to the actuator and observing the acceleration output of the plate using an accelerometer. A change in output is observed when the each screw is tightened or loosened. The torques are tuned properly when the accelerometer output has a pure sinusoidal shape with sufficient amplitude. It is generally assumed that the experimental results in this thesis have been obtained on a properly tuned system.

2.2 Test Setup and Voltage Input Profile

A proper test procedure and test setup are needed to properly characterize the response of the active clamp assembly. For this investigation, first order descending hysteresis curves are generated by inputting a set of triangular voltage profiles with decreasing peak amplitudes and constant voltage slope rates. Figure 2.3 illustrates an input voltage profile for descending hysteresis. The max amplitude of the triangle wave is 10 V and after repeating the 10 V wave for a second time, decreases by 1 V for every successive wave. The voltage input rate is 1 V/s.

Input Voltage Profile for Descending Hysteresis at 1 V/s
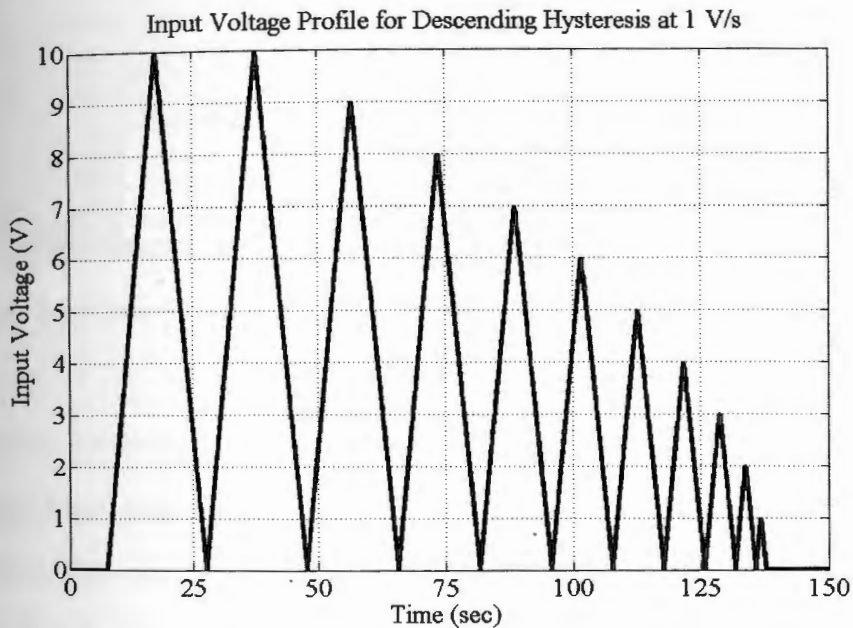
Figure 2.3. Input Voltage Profile to Generate Descending Hysteresis Curves (1 V/s)

Three different experimental setups were used to measure the system dynamic response to the given input profiles. Figure 2.4 details one of the setups used for the measurement of hysteresis. A LVDT (linear variable differential transducer) contact measurement pencil probe from Marposs S.p.A. is used for the measurement of hysteresis resulting from slow (ca. 1 - 10 V/s) voltage profiles. Above this

rate the measured data is too noisy, even when filtered. Therefore the range of dynamic inputs that can be used for system output measurement is limited.
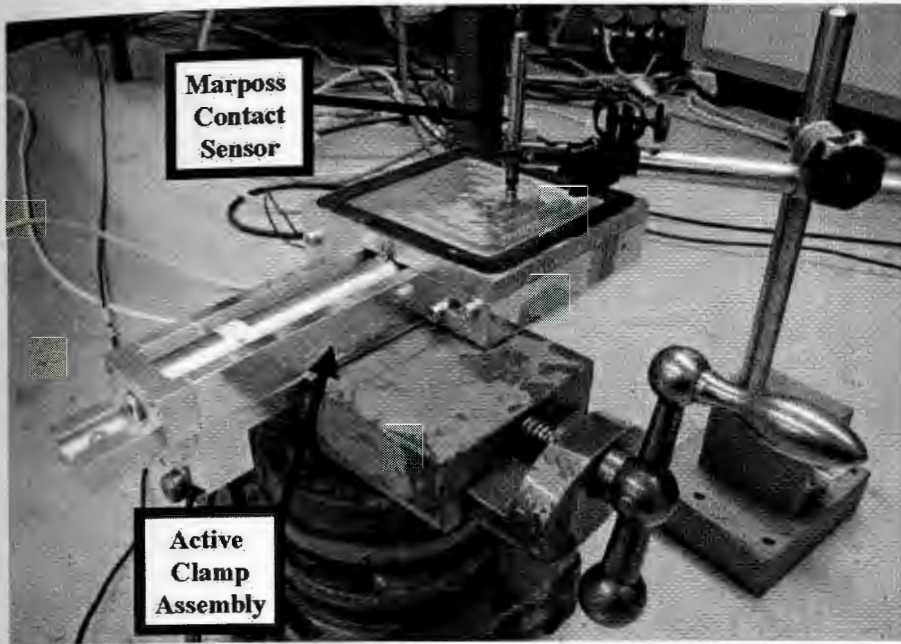
Figure 2.4. Test Setup with Marposs Contact Displacement Sensor Probe

Another setup used for this thesis is shown in Figure 2.5. This setup uses a scanning head vibrometer model OFV 056 from Polytec GmbH. Out of the three setups, this can measure the fastest dynamic responses with the least noise. However, it is also the most complicated setup to prepare for experimental testing, and therefore has been used sparingly.

The third setup used for system response analysis is shown in Figure 2.6. This setup uses the the laser triangulation positioning sensor model optoNCDT 1607 [41] from Micro-Epsilon Messtechnik GmbH & Co. KG. This sensor is able to measure faster dynamic responses than that of the Marposs sensor. However this sensor is also sensitive to noise (noise amplitude about 5 μm) requiring this output to be post-filtered using the Matlab function "smooth". Nevertheless, this became the most regularly used sensor for this research due to its easy setup and large
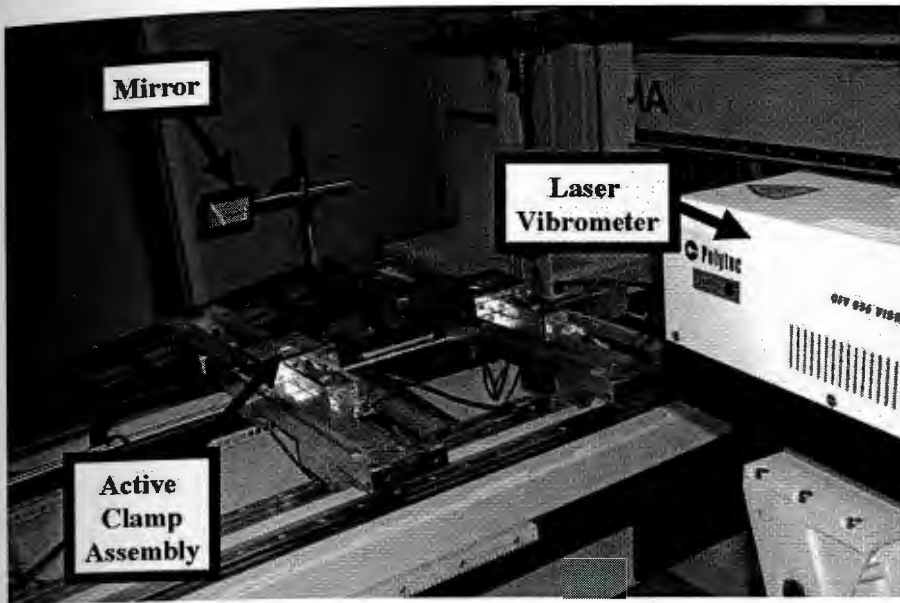
Figure 2.5. Test Setup with Laser Vibrometer Positioning Sensor

measurement bandwidth.

2.3 Hysteresis Response Characterization of the Active Clamp Assembly to Varying Conditions

The system's hysteresis output can be influenced by many factors. These include its assembly condition, the stiffness of the retraction spring, or the voltage signal input rate. In the following, these varying conditions will be compared to each other by observing the resulting displacement at 10 V input and the *area* (computed using Matlab function "trapz") within the major (0-10 V) hysteresis loop in $\mu m \cdot V$. This hysteresis area may be interpreted as being proportional to work losses incurred by traveling along the major loop. Mechanical work is defined as: $W = F \cdot x$, where F represents force and x is the corresponding displacement. The force imparted by a piezoelectric actuator may be determined through the following equation: $F = u \cdot d \cdot k_{eff}$, where u is the input voltage, d is the position output to voltage strain input and k_{eff} is the effective stiffness of the piezoelectric actuator. Combining these two equations yields work losses in terms of system

Figure 2.6. Test Setup with Laser Triangulation Positioning Sensor

input voltage and output displacement. Furthermore, when there is no hysteresis effect present (i.e. the area under the u-x curve is the same for increasing as for decreasing voltage), there is no hysteretic work loss. The major hysteresis loops in the following were recorded by taking the output data resulting from the second $0 - 10$ input triangle shown in Figure 2.3, and normalizing the data such that the displacement at the beginning of the ascending triangle (i.e. at $0\ V$) is equal to 0 μm.

2.3.1 Hysteresis Response Characterization of the Actuator and Active Clamp Assembly

The maximum displacement and the hysteresis are highly affected by the system's assembly condition. Variations may be observed when the actuator's displacement and hysteresis are compared to that of the assembly and the assembly without the suction block plate. These effects are compared to each other in Figure

2.7 using the Marposs sensor for a 1 V/s input voltage triangle and the standard DF-2440 spring.
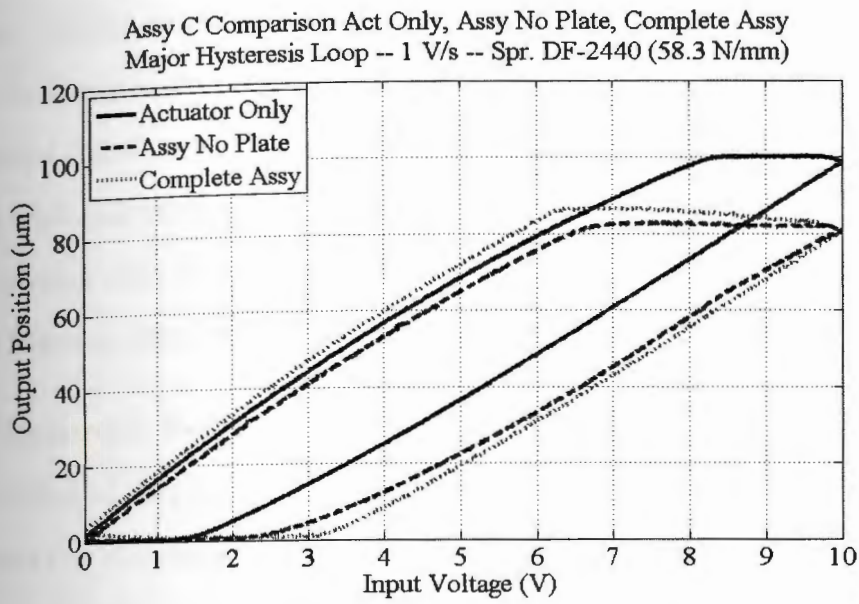
Figure 2.7. Various Assembly Conditions at 1V/s

Both the complete assembly and the assembly without the suction plate yield very similar looking hysteresis loops and displacements at 10 V, while the hysteresis loop appears thinner and the displacement is greater for the actuator alone. The actuator has a displacement of 98.46 μm at 10 V and a loop area of 237.39 $\mu m \cdot V$. The assembly without suction plate has a displacement of 80.70 μm at 10 V and a loop area of 279.68 $\mu m \cdot V$. The full assembly has a displacement of 80.08 μm at 10 V and a loop area of 347.04 $\mu m \cdot V$. This effect suggests that the weight of the plate likely does not play a major role in shaping the output of the hysteresis loop. But, the assembly of the other system components to the actuator does appear to make a significant impact on system output performance when compared to the actuator's output.

In particular, there appears to be an extension of the "flat" section at the ends

of the hysteresis curve, which occurs immediately following a sign change in input voltage rate. The plate velocity is roughly zero during this voltage direction change (remember, voltage rate only 1 V/s). The author believes that the flat sections from the assembly output is mostly due to static friction. The assembly requires an additional one to two volt change in equivalent actuator force to overcome the opposing frictional breakaway force before the suction plate starts to move again. The flat section seen on the actuator output is likely due to friction originating from the Marposs displacement probe rather than from the actuator itself.

2.3.2 Hysteresis Response Due to Differing Spring Stiffnesses

The effect of varying spring stiffnesses on the hysteresis loop were also compared using the Marposs sensor for an assembly at 1V/s. The standard spring used throughout this thesis is model DF-2440 with a spring constant of 58.3 N/mm. This response was compared to the assembly with spring model VD-263V-10 with a spring constant of 25.2 N/mm and spring model VD-207J-01 with a spring constant of 3.8 N/mm. The results of this study are shown in Figure 2.8.

It appears that using a spring with a lower stiffness simultaneously reduces the hysteresis loop area as well as increases the displacement at 10 V input voltage. The differences in loop shape between VD-263V-10 and VD-207J-01 appear marginal when compared to that from DF-2440. As stated above, the assembly with spring DF-2440 has a displacement of 80.08 μm at 10 V and a loop area of 347.04 $\mu m \cdot V$. The assembly with VD-263V-10 has a displacement of 102.3 μm at 10 V and a loop area of 160.15 $\mu m \cdot V$. The assembly with VD-207J-01 has a displacement of 112.5 μm at 10 V and a loop area of 216.86 $\mu m \cdot V$. When using less stiff springs, there is less downward force being exerted onto the horizontal wedge by the vertical wedge over the entire range of motion. This leads to a lower normal force between the wedges (i.e. less friction) and therefore less external force being
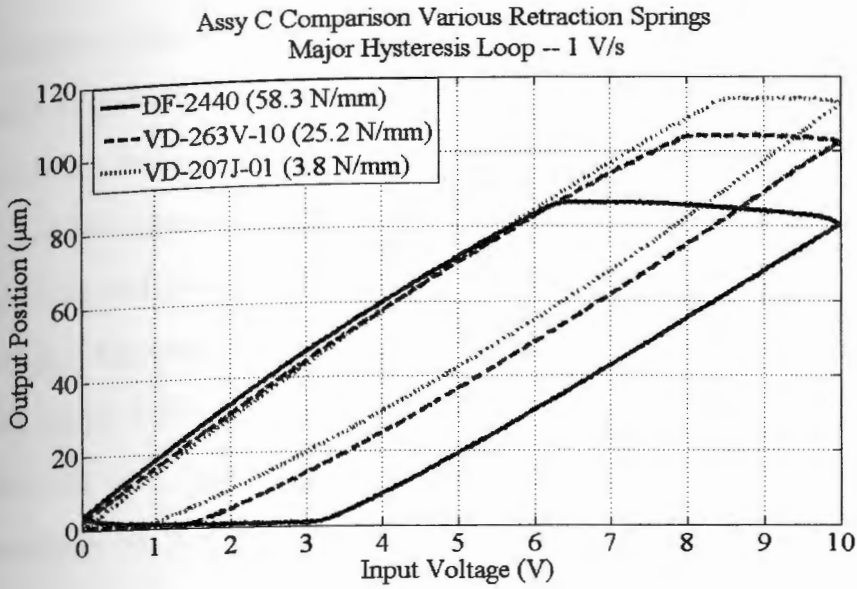
Figure 2.8. Hysteresis Output Using Various Springs at 1V/s

imparted onto the actuator. Since this external force is less, the hysteretic output over the entire motion range is therefore different.

This effect can partially be explained by the *loss in generated displacement* equation (Equation 2.1) due to a piezoelectric actuator acting against an elastic load found in [42].

$$\Delta L \approx \Delta L_0 \cdot \frac{k_T}{k_T + k_S} \tag{2.1}$$

In this equation, ΔL_0 is the original, unloaded maximum displacement of the piezoelectric actuator, k_T is the stiffness of the actuator, k_S is the stiffness of the elastic element and ΔL is the resulting maximum displacement of the loaded actuator.

The author could not apply this equation directly to relate the stiffness of a given spring to the output of the assembly. The actuator has a significantly larger stiffness than the springs, resulting in very little change in output position according to the above equation. However, Equation 2.1 does validate that the spring

18

stiffness has an inverse effect on the position output of the assembly. Static friction likely plays a significant role in the output displacement of the assembly. The level of static friction in the assembly dependent on the stiffness and compression of the spring. A stiffer spring increases the normal force that the vertical wedge exerts onto the horizontal wedge, which leads to elevated static frictional forces.

In Figure 2.9, the position output for 10 V input is plotted against the three retraction spring stiffnesses. In this case, an inverse linear relationship could be derived from this data. This relationship suggests that the position output behavior of the assembly can be characterized for any given spring stiffness.
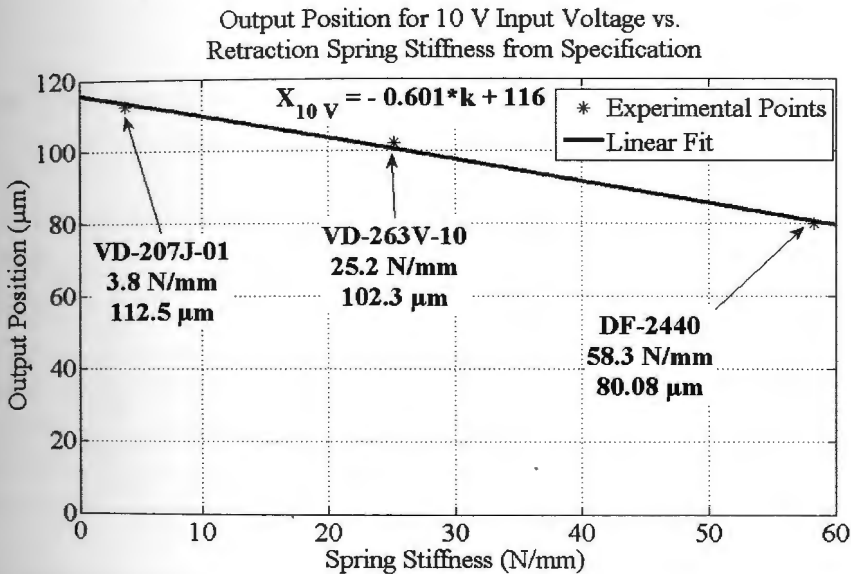
Figure 2.9. Position Output for 10 V Input vs. Spring Stiffness

2.3.3 Hysteresis Response Due to Differing Voltage Input Rates

The system's hysteresis loop is also influenced by the input voltage rate. The laser vibrometer was used to measure assembly B's response to voltage rates of 10, 100, 500, 1000 and 1500 V/s, while using the DF-2440 spring. The input voltage-output position response for each case is plotted in Figure 2.10.

Figure 2.10. Assembly B Spring DF-2440 8cNm with Varying Input Rates

Table 2.1. Maximum Output Positions and Major Loop Areas for Various Voltage Input Rates

Volt. In. Rate V/s	Max. Out. Pos. μm	Loop Area $\mu m \cdot V$
10	96.5	207.94
100	96.59	185.87
500	93.17	199.52
1000	99.14	126.38
1500	99.33	113.67

The resulting maximum output position and loop area for each input voltage rate is tabulated in Table 2.1. The maximum output position of the assembly does not appear to be affected by the input voltage rate. However, the loop area and particularly the shape of the hysteresis loop has been clearly changed by the input voltage rate. In particular, voltage rates of 1000 and 1500 V/s seem to have some sort of vibrational response. Later in this chapter, the author will use this data to relate the system's hysteretic displacement to its linear dynamic characteristics.

2.4 Linear Dynamic Characteristics of the Active Clamp Assembly

The author assumes that the system exhibits both nonlinear hysteretic as well as roughly linear dynamic qualities. Although the relationship between linear and nonlinear are not immediately obvious, one needs to extract the linear dynamic information from the system, so that the combined nonlinear system response characteristics are better understood. The author further proposes that this linear behavior can be sufficiently approximated by a second-order linear dynamic equation. The parameters of such a system (such as undamped natural frequency and damping factors) may be identified by observing the transient position output of assembly's plate to actuator step or impulse voltage inputs. Actuator B's step response behavior will be analyzed in the following.

The 1 volt step response of assembly B is shown in Figure 2.11. This response has a steady state value of 6.40μm, meaning a DC gain factor of 6.4 $\mu m/V$ for this response. The system's peak value is 10.09 μm at 0.00117 seconds, meaning 59.66% overshoot. The displacement of the second peak is 8.83 μm at 0.00351 seconds. Using this information, and assuming 2nd order response characteristics, one can determine the system's undamped natural frequency as well as its damping factor [43].

The system's *damped* natural frequency can be determined by analyzing the time between the first two peaks:

$$\omega_d = \frac{2 \cdot \pi}{t_{peak2} - t_{peak1}} = \frac{2 \cdot \pi}{0.00351 - 0.00117} = 2685 rad/sec = 427.3 Hz \qquad (2.2)$$

The system's damping factor may be determined in one of either two ways: by determining percent overshoot (POS) or comparing amplitude differences between peaks (PK). The damping factor determination by percent overshoot is as follows:

21
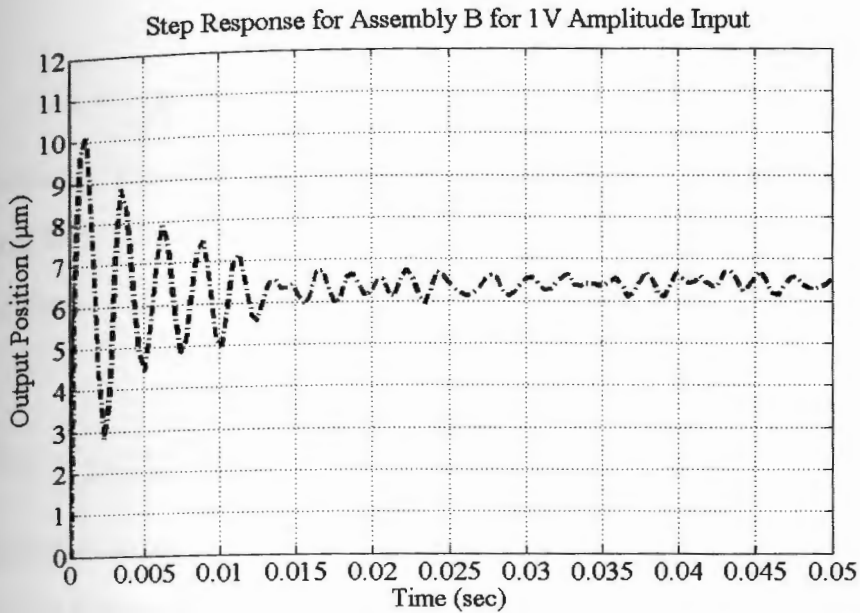
Figure 2.11. Assembly B Step Response

$$\zeta_{POS} = -\frac{ln(POS/100)}{\sqrt{\pi^2 + ln^2(POS/100)}} = -\frac{ln(59.66/100)}{\sqrt{\pi^2 + ln^2(59.66/100)}} = 0.1726 \qquad (2.3)$$

The damping factor determination by peak-to-peak amplitude, where P_k is the amplitude at a peak and P_{k+N} is the amplitude at N peak periods later is as follows:

$$
\begin{aligned}
\zeta_{PP} &= -\frac{ln(P_{k+N}/P_k)}{\sqrt{4 \cdot \pi^2 \cdot N^2 + ln^2(P_{k+N}/P_k)}} \\
&= -\frac{ln(8.83/10.09)}{\sqrt{4 \cdot \pi^2 \cdot 1^2 + ln^2(8.83/10.09)}} = 0.0212 \qquad (2.4)
\end{aligned}
$$

Neither of these damping factors appear to accurately represent the damping - 0.1726 gives too much damping and 0.0212 gives too little damping. As a compromise, these two damping factors are averaged. This yields a damping factor of $\zeta = 0.0969$. This damping factor may then be used with the damped natural frequency to determine the system's undamped natural frequency:

22

$$\omega_n = \frac{\omega_d}{\sqrt{1 - \zeta^2}} = \frac{2685}{\sqrt{1 - 0.0969^2}} = 2698 rad/sec = 429.4 Hz \qquad (2.5)$$

Combining the values gathered for undamped natural frequency, damping factor and DC-Gain, the assembly B's 2nd order linear transfer function has the following form:

$$G(s) = \frac{DC \cdot \omega_n^2}{s^2 + 2 \cdot \zeta \cdot \omega_n \cdot s + \omega_n^2} = \frac{6.4 \cdot 2698^2}{s^2 + 2 \cdot 0.0969 \cdot 2698 \cdot s + 2698^2} \qquad (2.6)$$

The system's step response and the simulated step response from Equation 2.6 are shown in Figure 2.12. Due to modeling errors and nonlinearities (mostly due to hysteresis effects), this model does not yield a perfect fit, it is however sufficient for the purposes of this study.
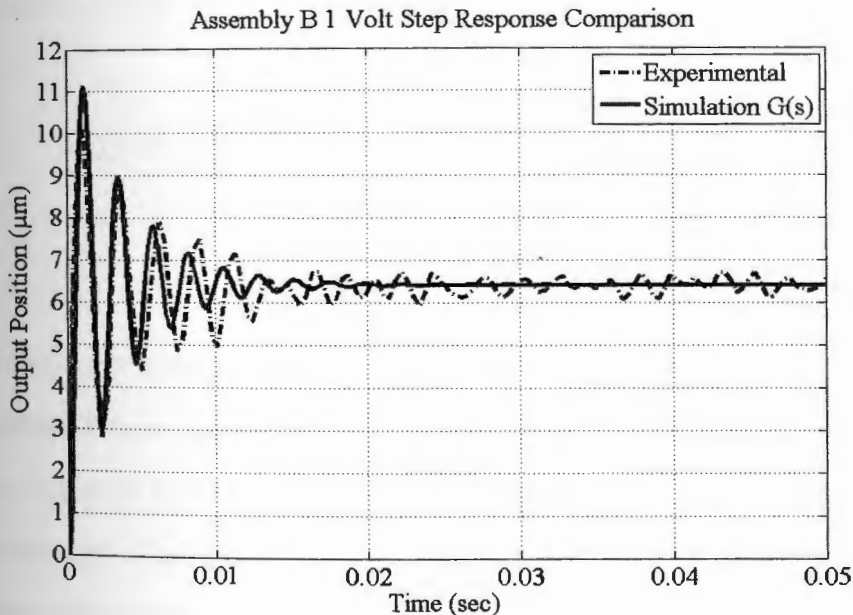
Figure 2.12. Assembly B Experimental and Simulated Linear Step Response

It is also appropriate to determine the system's effective actuated mass m_{eff}, effective viscous damping constant c_{eff} and effective stiffness k_{eff}. This data can

Table 2.2. Mass of Moving Components from Active Clamp	
Top Plate with Two Screws	426.7 g
Horizontal Wedge with Nut	59.1 g
Vertical Wedge	104.0 g
Equivalent Mass of Spring DF-2440 ($m/3$)	3.9 g
Spring Screw and Washer	5.6 g
Equivalent Mass of Actuator	123.3 g
Total Mass	723 g or **0.72 kg**

then be used to determine the system's force balance equation. The mass of each moving component in the active clamp is listed in Table 2.2. The effective mass of the piezoelectric actuator is given by taking one-third of the total mass of the actuator [44].

The effective actuated mass of the system has been determined to be 0.72 kg. Using this data and data concerning natural frequency and damping factors, the effective viscous damping and stiffness may be derived:

$$k_{eff} = \omega_n^2 \cdot m_{eff} = 2698^2 \cdot 0.72 = 5.24 \cdot 10^6 N/m \tag{2.7}$$

$$c_{eff} = 2 \cdot \zeta \cdot \sqrt{k_{eff} \cdot m_{eff}}$$

$$= 2 \cdot 0.0969\sqrt{5.24 \cdot 10^6 \cdot 0.72} = 376.4 N \cdot s/m \tag{2.8}$$

The step response test was conducted again for assembly A to validate the results obtained from assembly B. This assembly's response characteristics were also very similar to those depicted above. This suggests that the linear response characteristics of all assemblies may be sufficiently modeled using a simple second-order system description.

2.5 Relationship Between Linear and Nonlinear Hysteretic System Behavior

The author assumes that the total nonlinear response characteristics of a piezoelectrically actuated system may be split into linear dynamic and nonlinear,

rate-independent hysteretic responses. Systems with hysteresis can be defined as a "series, parallel or feedback connection of a hysteresis operator and a dynamical system" [45]. This thesis models the active clamp assembly's hysteresis as a phenomenon in series or in parallel with the system's (mostly) linear dynamic behavior. These two linear-hysteretic system variants are depicted in block diagram form in Figure 2.13.
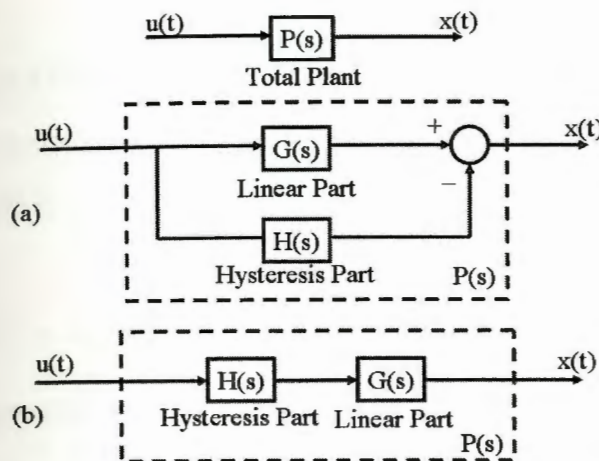
Figure 2.13. Block Diagram Depicting Hysteresis in Series (a) and in Parallel (b) with Linear System Behavior

Accurate modeling of the total nonlinear plant P(s) across all input signal frequency ranges requires models of the system's hysteresis (H(s)) and the linear dynamic component (G(s)). The Bouc-Wen modeling procedure tries to explicitly model the hysteresis component H(s) as a phenomenon in parallel with a linear dynamic system, while the Preisach technique models the total nonlinear response P(s) for signal input rates where the linear part acts like a static system (i.e. the velocity and acceleration terms are close to zero). By using each feed-forward model-based hysteresis compensation strategy outlined in the forthcoming chapters, the rate-independent hysteretic response is essentially canceled out leaving an exclusively linear dynamic system output response.

25

By assuming that the system's nonlinear hysteresis (H(s)) is purely rate-independent, the loop shape variations observed in Figure 2.10 should originate only from the linear part (G(s)) of system response. It should therefore be possible to use the identified linear model G(s) and filter the output shown in the figure. This would then yield the purely hysteretic component of the response H(s). A plot of signal input to H(s) output for each input signal rate would yield a set of matching loops.

Using the model found in [16], hysteresis effects which are in parallel with a linear dynamic system 2nd order system may be described through the following force balance equation:

$$m_{eff} \cdot \ddot{x}(t) + c_{eff} \cdot \dot{x}(t) + k_{eff} \cdot x(t) = k_{eff} \cdot (d \cdot u(t) - h(u(t)))　\quad (2.9)$$

Here $x(t)$ represents the total response of the system, d is the voltage to displacement constant, u is the input voltage and $h(u)$ represents the hysteresis displacement, which is a function of u. The rate-independent hysteresis function $h(u)$ may be determined by rearranging Equation 2.9. The resulting Equation 2.10 may be implemented by the block diagram shown in Figure 2.14.

$$h(u(t)) = d \cdot u(t) - \frac{m_{eff}}{k_{eff}} \cdot \ddot{x}(t) - \frac{c_{eff}}{k_{eff}} \cdot \dot{x}(t) - x(t) \quad (2.10)$$

One can determine the shape of the rate-independent hysteresis loop function $h(u(t))$ from experimental data using this conversion function with the voltage input signal and the measured output position. This function for assembly B, spring DF-2440 and voltage rates 10, 100, 500, 1000 and 1500 V/s is shown in Figure 2.15.

This plot looks different from previous plots of hysteresis, since its output only represents the change from linear output due to hysteresis, instead of the
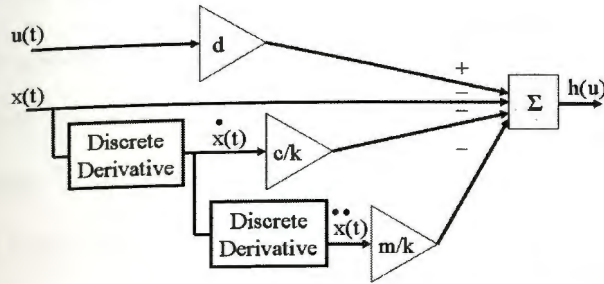
Figure 2.14. Block Diagram for Determining Rate-Independent Hysteresis Function From Voltage Input and Displacement Output Data
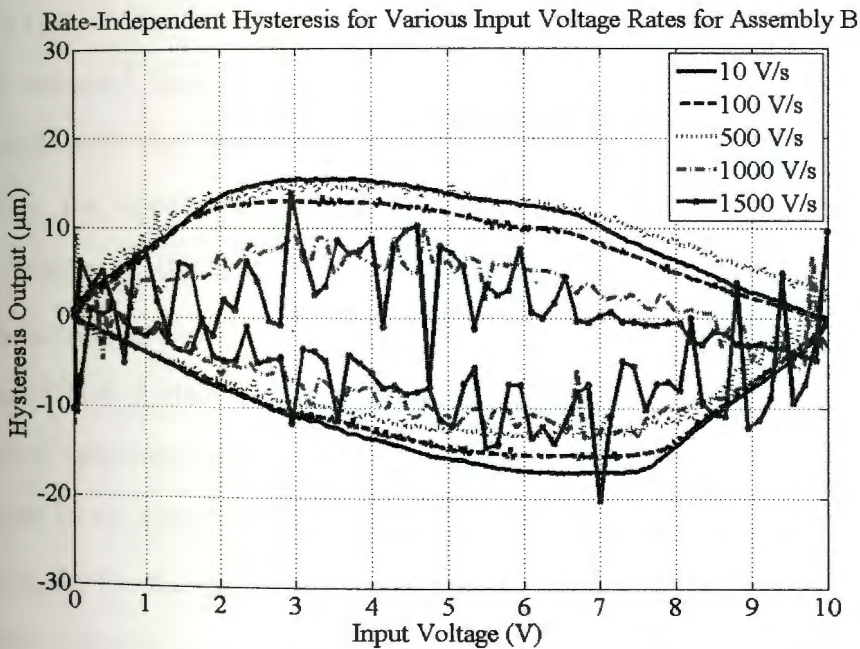
Figure 2.15. Plot of Pure Outer Loop Hysteresis Response without Linear Dynamics for Various Input Voltage Rates

total nonlinear output of the system. If the system had a purely linear response, the output of this plot would be a straight line along $0\mu m$. The rate independent hysteresis function appears to hold very well for 10, 100 and 500 V/s input voltage rates. There seems to be some discrepancy as well as noise in the loop for 1000 and 1500 V/s input rates. The discrepancies are likely due to linear system modeling errors, unmodeled non-hysteresis related nonlinearities, measurement errors and perhaps a certain degree of rate-dependence in the system. The noise present results from the differentiation of the experimental displacement data $x(t)$. Any noise that may have been present in $x(t)$ would be amplified by a factor of c_{eff}/k_{eff} for the first differentiation and by m_{eff}/k_{eff} for the second differentiation. Despite the rate-independence discrepancies for 1000 and 1500 V/s, this thesis will assume that the system's hysteresis is primarily a rate-independent phenomenon, and that the linear part of the response can be described as a 2nd order system.

It is assumed that the system's output for a 10 V/s input is fully rate-independent and the linear dynamics do not play a role ($\ddot{x}(t) \approx \dot{x}(t) \approx 0$). Using the rate-independent hysteresis function $h(u)$ from the 10 V/s test, the output of the system should fulfill the following static position equation: $x_{LinearFiltered10V/s}(t) = d \cdot u(t) - h(u)$. When $x_{LinearFiltered10V/s}(t) - x_{NoFilter10V/s}(t) = 0$, then $x_{NoFilter10V/s}$ may be used in general to derive the rate-independent hysteresis function without worrying that the linear rate-dependent effects need to be filtered. Figure 2.16 plots the function $x_{LinearFiltered10V/s}(t) - x_{NoFilter10V/s}(t)$ for the major hysteresis loop of assembly B with spring DF-2440 and 8 cNm set screw torque.

This figure shows that the position error between the calculated static hysteresis loop and that derived for 10 V/s is almost non-existent. For this reason, it is safe to model system hysteresis with up to 10 V/s hysteresis loop data.
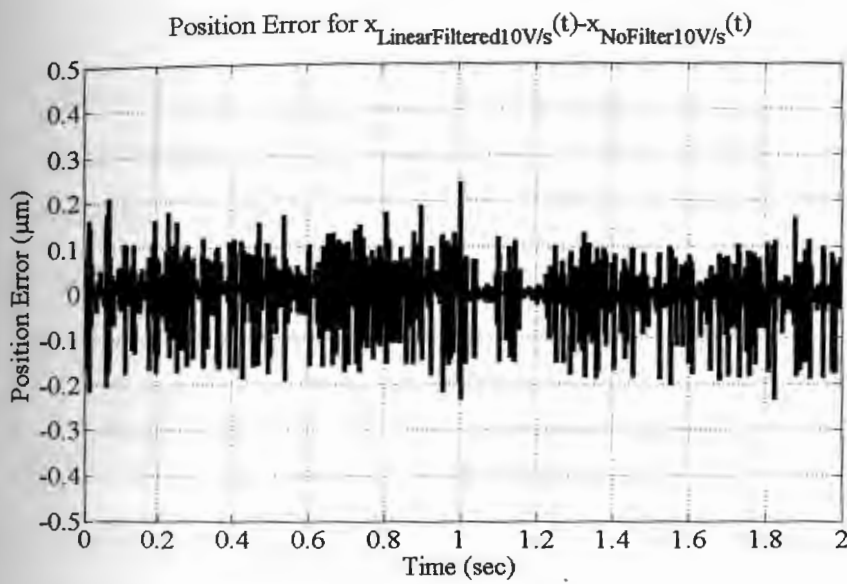
Figure 2.16. Difference Between Hysteresis Curves for Static Major Loop Hysteresis and Hysteresis for 10 V/s for Assembly B

CHAPTER 3

Bouc-Wen Hysteresis Modeling and Compensation

3.1 Bouc-Wen Model Formulation

Using the formulation developed by Bouc and Wen, the hysteresis dependency between a state variable z and an excitation y is described by the following relation:

$$\dot{z} = A \cdot \dot{y} - \beta \cdot |\dot{y}| \cdot z \cdot |\dot{z}|^{n-1} - \gamma \cdot \dot{y} \cdot |z|^n \tag{3.1}$$

The parameter A controls the restoring force amplitude, and parameters β and γ control the shape of the hysteresis loop. The parameter n controls the transition between elastic and plastic responses. Since the piezoelectric actuator is assumed to operate as a fully elastic structure, the parameter n can be assumed to be equal to one. Therefore Equation 3.1 can be simplified into the following form:

$$\dot{z} = A \cdot \dot{y} - \beta \cdot |\dot{y}| \cdot z - \gamma \cdot \dot{y} \cdot |z| \tag{3.2}$$

It is convenient to further modify Equation 3.2 to describe the relationship between an input voltage $u(t)$ and an hysteretic component of output position $h(t)$. This equation has the form:

$$\dot{h} = \alpha \cdot d \cdot \dot{u} - \beta \cdot |\dot{u}| \cdot h - \gamma \cdot \dot{u} \cdot |h| \tag{3.3}$$

The effective linear relationship between input voltage and system output position x is described by d. The value of d may be determined using identification algorithm described below.

The hysteretic state $h(t)$ could then be used for the calculation of output position $x(t)$ based on the input voltage $u(t)$. The Bouc-Wen model assumes that hysteresis is a phenomena occurring in parallel with linear effects. For example,

30

assuming that the piezoelectrically actuated system has a linear component that behaves like a 2nd order mass-spring-damper system, the force balance equation for this system would then have the following form:

$$m \cdot \ddot{x} + c \cdot \dot{x} + k \cdot x = k \cdot (d \cdot u - h) \tag{3.4}$$

Here m represents the system's effective mass, c represents effective linear viscous system damping and k represents effective linear system stiffness. The parameter m can be estimated as the sum of all moving part masses plus the effective mass of the piezoelectric actuator. The parameters c and k can then be estimated using the value of m and the damped natural frequency and damping factor observed through step or impulse response tests.

3.2   Identification Procedure for Bouc-Wen Hysteresis Parameters

There are several methods available for the identification of parameters α, β, γ and d. The input to the system is first cycled so that the system hysteretic output position behavior is recorded experimentally. An input profile like the one found in Figure 2.3 in Chapter 2 may be used for this purpose. After this step, one may try *tuning* the model parameters by hand until the simulated response roughly fits that of the experimental data. The second option is to develop a formal identification algorithm for the determination of each parameter.

There are several formal identification algorithms available for the determination of Bouc-Wen parameters. In [16], a optimizing parameter estimator was developed based on the theory of invariant imbedding. The publication [18] used an efficient adaptive on-line identification method, [19] employed modified quadratic programming while [21] utilized a real-coded genetic algorithm for parameter identification.

Most of these identification methods share the common characteristic that

31

they determine parameters which minimize a given cost function J. In most cases, a quadratic-based cost function was used for identification. Such a cost function takes the form:

$$J = \int_0^T (x(t) - \hat{x}(t))^2 dt = \sum_{k=0}^N (x_k - \hat{x}_k)^2 \qquad (3.5)$$

or:

$$J = \sqrt{\frac{\sum_{k=0}^N (x_k - \hat{x}_k)^2}{N}} \qquad (3.6)$$

In these cost functions, $x(t)$ and x_k represent measured output data at time t or sample k. $\hat{x}(t)$ or $\hat{x}_k$ represent the estimated output for a certain α, β, γ and d. N represents the total number of sampled data points. Equation 3.6 is used in this thesis for the identification of Bouc-Wen parameters.

The Matlab function "fmincon" is used to identify the Bouc-Wen parameters from experimental data. The function "attempts to find the constrained minimum of a scalar function of several variables starting at an initial estimate." [46]. It tries to locate variables (α, β, γ and d) which minimize the cost function in Equation 3.6. The function to be minimized and the constraints on the variables must be continuous. This function relies on user-provided lower and upper bounds as well as initial values for each of the variables.

In this case, x_k is the position output for a given time index k and $\hat{x}_k$ is the estimated value of x_k for index k based on the output resulting from Equations 3.3 and 3.4.

Using the assumption of linear rate independence for input voltage rates less than or equal to 10 V/s (meaning $\dot{x} \approx \ddot{x} \approx 0$ – see Figure 2.16 from Chapter 2), Equation 3.4 may be simplified into Equation 3.7 to accelerate the identification process.

$$m \cdot 0 + c \cdot 0 + k \cdot x = k \cdot (d \cdot u - h)$$

$$x = d \cdot u - h \tag{3.7}$$

This form allows the proper identification of parameters α, β, γ and d without needing to separately identify the linear parameters m, c and k. To further accelerate the process, the experimental outer loop measurement data is used for identification.

The differential equations governing the complete Bouc-Wen hysteresis model may be set up in a form which is solvable using the ordinary differential equation solver in Matlab. Since the hysteresis compensation algorithm would later need to be built in Simulink, the author instead set up the differential equations in block diagram form and implemented the differentiation and integration operations using the *Discrete Derivative* and *Discrete Time-Integration* Simulink blocks.

The selection of proper lower and upper bounds is very important for the correct determination of minimizing Bouc-Wen parameters. Improper selection of lower and upper bounds cause the function's search mechanism to find a *local* rather than the *global* function minimum. The resulting hysteresis loop may not sufficiently *fit* to the experimentally measured loop. For this reason, the user may need to repeat the process with varying the lower and upper bound combinations until the proper parameters are located.

3.2.1 Identification of Hysteresis Parameters in Actuators A and B

The Bouc-Wen model of hysteresis was determined for actuators A and B using experimental data from 1 V/s outer loop hysteresis curves sampled at 1 kHz and the identification procedure described above. The selected initial values and lower and upper bounds for each Bouc-Wen parameter is listed in Table 3.1.

Table 3.1. Initial Values and Bounds for Identification of Bouc-Wen Parameters for Actuators A and B

	Initial Value	Lower Bound	Upper Bound
α	1.0	0	5
β	0.5	0	5
γ	0.5	-2	5
$d\ (\mu m/V)$	12	10	14

The comparison of experimental output and identified Bouc-Wen model for actuator A are shown in the input voltage to output position plot in Figure 3.1. Likewise, the time to output position plot for actuator B is shown in the input voltage to output position plot in Figure 3.2. The identified parameters and cost functions are tabulated in Table 3.2.
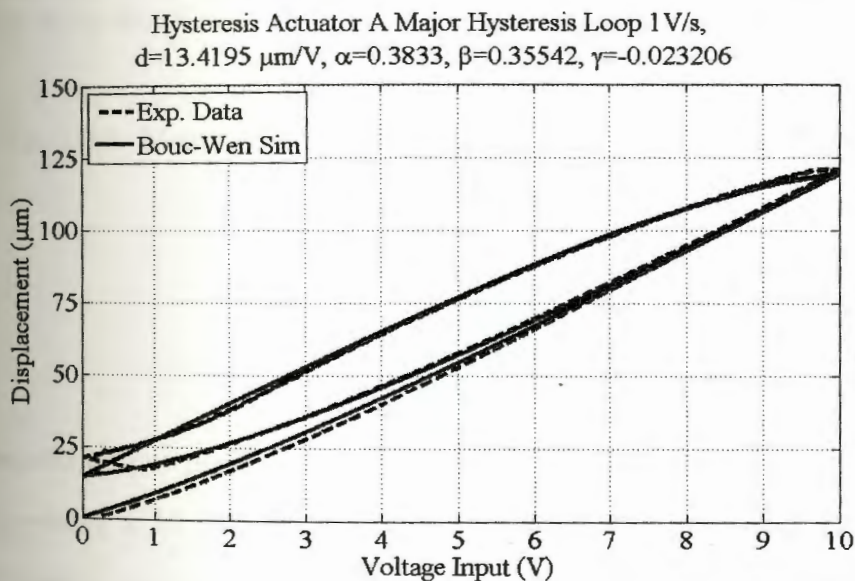
Figure 3.1. Input Voltage to Output Position Plot Comparing Experimental and Identified Bouc-Wen Loops for Actuator A

Both identified model output appear to fit the shape of the experimental hysteresis curves well. However, the parameters determined from these models cannot be directly used for the compensation of hysteresis in the assemblies. Referring back to Figure 2.7 in Chapter 2, the assembly condition specifically affects hystere-
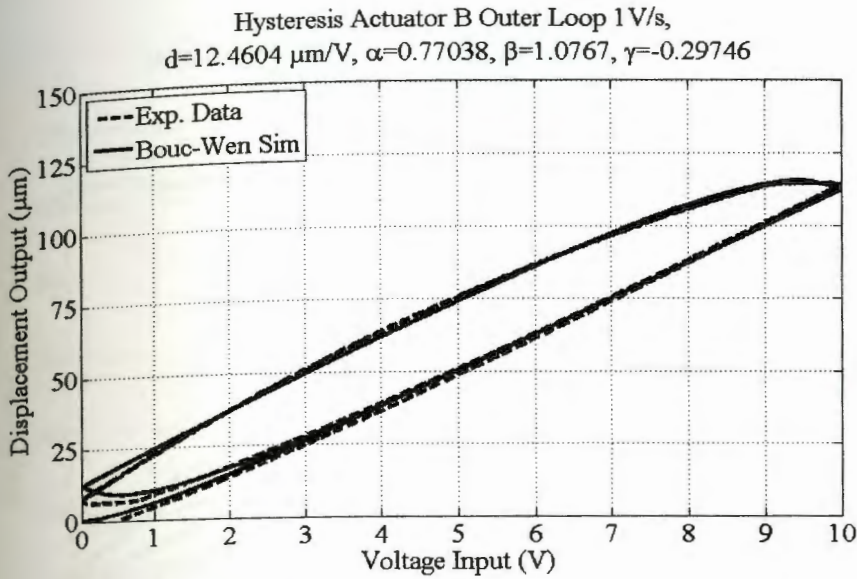
Figure 3.2. Input Voltage to Output Position Plot Comparing Experimental and Identified Bouc-Wen Loops for Actuator B

Table 3.2. Identified Bouc-Wen Parameters for Actuators A and B

Actuator	A	B
α	0.38	0.77
β	0.36	1.08
γ	-0.02	-0.30
d (μm)	13.42	12.46
J (RMS)	0.485	0.451

sis shape and output position at 10 V. One option for applying these parameters to the assembly is to maintain the values of α, β and γ from the actuator and then re-identify the parameter d using the major hysteresis loop data from the assembly.

The comparison of experimental output and identified Bouc-Wen model for assembly A using the parameters from actuator A are shown in the input voltage to output position plot in Figure 3.3. Likewise, the input voltage to output position plot for assembly B using the parameters from actuator B is shown in Figure 3.4.

The identified values for the voltage to displacement constant d for assemblies
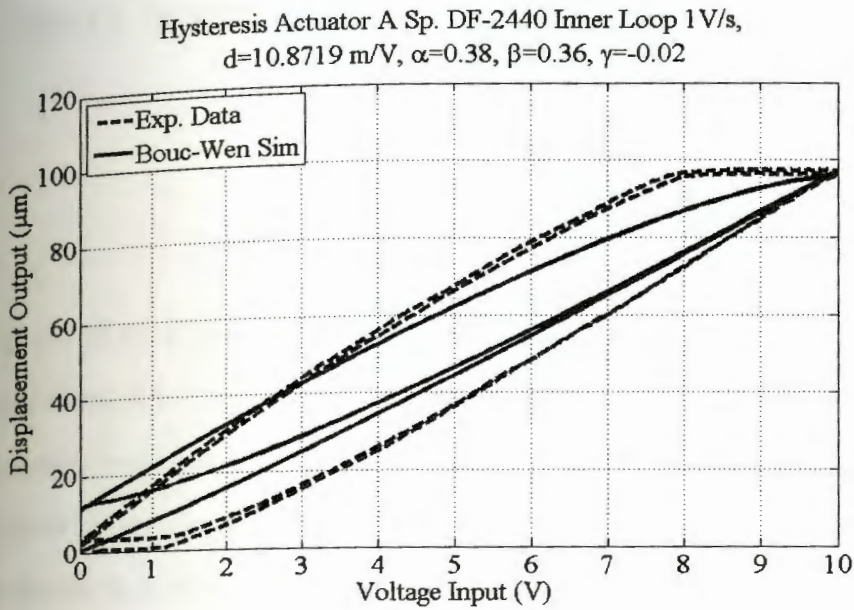
Figure 3.3. Input Voltage to Output Position Plot Comparing Experimental and Identified Bouc-Wen Loops for Assembly A Using Actuator A Parameters
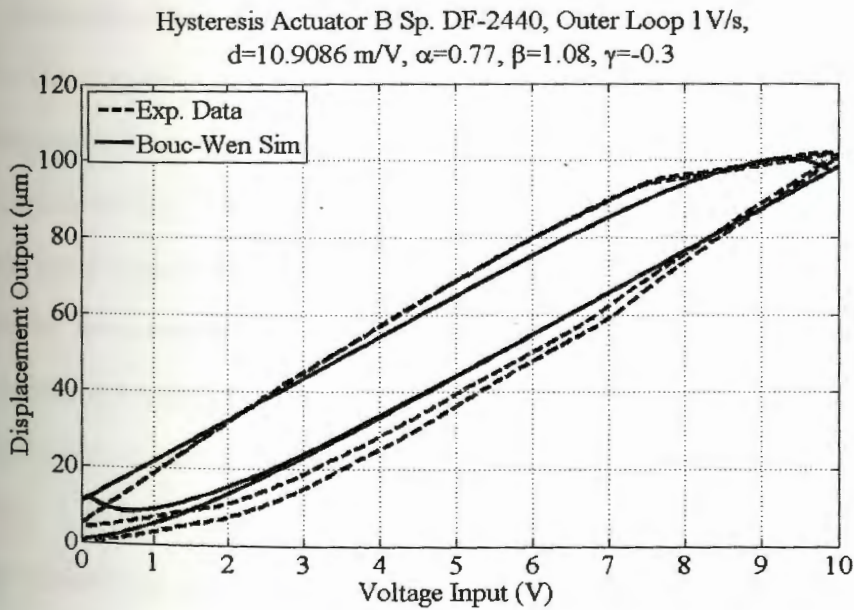
Figure 3.4. Input Voltage to Output Position Plot Comparing Experimental and Identified Bouc-Wen Loops for Assembly B Using Actuator B Parameters

Table 3.3. Identified Bouc-Wen Parameters for Assemblies A and B

Assembly	A	B
α	1.79	1.34
β	1.29	1.29
γ	-0.21	-0.16
d (μm)	10.51	10.84
J (RMS)	0.336	0.320

A and B are 10.87 $V/\mu m$ and 10.91 $V/\mu m$ with the cost function values of 0.705 RMS and 0.414 RMS respectfully. These models do not fully describe the respective assembly hysteresis behaviors. This is a particular problem with assembly A, as evidenced by its significantly larger RMS value compared to actuator A. Figure 3.3 also shows that experimental hysteresis curve is much wider than the model's hysteresis. However, a compensation algorithm using the identified parameters may still be effective in at least reducing the hysteresis effect in the assemblies. This will be investigated later in this chapter.

3.2.2 Identification of Hysteresis Parameters in Assemblies A and B

The identification procedure may also be used to determine all four Bouc-Wen parameters from the assembly data directly. The comparison of experimental output and identified Bouc-Wen model for assembly A are shown in the input voltage to output position plot in Figure 3.5. Likewise, the input voltage to output position plot for assembly B is shown in Figure 3.6. The identified parameters and cost functions are tabulated in Table 3.3.

The identified hysteresis loops initially appears to fit fairly well to the measured data. The RMS cost function value is also quite low for both models. However, the Bouc-Wen model fails to model the ends of the hysteresis curve. As explained in Chapter 2, these "flat" parts of the experimental hysteresis curves are likely due to static frictional forces. The Bouc-Wen model does not have parameters related to static friction and for this reason it is not particularly suitable for

Hysteresis Actuator A Sp. DF-2440, Outer Loop 1 V/s,
d=10.5135 μm/V, α=1.7899, β=1.2927, γ=0.21444
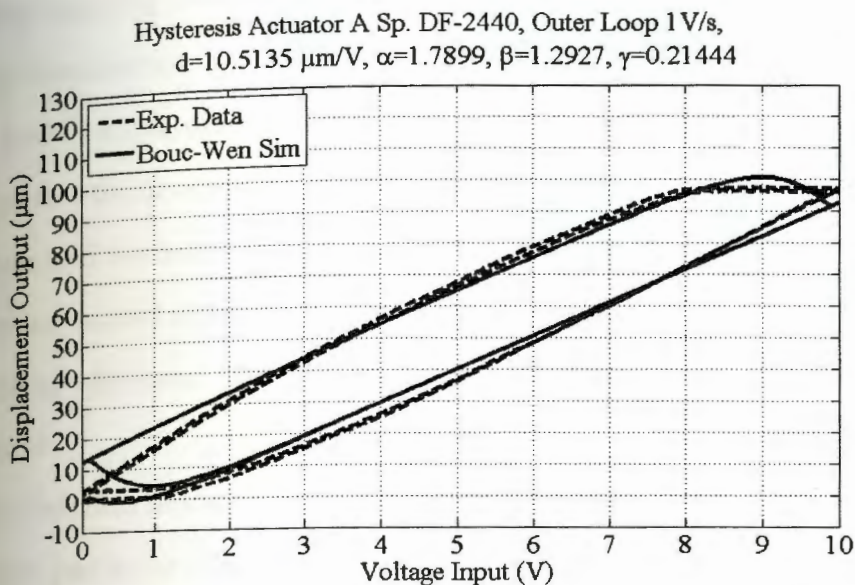
Figure 3.5. Input Voltage to Output Position Plot Comparing Experimental and Identified Bouc-Wen Loops for Assembly A

Hysteresis Actuator B Sp. DF-2440, Outer Loop 1 V/s,
d=10.8373 μ m/V, α=1.3427, β=1.2916, γ=-0.16127
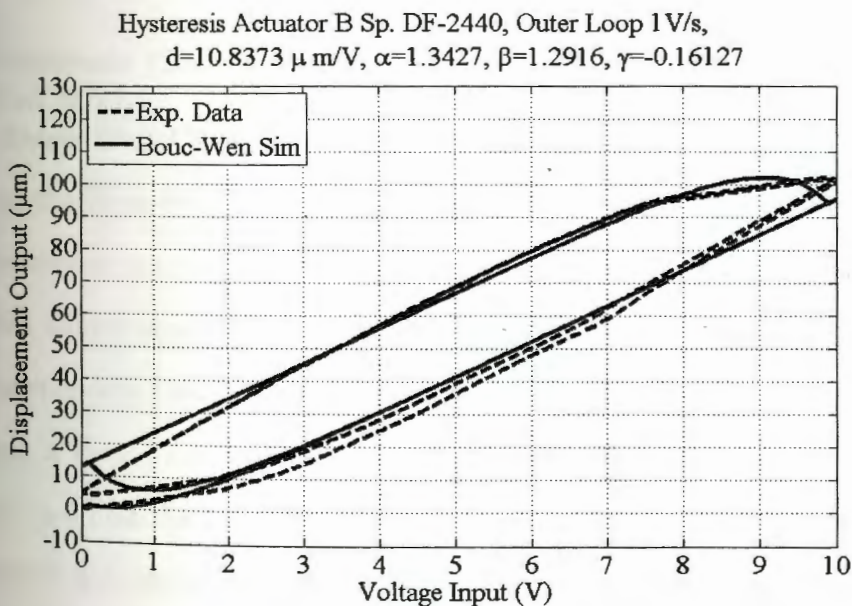
Figure 3.6. Input Voltage to Output Position Plot Comparing Experimental and Identified Bouc-Wen Loops for Assembly B

accurately modeling systems exhibiting such dominant behavior.

The identification routine tries to determine Bouc-Wen parameters which make a best fit to the given dataset. The resulting models have a hysteresis curve which appears to curve upward between 10 to 8 or 7 volt input. This curved shape could later lead to control signal saturation issues. The desired (before saturation) feed-forward control signal output may be greater than 10 V when the reference input voltage decreases from 10 V. This will be examined in more detail later in the chapter.

The identified model also appears to exhibit unusual behavior near 0 and near 10 V input just before the curving begins at either end of the hysteresis loop. At these points, it appears that the simulation enters a short region of linearity. This is most likely a numerical integration solver error resulting from the discontinuous voltage signal where the input voltage profile immediately switches from a positive to a negative slope.

3.3 Hysteresis Compensation Method and Simulation Using Bouc-Wen Model

3.3.1 Bouc-Wen Compensation Method

Once the Bouc-Wen modeling parameters α, β and γ have been determined, these parameters may be used directly for the compensation of hysteresis. Since the Bouc-Wen model assumes that the total hysteretic nonlinear system response has a rate-independent hysteresis component which runs in parallel with linear system dynamics, a Bouc-Wen hysteresis *observer* may be implemented to predict this behavior based on the identified modeling parameters. This predicted hysteresis may be used directly to calculate a compensating control voltage.

The feed-forward Bouc-Wen parallel hysteresis observer compensation has the block diagram form shown in Figure 3.7. The term u_{ref} refers to the reference voltage input term corresponding to a reference position $x_{ref} = u_{ref} \cdot d$ that is to

be tracked, $\hat{h}(u_{ref})$ refers to the Bouc-Wen calculated hysteresis output, $1/d$ is the inverse of the identified input voltage to output position constant. The term u_{ff} is then the reference feed-forward input voltage needed to track x_{ref}.
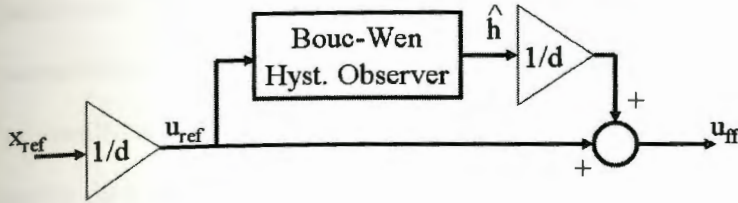
Figure 3.7. Feed-Forward Bouc-Wen Parallel Hysteresis Observer Compensation Block Diagram

Based on Equation 3.3, this feed-forward compensator may also be implemented digitally with the following set of equations using Δt as the sampling rate:

$$\hat{h}[k] = \hat{h}[k-1] + \Delta t \cdot (\alpha \cdot d \cdot \dot{u}_{ref}[k-1] - \beta \cdot |\dot{u}_{ref}[k-1]| \cdot \hat{h}[k-1]$$
$$-\gamma \cdot \dot{u}_{ref}[k-1] \cdot |\hat{h}[k-1]|) \tag{3.8}$$
$$u_{ff} = u_{ref} + \frac{\hat{h}[k]}{d} \tag{3.9}$$

Substituting u_{ff} for u in Equation 3.4 gives:

$$m \cdot \ddot{x} + c \cdot \dot{x} + k \cdot x = k \cdot (d \cdot u_{ref} - h + \hat{h}) \tag{3.10}$$

Assuming that $h \approx \hat{h}$, the hysteresis terms should cancel each other out, and then the system should behave like a linear second order system.

3.3.2 Simulated Parallel Bouc-Wen Hysteresis Compensation

The Bouc-Wen parameters determined in Chapter 3 have been used for the compensation of parallel hysteresis. Two different types of parameter sets were proposed for the assembly: one where the parameters α, β and γ where identified

from the unloaded actuator hysteresis response and d was based on the assembly, and the other where the parameters α, β, γ and d were identified from the assembly's hysteresis curves directly.

The simulations are based on sending a feed-forward signal into a Bouc-Wen model whose parameters α, β, γ and d match that of the feed-forward control algorithm. The resulting simulation output represents an idealized case which does not necessarily directly reflect the actual hysteresis reduction when the feed-forward algorithm is implemented experimentally. However, the output from these simulations is useful in understanding the reference to feed-forward input voltage relationship as well as for comparing the system output with parameters based on the actuator with those from the assembly.

Based on Figure 3.3, the parameters for assembly A based on the unloaded actuator are $\alpha = 0.38$, $\beta = 0.36$, $\gamma = -0.02$ and $d = 10.87$ μm. Figure 3.8 illustrates the reference voltage input (u_{ref}), and the feed-forward voltages before (u_{ff} no sat.) and after 0 to 10 V saturation (u_{ff} sat. 0-10 V) for the given reference input signal. The corresponding simulated reference input voltage and position output are shown in Figure 3.9. The major loop area for the uncompensated system is 205.11 $\mu m \cdot V$. On the other hand, the major loop area for the compensated system is 13.79 $\mu m \cdot V$. This suggests a 93.28% reduction in major hysteresis loop area. The displacement output for both cases for 10 V input is 93.52 μm.

The output of the Bouc-Wen controller is diminished by the saturation. All computed feed-forward inputs which fall below 0 volts are held at 0 V. All feed-forward inputs above 10 volts are held at 10 V. The computed voltage before saturation does not appear to go above 11 V or below -1 V. This seems to have no effect on the calculated maximum output of the actuator, however the output position does not return to zero when the reference output falls below 1 volt refer-

ence input (see lower left corner of Figure 3.9). This control algorithm is therefore not effective in the 0 to 1 V reference voltage input range. The controller could however significantly reduce hysteresis.
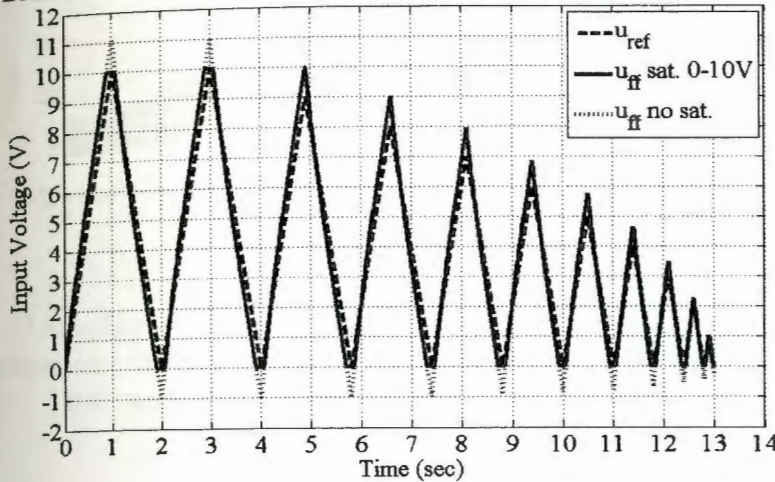
Figure 3.8. Assembly A Simulated 10 V/s Reference Input Voltage and Bouc-Wen Hysteresis Compensated Voltage for $\alpha = 0.38$, $\beta = 0.36$, $\gamma = -0.02$ and $d = 10.87 \mu m$

Based on Figure 3.4, the parameters for assembly B based on the unloaded actuator are $\alpha = 0.77$, $\beta = 1.08$, $\gamma = -0.3$ and $d = 10.91$ μm. Figure 3.10, illustrates the reference voltage input (u_{ref}), and the feed-forward voltages before (u_{ff} no sat.) and after 0 to 10 V saturation (u_{ff} sat. 0-10 V). The corresponding simulated reference input voltage and position output are shown in Figure 3.11. The major loop area for the uncompensated system is 181.23 $\mu m \cdot V$, while the displacement output at 10 V is 100.9 μm. On the other hand, the major loop area for the compensated system is 13.73 $\mu m \cdot V$, while the displacement output at 10 V is 98.33 μm. The control could reduce hysteresis by 92.42%

Like with actuator A, the output of the Bouc-Wen controller is diminished by the saturation. The voltage again does not appear to go beyond 1 V above or

Assembly A Simulation Comparison of 10V/s Uncompensated Experimental
Position and Parallel Bouc-Wen Compensated Position to Input
Reference Voltage, d=10.87 μ m/V, α=0.38, β=0.36, γ=-0.02
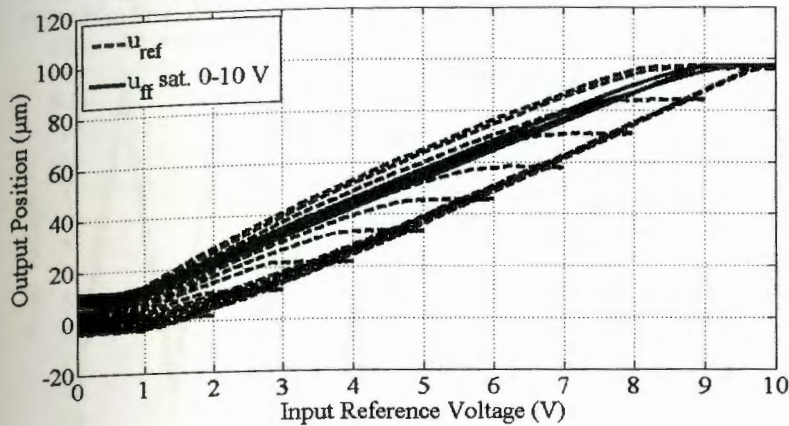
Figure 3.9. Assembly A Simulated 10 V/s Reference Voltage Input to Position
Output Comparison for Bouc-Wen Hysteresis Compensated Voltage for $\alpha = 0.38$,
$\beta = 0.36$, $\gamma = -0.02$ and $d = 10.87\mu m$

below saturation. The position output also does not return to $0~\mu m$. The controller
could however significantly reduce hysteresis.

Referring to Figure 3.5, the parameters for assembly A based on identifying
the assembly directly are $\alpha = 1.79$, $\beta = 1.29$, $\gamma = -0.21$ and $d = 10.51~\mu m$.
Figure 3.12, illustrates the reference voltage input (u_{ref}), and the feed-forward
voltages before $(u_{ff}$ no sat.$)$ and after 0 to 10 V saturation $(u_{ff}$ sat. 0-10 V$)$. The
corresponding simulated reference input voltage and position output are shown in
Figure 3.13. The major loop area for the uncompensated system is 205.11 $\mu m \cdot V$,
while the displacement for 10 V input is 93.52 μm. On the other hand, the major
loop area for the compensated system is 34.30 $\mu m \cdot V$, while the displacement for
10 V input is 87.68 μm. The compensated system achieves an 83.28% reduction
in major loop hysteresis area.

Similar to the cases where the Bouc-Wen parameters are based on the actu-
ator, the computed feed-forward signal is also restricted by saturation. However,
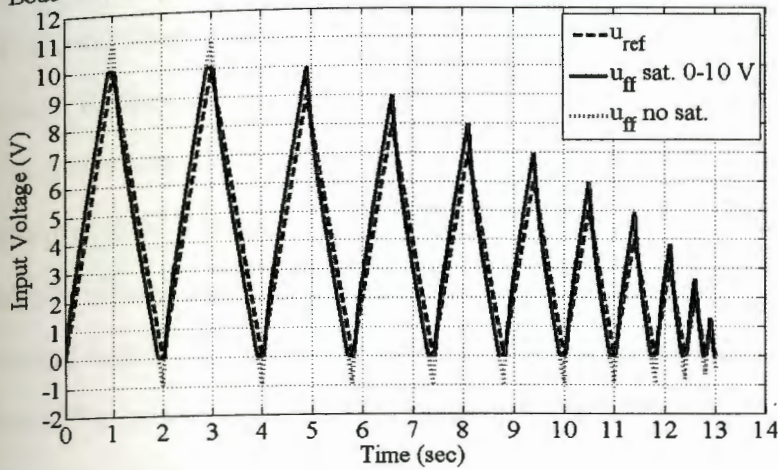
Figure 3.10. Assembly B Simulated 10 V/s Reference Input Voltage and Bouc-Wen Hysteresis Compensated Voltage for $\alpha = 0.77$, $\beta = 1.08$, $\gamma = -0.3$ and $d = 10.91\mu m$
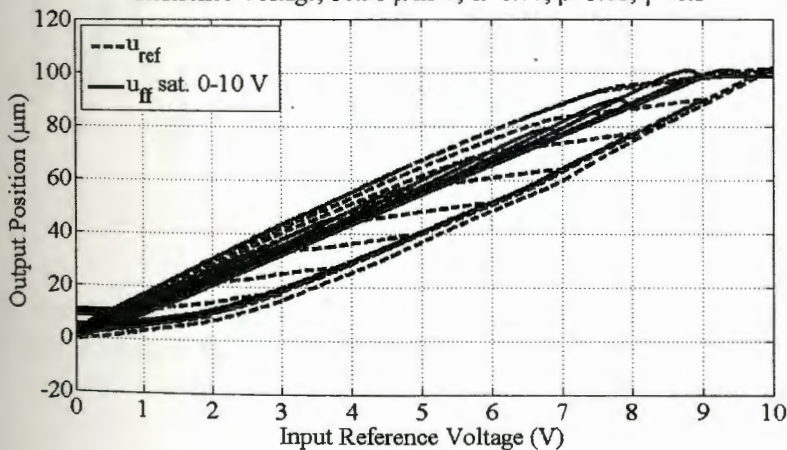
Figure 3.11. Assembly B Simulated 10 V/s Reference Voltage Input to Position Output Comparison for Bouc-Wen Hysteresis Compensated Voltage for $\alpha = 0.77$, $\beta = 1.08$, $\gamma = -0.3$ and $d = 10.91\mu m$

in this case, the voltage level goes almost 2 volts beyond the saturation limits. This leads to some unusual behavior observed in the voltage input to position output plot. The controlled output does not reach its maximum output at 10 volt reference input. Rather, the hysteresis loops suddenly curves upward soon after decreasing from the loop maximum voltage input. The position output also never goes back down to zero. Instead, the position output is at almost 20 μm for zero input. When the voltage input increases again, the position loops back downward before increasing again. This behavior can also be partially explained by Figure 3.5. The Bouc-Wen model does not match the hysteresis behavior well at either end of the hysteresis loop, and instead has a curved shape. The curved shape in the controlled output is roughly analogous to the curved shape found in the controlled output.
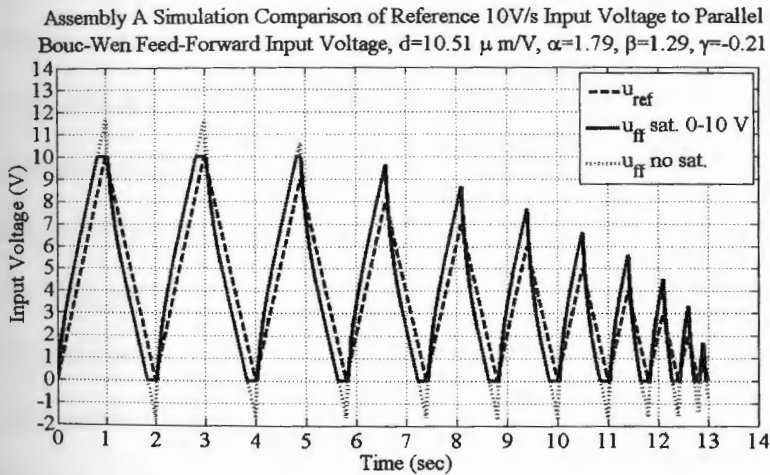
Figure 3.12. Assembly A Simulated 10 V/s Reference Input Voltage and Bouc-Wen Hysteresis Compensated Voltage for $\alpha = 1.79$, $\beta = 1.29$, $\gamma = -0.21$ and $d = 10.51$ μm

In Figure 3.6, the parameters for assembly B based on identifying the assembly directly are $\alpha = 1.34$, $\beta = 1.29$, $\gamma = -0.16$ and $d = 10.84$ μm. Figure 3.14, illustrates the reference voltage input (u_{ref}), and the feed-forward voltages before

Assembly A Simulation Comparison of 10V/s Uncompensated Experimental Position and Parallel Bouc-Wen Compensated Position to Input Reference Voltage, d=10.51 μ m/V, α=1.79, β=1.29, γ=-0.21
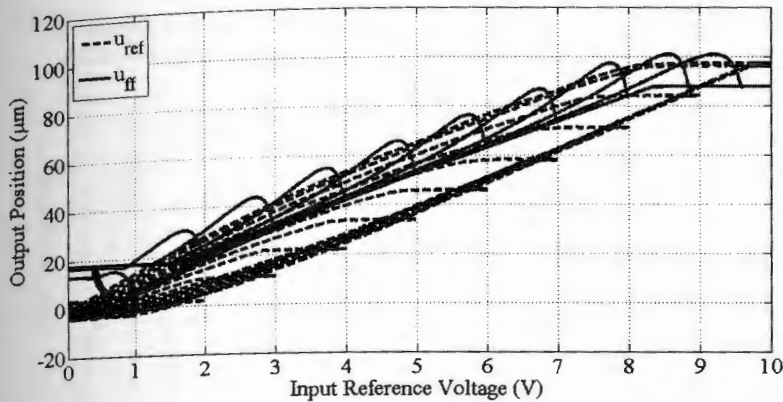
Figure 3.13. Assembly A Simulated 10 V/s Reference Voltage Input to Position Output Comparison for Bouc-Wen Hysteresis Compensated Voltage for $\alpha = 1.79$, $\beta = 1.29$, $\gamma = -0.21$ and $d = 10.51~\mu m$

(u_{ff} no sat.) and after 0 to 10 V saturation (u_{ff} sat. 0-10 V). The corresponding simulated reference input voltage and position output are shown in Figure 3.15. The major loop area for the uncompensated system is 181.23 $\mu m \cdot V$, while the displacement output at 10 V is 100.9 μm. On the other hand, the major loop area for the compensated system is 18.99 $\mu m \cdot V$, while the displacement output at 10 V is 95.55 μm. The reduction in major hysteresis loop area is 89.52%.

As with the directly identified assembly A, the computed control signal also exceeds the saturation limits by almost two volts. This, coupled with the rounded hysteresis shape at either end of 3.6, leads to the looped shapes in the controlled output position.

Although the feed-forward simulation of both model types appear to be able to significantly reduce the level of assembly hysteresis, the author prefers the results from the actuator model-based parameters. The actuator-based controlled output appears to reach roughly maximum output at 10 volts. Furthermore, the output position for this case at zero volts appears to be closer to zero than that

46
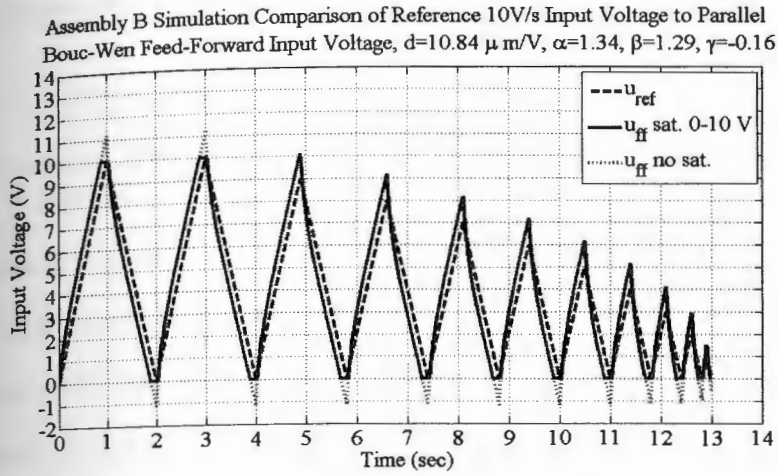
Figure 3.14. Assembly B Simulated 10 V/s Reference Input Voltage and Bouc-Wen Hysteresis Compensated Voltage for $\alpha = 1.34$, $\beta = 1.29$, $\gamma = -0.16$ and $d = 10.84$ μm
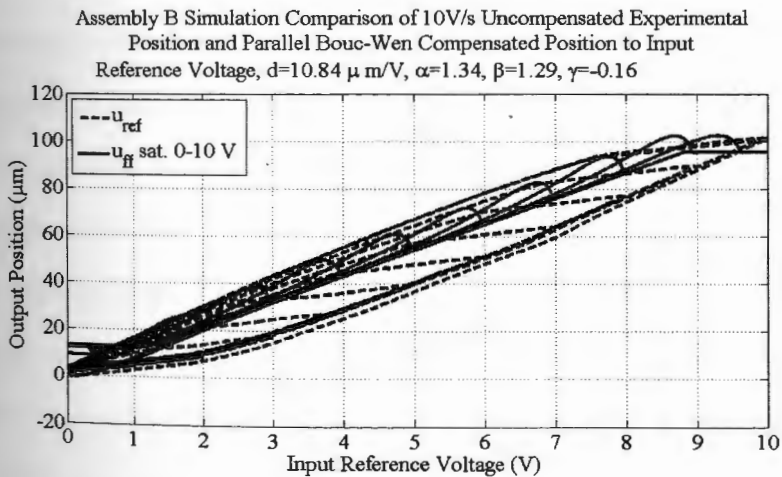
Figure 3.15. Assembly B Simulated 10 V/s Reference Voltage Input to Position Output Comparison for Bouc-Wen Hysteresis Compensated Voltage for $\alpha = 1.34$, $\beta = 1.29$, $\gamma = -0.16$ and $d = 10.84$ μm

of the ▓▓▓mbly-based controlled output. For these reasons, the following exper-
iments were carried out only using the feed-forward controller based on actuator
parameters.

3.4 Experimental Parallel Bouc-Wen Hysteresis Compensation for 0 to 10 V Range

The actuator parameter-based hysteresis compensator was tested on the ex-
perimental setup using profiles similar to that shown in Figure 2.3 in Chapter 2,
but with slopes of 10, 100, 500, 1000 and 1500 V/s. The resulting plots of reference
input voltage to output position for the uncompensated and compensated systems
are shown correspondingly in Figures 3.16, 3.17, 3.18, 3.19, 3.20. The output dis-
placement at 10 V reference input and the area of the major hysteresis loop for
both uncompensated and compensated systems are detailed in Table 3.4.

The experimental feed-forward control results using the Bouc-Wen compen-
sation model based on the model of actuator A appear to reduce the assembly's
level of hysteresis between voltage input to position output. The resulting input
voltage to output position loops for 10, 100 and 500 V/s for the controlled system
generally appear to have reductions in hysteretic area. This relationship seems to
disappear at 1000 and 1500 V/s, where the controlled system's hysteretic area at
1000 V/s approaches that of the uncompensated system and at 1500 V/s it ap-
pears to be slightly larger. The average reduction for all input voltages is 29.26%.
The controller does not completely eliminate hysteretic effects since the Bouc-Wen
model itself does not completely encompass the entire hysteresis loop (Figure 3.3).
However, there appears to be a general improvement in linearizing the system's
output.

The next chapter will investigate the Classical Preisach modeling and feed-
forward hysteresis compensation technique.

Figure 3.16. Assembly A 10 V/s Experimental Reference Voltage Input to Position Output Comparison for Bouc-Wen Hysteresis Compensated Voltage for $\alpha = 1.79$, $\beta = 1.29$, $\gamma = 0.21$ and $d = 10.51 \ \mu m$

Figure 3.17. Assembly A 100 V/s Experimental Reference Voltage Input to Position Output Comparison for Bouc-Wen Hysteresis Compensated Voltage for $\alpha = 1.79$, $\beta = 1.29$, $\gamma = 0.21$ and $d = 10.51 \ \mu m$

Figure 3.18. Assembly A 500 V/s Experimental Reference Voltage Input to Position Output Comparison for Bouc-Wen Hysteresis Compensated Voltage for $\alpha = 1.79$, $\beta = 1.29$, $\gamma = 0.21$ and $d = 10.51$ μm

Figure 3.19. Assembly A 1000 V/s Experimental Reference Voltage Input to Position Output Comparison for Bouc-Wen Hysteresis Compensated Voltage for $\alpha = 1.79$, $\beta = 1.29$, $\gamma = 0.21$ and $d = 10.51$ μm

Assembly A Comparison of 1500V/s Uncompensated Experimental Position and Parallel Bouc-Wen Feed-Forward Compensated Position to Input Reference Voltage, d=10.87 µ m/V, α=0.38, β=0.36, γ=-0.02
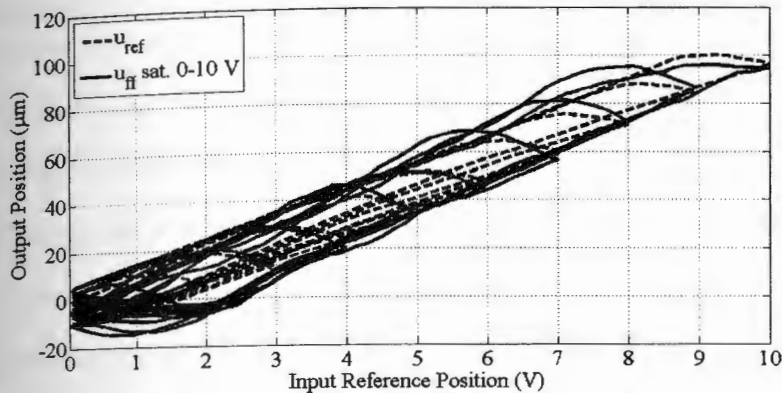
Figure 3.20. Assembly A 1500 V/s Experimental Reference Voltage Input to Position Output Comparison Bouc-Wen Hysteresis Compensated Voltage for $\alpha = 1.79$, $\beta = 1.29$, $\gamma = 0.21$ and $d = 10.51 \ \mu m$

Table 3.4. Assembly A Experimental Displacement at 10 V Reference Input and Major Loop Area for Uncompensated (Unc.) and Bouc-Wen Compensated (Comp.) Systems

Input Rate (V/s)	10	100	500	1000	1500
Unc. Pos. at 10 V (μm)	93.52	97.14	96.76	97.22	99.25
Unc. Loop Area $(\mu m \cdot V)$	205.11	174.11	185.68	178.92	139.07
Comp. Pos. at 10 V (μm)	93.53	95.85	95.61	95.68	100.10
Comp. Loop Area $(\mu m \cdot V)$	96.97	83.54	101.34	135.06	178.53
% Red. in Maj. Loop Area	52.72	52.02	45.42	24.51	-28.37

51

CHAPTER 4

Classical Preisach Hysteresis Modeling and Compensation

4.1 The Preisach Hysteresis Model
4.1.1 Comparison of Classical and Generalized Preisach Methods

This chapter concentrates on the Classical Preisach method for modeling and feed-forward compensation of hysteresis. The author recognizes two types of Preisach-based methods for the rate-independent modeling of hysteresis: Classical and Generalized Preisach modeling techniques. Both methods differ in their complexity, their assumptions concerning hysteretic system behavior and the types of input that may be used. The Classical Preisach technique however assumes that the hysteresis loops fulfill the congruency property. Figure 4.1 illustrates piezo-electric hysteresis effect with gradually decreasing voltage input maximum values. The changes in displacement output Δ_1 (for the major outer ascending curve) and Δ_2 (for the minor inner ascending curve) are compared for the a given voltage input increase from u_1 to u_2. When assuming congruent hysteresis loops, Δ_1 and Δ_2 would be equal. In practice, this is not the case for piezoelectric actuator hysteresis.

The primary objective in using the Classical Preisach method is to avoid using inputs which would cause displacement output along a minor inner ascending curve. This means that the input should be cycled in such a way that a decreasing voltage profile should always "go back down to zero" before increasing again. The Generalized Preisach model does not require this condition and can be used for any arbitrary input profile. The Classical Preisach method uses measured input/output data from the major ascending loop and a set of first order descending curves. The Generalized Preisach method uses this data, and also measured data from second order curves ascending curves attached to the first order descending curves.
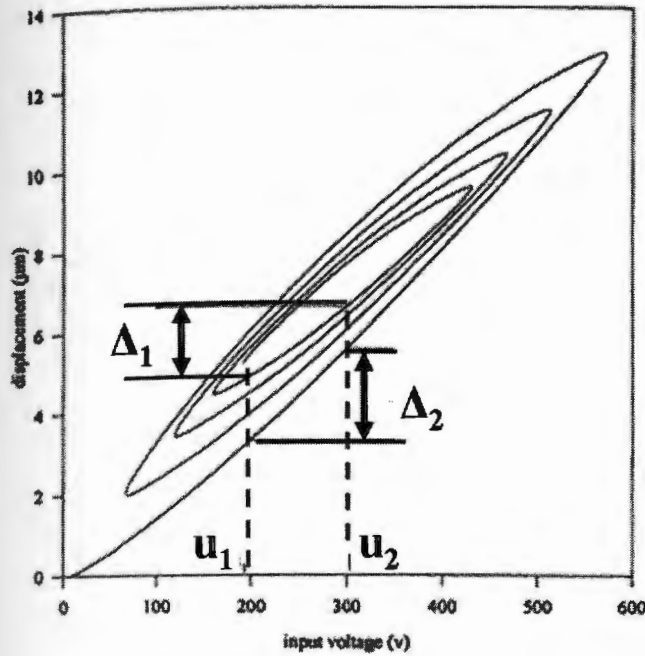
Figure 4.1. Hysteresis Curves Illustrating Congruency Property (graphic modified from [1])

Figure 4.2 illustrates the concepts of major and minor loops as well as first order descending curves and second order ascending curves.

4.1.2 Classical Preisach Model General Form for Piezoelectric Actuators

The Preisach model has the following form for the voltage-displacement characteristics of piezoelectric actuators:

$$x(t) = \iint_{\alpha \geq \beta} \mu(\alpha, \beta) \gamma_{\alpha\beta} \left[u(t) \right] d\alpha d\beta \tag{4.1}$$

The term $x(t)$ describes the output response of the piezoelectric actuator; α and β correspond accordingly to *up* and *down* voltage input threshold switching value parameters; $\mu(\alpha, \beta)$ is a weighting function for a given α and β; $\gamma_{\alpha\beta}\left[u(t)\right]$ represents a hysteresis operator whose value is dependent on input $u(t)$.
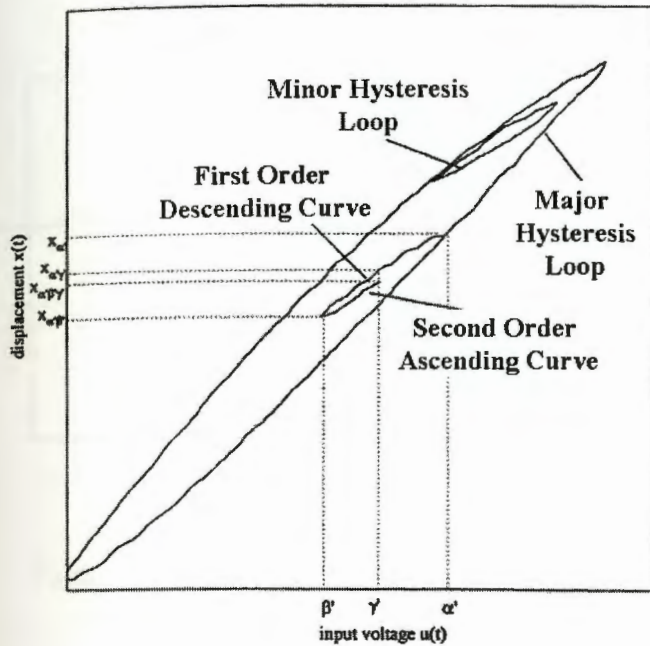
Figure 4.2. Hysteresis Curves Illustrating Various Loop Properties (graphic modified from [2])

The block diagram equivalent of the Preisach model can be interpreted as a voltage signal inputted into a set of parallel connected two-position relays (representing $\gamma_{\alpha\beta}[u(t)]$) in series with gain factors (representing $\mu(\alpha, \beta)$). The output of these gain factors are recombined into a summer, whose output represents the piezoelectric actuator position output $x(t)$. A relay is activated (*up position*) when the input voltage is greater than or equal to its given α voltage parameter. The relay is then deactivated (*down position*) when the input voltage is less than or equal to its given β voltage parameter. A block diagram of this concept is depicted in Figure 4.3.

Since piezoelectric materials are polarized, only an input voltage in the direction of polarization will cause an expansion of the material. This property effectively limits the input voltage to the 0 to U_{max} range and the output to the 0 to x_{max} range. When applying this characteristic to the Preisach block diagram,

54
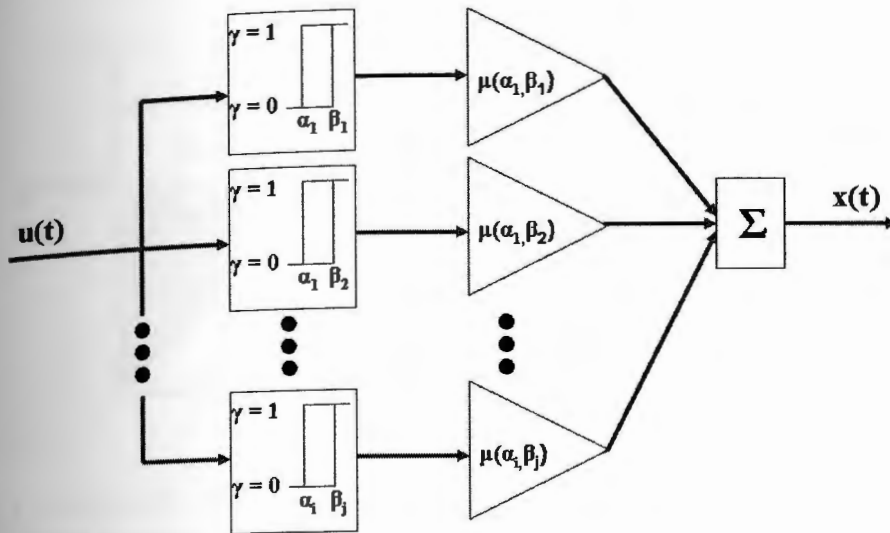
Figure 4.3. Preisach Model as Block Diagram

the relay's state can be mathematically interpreted as having a gain factor of 1 in the up position and a gain factor of 0 in the down position.

The state of each relay may also be described by a so-called Preisach triangle (see Figure 4.4). This is an α/β plot with triangle T_0 representing all relays. When the voltage is increased from 0 to $u(t) = \alpha'$ (Figure 4.4, left), the shaded region S^+ represents the relays which are activated and the area S^- represents the relays which remain deactivated. The region T_1 (Figure 4.4, right) represents the relays which are deactivated by switching the input voltage direction from α' down to β'.

Using this understanding of Preisach modeling, the output $x(t)$ is dependent on the sum of the gain factors found in region S^+. Going back to Equation 4.1, the integral can be rearranged to cover the output over S^+. In other words, the summation only covers those weighting factors where the output of the $\gamma_{\alpha\beta}[u(t)]$ relays equal one. The other weighting factors are ignored, since they are then multiplied by zero. Equation 4.1 can then be rewritten into Equation 4.2.

55
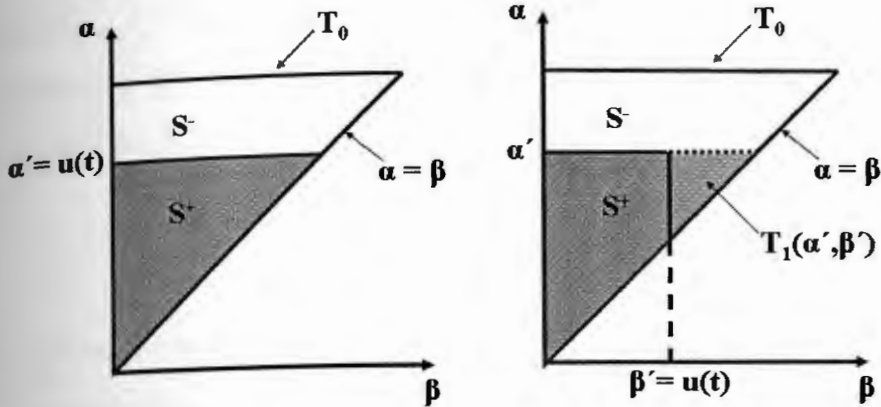
Figure 4.4. Preisach Triangle for Voltage Input Increase from 0 to α' (left) and Voltage Input Decrease from α' to β'

$$x(t) = \iint_{S^+(t)} \mu(\alpha, \beta) d\alpha d\beta \tag{4.2}$$

4.1.3 Weighting Function Determination and the Classical Preisach Model

The next step in applying this model is the identification of weighting functions $\mu(\alpha, \beta)$ for given values of α and β. When applying the Classical Preisach modeling technique, these weighting functions are dependent on position data from the major increasing hysteresis loop for increasing voltage input and from a set first order reversal curves attached to the major hysteresis loop for decreasing voltage input. An example of an input profile for obtaining the major ascending loop and the set of first order reversal curves is found in Figure 2.3. Since the Classical Preisach model assumes that the input voltage is always cycled between zero and a given voltage maximum, the weighting function for increasing voltage is determined from the major ascending loop displacement where $\beta = 0$, i.e. $\mu(\alpha = u(t), 0)$. On the other hand, the weighting function for decreasing voltage is attained from a first order reversal curve starting at $u(t) = U_{LocalMax}$ back down to $u(t) = 0$, i.e.

$\mu(\alpha = U_{LocalMax}, \beta = u(t))$. The function $X(\alpha', \beta')$ is derived in Equation 4.3 in order to determine the proper weighting function from experimental data. This function is valid for a given α' and β' and when the input voltage is decreasing.

$$X(\alpha', \beta') = x_{\alpha'} - x_{\alpha'\beta'} \tag{4.3}$$

$X(\alpha', \beta')$ represents the change in position as the input $u(t)$ decreases from α' to β'. $x_{\alpha'}$ is the position output at the top of the first order reversal curve branch (maximum position output for given reversal curve), and $x_{\alpha'\beta'}$ is the output at voltage β' along the same reversal curve. This process is essentially equivalent to what one sees in Figure 4.4. Here (left side), voltage $u(t)$ first increased to α', which leads to an output $x_{\alpha'}$. The voltage input subsequently decreases (right side) to $u(t) = \beta'$, giving a positional output of $x_{\alpha'\beta'}$. The function $X(\alpha', \beta')$ is therefore equivalent to the total output which was *turned off* by decreasing voltage from α' to β', or the sum of weighting function outputs found in $T_1(\alpha', \beta')$. Using this fact, $X(\alpha', \beta')$ may be redefined using Equation 4.2 as:

$$X(\alpha', \beta') = \iint_{T_1(\alpha', \beta')} \mu(\alpha, \beta) d\alpha d\beta \tag{4.4}$$

The weighting function for a given α' and β' **within** S^+ (therefore reciprocal of above) could then be determined through double partial differentiation:

$$\mu(\alpha', \beta') = -\frac{\partial^2 X(\alpha', \beta')}{\partial \alpha' \partial \beta'} \tag{4.5}$$

This calculation, however, is unnecessary. Instead, the actual output of $X(\alpha', \beta')$ may be used directly for determining the position output $x(t)$ for descending voltage input. Equation 4.2 may be modified to account for discrete voltage direction changes for software implementation [2]. For increasing voltage input $u(t)$, the output of the modified Preisach model has the general form:

57

$$x(t) = \sum_{k=1}^{N} \left[X(\alpha'_k, \beta'_{k-1}) - X(\alpha'_k, \beta'_k) \right] + X(u(t), \beta'_N) \tag{4.6}$$

And for decreasing voltage input $u(t)$, the output of the Preisach model has the general form:

$$x(t) = \sum_{k=1}^{N-1} \left[X(\alpha'_k, \beta'_{k-1}) - X(\alpha'_k, \beta'_k) \right] + \left[X(\alpha'_N, \beta'_{N-1}) - X(\alpha'_N, u(t)) \right] \tag{4.7}$$

For a given number of voltage change directions k, $X(\alpha'_k, \beta'_{k-1})$ represents the position change for a voltage increase from β_{k-1} to α_k, $X(\alpha'_k, \beta'_k)$ represents the position change from α'_k down to β'_k, $X(u(t), \beta'_N)$ is the position output change for the current $u(t)$ after increasing voltage from β'_N and $X(\alpha'_N, u(t))$ represents the position output change for the current $u(t)$ after decreasing from β'_N.

4.1.4 Preisach Data Point Mesh and Interpolation

The practical implementation of the Preisach Model comprises a discrete mesh (in the form of a lookup table) of α and β values with corresponding $X(\alpha', \beta')$. A plot of this mesh on the Preisach Triangle can be found in Figure 4.5 for discrete α values of $\delta = 1V$, and discrete β values for each α of $\delta = 1V$.

A given $u(t)$ usually will not be found in the defined α/β mesh. For example, the given voltage input may be represented by α_1, β_1 or α_2, β_2. In these cases, an interpolation is necessary to determine the given output from the neighboring mesh points. As seen in Figure 4.6, the mesh points are denoted as $\alpha_0, \beta_0, \alpha_1, \beta_1$, α_2, β_2 and α_3, β_3 for a square and $\alpha_0, \beta_0, \alpha_2, \beta_2$ and α_3, β_3 for a triangle.

The output $X(\alpha', \beta')$ when located within a rectangular-shaped mesh can be calculated by:

Preisach Triangle of α / β Meshpoints for dα=1 V and dβ=1 V
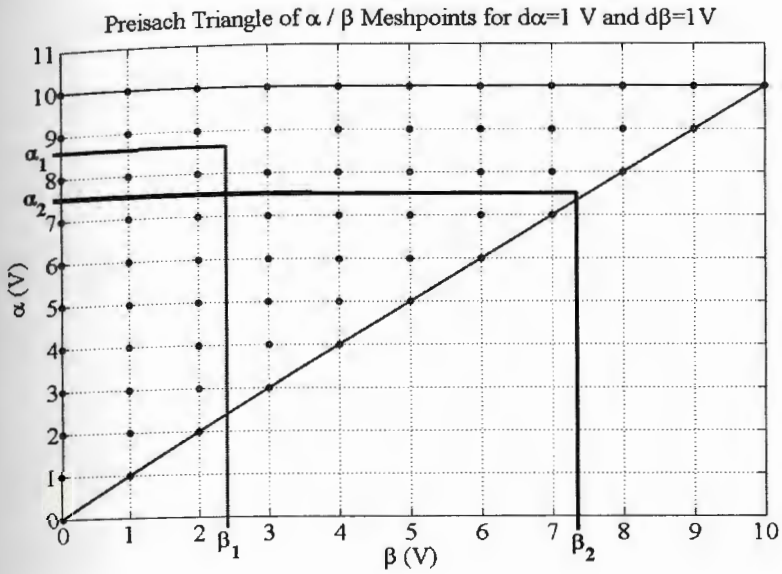
Figure 4.5. Discretization of the Preisach Triangle
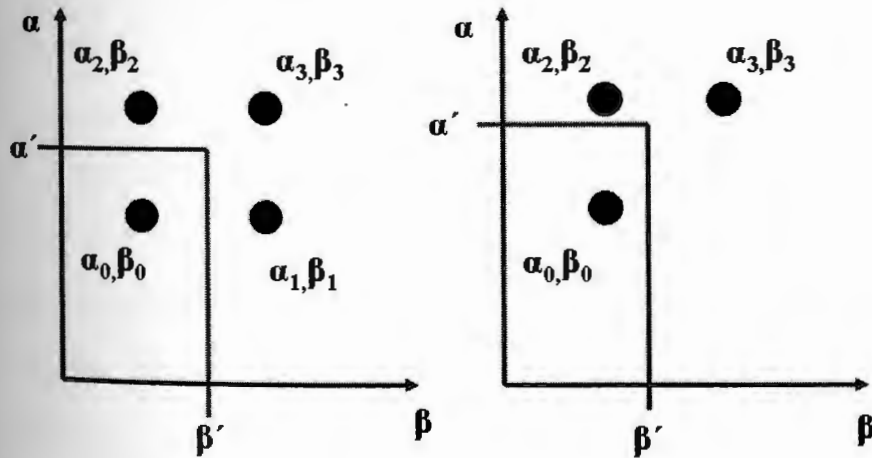
Figure 4.6. Interpolated Output for Location Within Square or Triangle Mesh Points

$$X(low) = \frac{\beta_1 - \beta'}{\beta_1 - \beta_0} \cdot X(\alpha_0, \beta_0) + \frac{\beta' - \beta_0}{\beta_1 - \beta_0} \cdot X(\alpha_1, \beta_1)$$

$$X(hi) = \frac{\beta_3 - \beta'}{\beta_3 - \beta_2} \cdot X(\alpha_2, \beta_2) + \frac{\beta' - \beta_2}{\beta_3 - \beta_2} \cdot X(\alpha_3, \beta_3)$$

$$X(\alpha', \beta') = \frac{\alpha_3 - \alpha'}{\alpha_3 - \alpha_0} \cdot X(low) + \frac{\alpha' - \alpha_0}{\alpha_3 - \alpha_0} \cdot X(hi) \tag{4.8}$$

The output $X(\alpha', \beta')$ when located within a triangular-shaped mesh can be calculated by:

$$X(left) = X(\alpha_0, \beta_0) - \frac{(X(\alpha_0, \beta_0) - X(\alpha_2, \beta_2)) \cdot (\alpha_0 - \alpha')}{\alpha_0 - \alpha_2}$$

$$X(right) = X(\alpha_0, \beta_0) - \frac{(X(\alpha_0, \beta_0) - X(\alpha_3, \beta_3)) \cdot (\alpha_0 - \alpha')}{\alpha_0 - \alpha_3}$$

$$\beta(left) = \frac{(\alpha' - \alpha_0) \cdot (\beta_2 - \beta_0)}{\alpha_2 - \alpha_0} + \beta_0$$

$$\beta(right) = \frac{(\alpha' - \alpha_0) \cdot (\beta_3 - \beta_0)}{\alpha_3 - \alpha_0} + \beta_0$$

$$X(\alpha', \beta') = X(right) - \frac{(X(right) - X(left)) \cdot (\beta(right) - \beta')}{\beta(right) - \beta(left)} \tag{4.9}$$

4.2 Classical Preisach Model of Hysteresis for the Active Clamping Systems

Two separate meshes have been used for the modeling of rate-independent hysteresis in the 0 to 10 volt range. The first mesh assumes α values ranging from 0 to 10 volts in 1 volt increments ($d\alpha = 1$). The β values then range from each α to 0 volts in 1 volt decrements ($d\beta = 1$). The second mesh is similar to the first except that the β values range from each α to 0 volts in 0.1 volt decrements ($d\beta = 0.1$).

Figure 4.7 shows the Preisach triangle for input voltages of 0 to 10 V with $d\alpha = 1$ and $d\beta = 1$ and each point representing a discrete α/β pair. The corresponding displacement points for each α/β location for actuator B with 10 V/s input voltage rate is shown in Figure 4.8.

60

Preisach Triangle of α and β Switching Voltages for dα=1 V and dβ=1 V
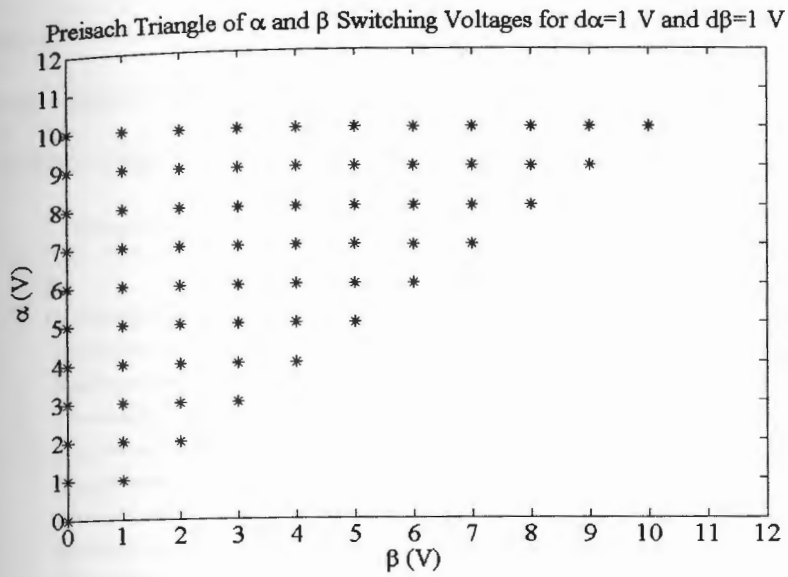
Figure 4.7. Preisach Triangle for $d\alpha = 1V$ and $d\beta = 1V$

Output Position for Given α and β Switching Values
dα = 1 V dβ=0.1 V
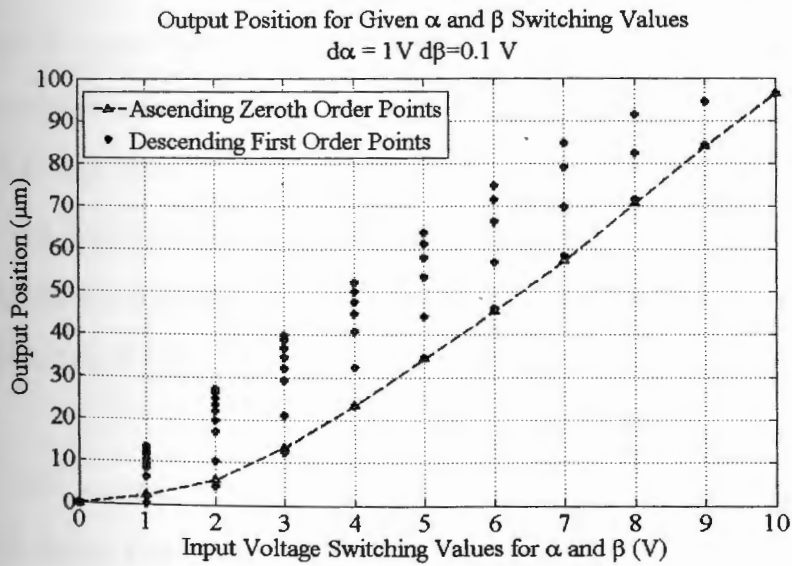
Figure 4.8. Assembly B 10 V/s Preisach Output Points for $d\alpha = 1 \ V$ and $d\beta = 1 \ V$

Figure 4.9 shows the Preisach triangle for input voltages of 0 to 10 V with $d\alpha = 1$ and $d\beta = 0.1$ and each point representing a discrete α/β pair. The corresponding displacement points for each α/β location for actuator B with 10 V/s input voltage rate is shown in Figure 4.10.
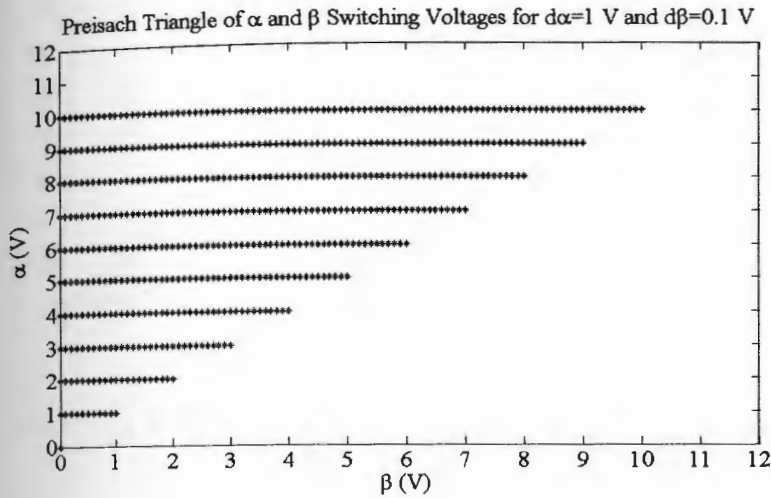
Figure 4.9. Preisach Triangle for $d\alpha = 1\ V$ and $d\beta = 0.1\ V$

In order to prove the viability of these models, it is helpful to compare their simulated properties to the original modeled experimental data. Figure 4.11 shows for $d\alpha = 1\ V$ and $d\beta = 1\ V$ an input voltage / output position plot to compare simulated and experimental hysteresis loops. The root mean square for the error between simulation and experiment has also been calculated using the cost function found in Equation 3.6 found in Chapter 3. The result of this calculation is 1.0827 RMS.

The same analysis has been undertaken for $d\alpha = 1\ V$ and $d\beta = 0.1\ V$. Figure 4.12 shows this same data on a input voltage / output position plot to compare simulated and experimental hysteresis loops. The RMS error between the experimental data and the simulation is 1.0162 RMS.

For consistency, assembly A has also been modeled with $d\alpha = 1\ V$ and

62
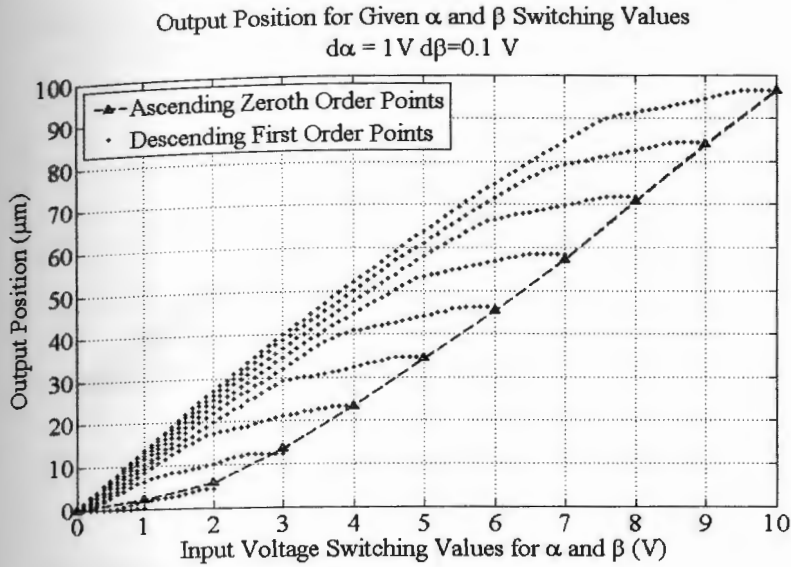
Figure 4.10. Assembly B 10 V/s Preisach Output Points for $d\alpha = 1\ V$ and $d\beta = 0.1\ V$
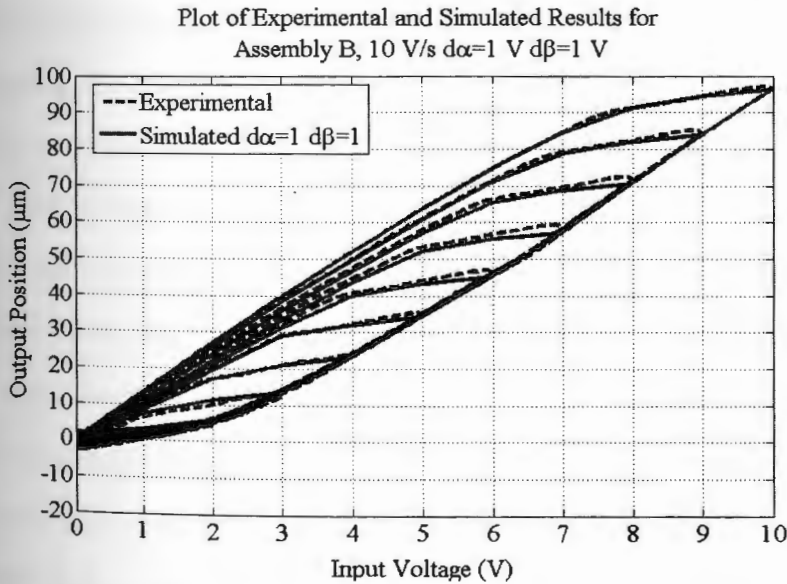
Figure 4.11. Hysteresis Loop Output for Assembly B 10V/s Experimental and Simulated Data with $d\alpha = 1V$ and $d\beta = 1V$

Plot of Experimental and Simulated Results
for Assembly B, 10 V/s dα=1 V dβ=0.1 V
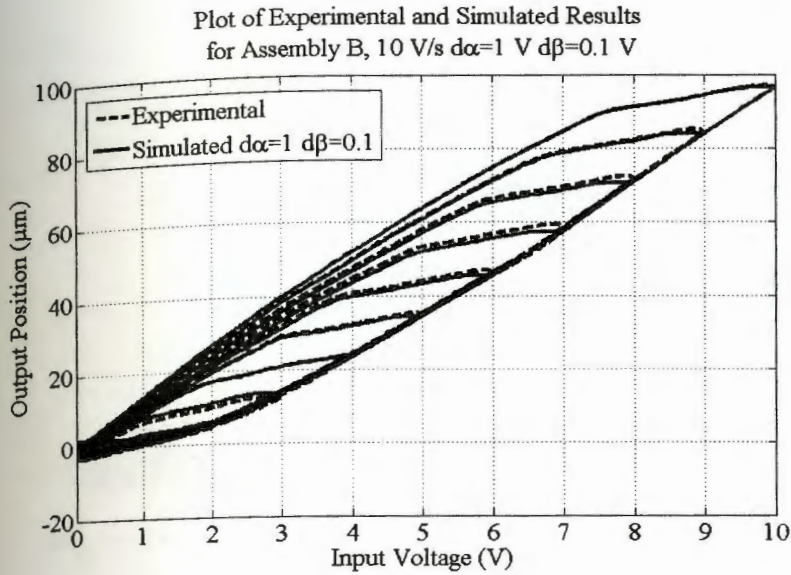
Figure 4.12. Hysteresis Loop Output for Assembly B 10V/s Experimental and Simulated Data with $d\alpha = 1\ V$ and $d\beta = 0.1\ V$

$d\beta = 0.1\ V$. Figure 4.13 shows an input voltage / output position plot to compare simulated and experimental hysteresis loops. The RMS error between the experimental data and the simulation is $3.2762\ RMS$.

Comparing the modeling results for assemblies A and B, it appears that the model for B conforms better with its experimental output. The Preisach modeling procedure used in this thesis is defined so that the output position at zero volts on the zeroth order ascending curve is the defined minimum position output, even for the first order descending curves. The assembly A's experimental output, as shown in Figure 4.13, tends to shift downward more dramatically for each consecutive decreasing amplitude triangular voltage input. However, the model keeps a floor at the zeroth order output at 0 volts. Any experimental first order descending output which falls below the zero mark is automatically recorded as zero output on the Preisach model. This also explains the relatively large RMS value when compared to the Bouc-Wen model RMS values in Chapter 3. The Bouc-Wen

Plot of Experimental and Simulated Results for
Assembly A, 10 V/s dα=1 V dβ=0.1 V
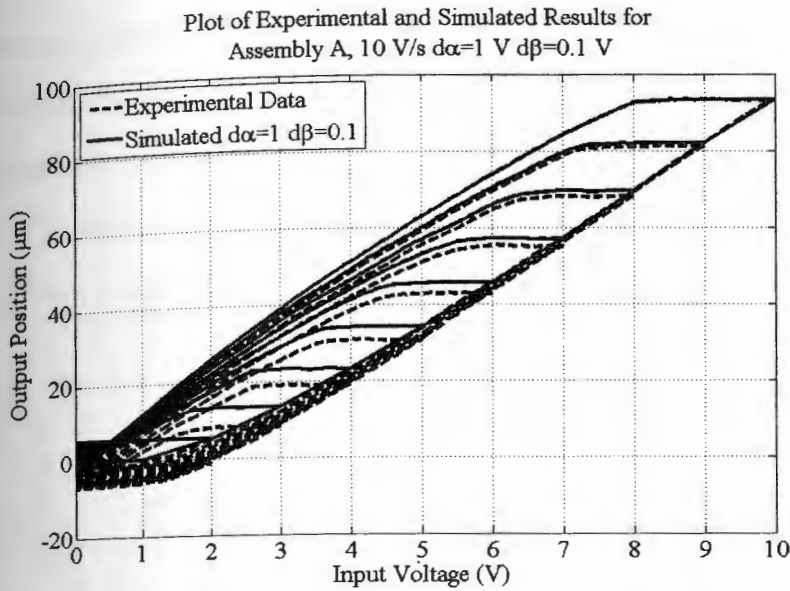
Figure 4.13. Hysteresis Loop Output for Assembly A 10V/s Experimental and Simulated Data with $d\alpha = 1\ V$ and $d\beta = 0.1\ V$

technique focused on modeling the outer loop hysteresis, and the error was based on this result. On the other hand, the Preisach model is based on not only the outer loop, but a set of first order descending curves off of the ascending branch. This larger amount of data left more room for "error". However, by looking at both input/output plots, it appears that the Preisach model is sufficient in modeling these hysteresis loops.

4.3 Classical Preisach Model of Hysteresis for Sinusoidal Input Signals with Offset

The X-Filtered LMS algorithm used for workpiece noise and vibration control typically sends a sinusoidal controlling signal with an amplitude of roughly 1 to 3 volts a frequency of 300 Hz and a voltage *offset* from 0 V D/A output of positive 5 or 6 volts. For example, an input sinusoid with an offset of 6V and an amplitude of 2 V has an input range of 4 to 8 V. As stated earlier in this chapter, the Classical Preisach model requires that the descending loop input voltage to return to zero

before increasing again. Since the above stated example always "returns" to 4 volts instead of 0 volts, the author proposes the concept of an offset Classical Preisach model of hysteresis, where the modeled major hysteresis loop ranges in the 4 to 8 volt range. The input voltage profile for this model can be found in Figure 4.14.

Input Voltage Profile for Descending Offset Hysteresis from 4 and 8 V at 10 V/s
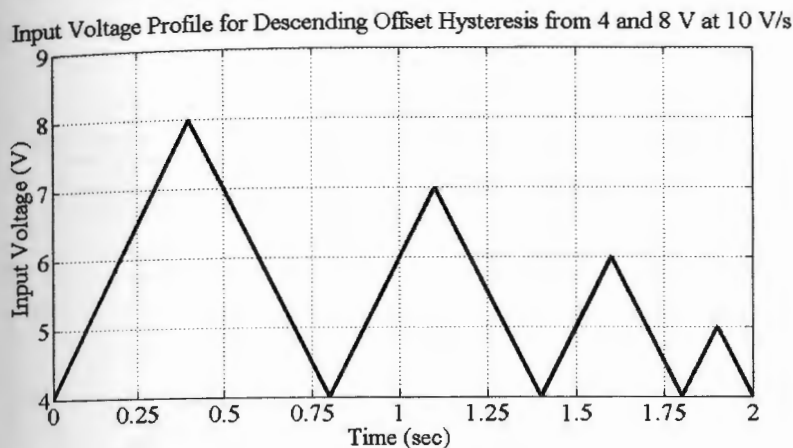
Figure 4.14. Input Voltage Profile for Descending Offset Hysteresis from 4 to 8 V at 10 V/s

This input profile was used to determine the rate independent hysteretic system output in the 4 to 8 volt range. The Classical Preisach model for assembly A was identified in this range with $d\alpha = 1\ V$ and $d\dot{\beta} = 0.1\ V$. The system output and corresponding model output can be found in the input voltage and output position plot is shown in Figure 4.15. The RMS error between the experimental data and the simulation is 0.5380 RMS.

At first look, there appears to be a high level of oscillation in both plots in Figure 4.15. This oscillation is present due to noise measurements from the laser triangulation sensor. Furthermore, the displacement axis scale is less than a quarter of that from previous plots. So any signal noise present appears to be much larger in this figure than when the scale ranges from 0 to 100 μm or 0 to 120 μm. Nevertheless, the low RMS error between the experimental measurement

and the simulation seem to prove that Offset Classical Preisach model is viable for modeling hysteresis between a lower bound and an upper bound. This model will prove useful when developing a feed-forward control algorithm to prevent system hysteresis for sinusoid control signal loops which do not cycle between zero and some maximum value.
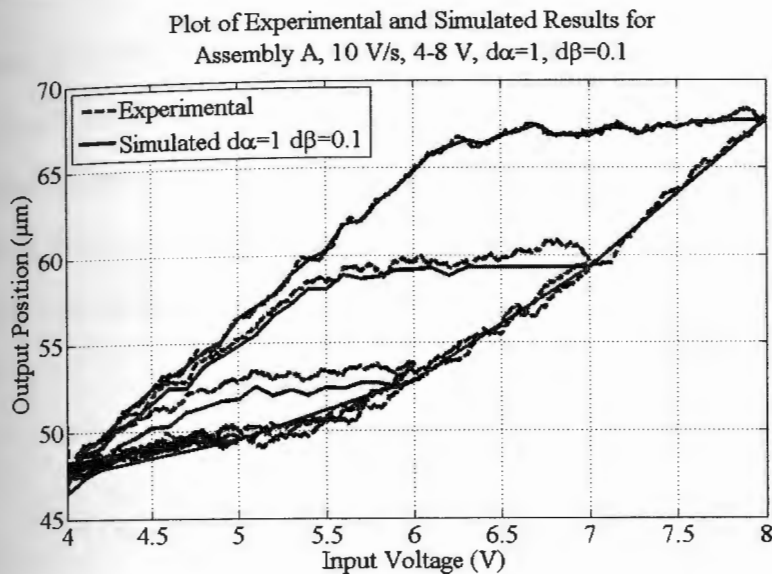
Figure 4.15. Input Voltage to Output Position Plot of Experimental and Classical Preisach Offset Hysteresis Model for Assembly A for 4 to 8 V at 10 V/s with $d\alpha = 1 \ V$ and $d\beta = 0.1 \ V$

4.4 Hysteresis Compensation Methods Using Preisach Model
4.4.1 Parallel Hysteresis Compensation Method

The parallel Preisach hysteresis compensation model has a very similar structure to the Bouc-Wen hysteresis compensation setup. The Preisach hysteresis function, used to determine system response for a given input voltage, is used as a system observer for calculating total system output. A Preisach system model is used which gives essentially rate-independent output (no rate dependency from linear system) for very low voltage rate inputs (i.e. 10 V/s). The output of this model is then used to determine the pure hysteresis output $\hat{h}_{Preisach}$ from the ref-

erence position input and the output of the Preisach block. The $\hat{h}_{Preisach}$ term is equivalent to the h function from Bouc-Wen. In a similar sense to Equation 3.7 in Chapter 3, this $\hat{h}_{Preisach}$ term can be calculated through the following equation:

$$\hat{h}(u) = d \cdot u_{ref} - \hat{x}_{Preisach} \tag{4.10}$$

The term d is calculated by determining the change in displacement over the minimum to maximum input voltage range, and dividing this value by the length of this voltage range.

The block diagram implementation of Preisach parallel feed-forward hysteresis compensation can be found in Figure 4.16.
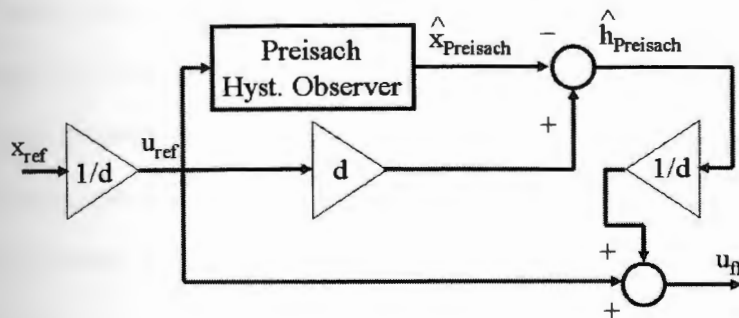
Figure 4.16. Feed-Forward Preisach Parallel Hysteresis Observer Compensation Block Diagram

4.4.2 Series Hysteresis Compensation Method

One can also compensate for hysteresis by implementing a Preisach inverse hysteresis model. This model is the same as the Classical Preisach model derived in Chapter 4, except that it runs in reverse - it accepts a desired position input, and using the Classical Preisach model, calculates the corresponding input voltage. This concept is illustrated in the block diagram in Figure 4.17.

68
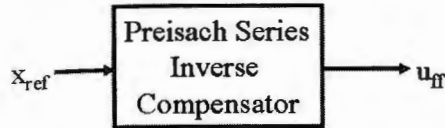
Figure 4.17. Feed-Forward Preisach Series Inverse Hysteresis Compensation Block Diagram

4.5 Hysteresis Compensation Simulation Using Preisach Model

As with the simulations of feed-forward control using Bouc-Wen, the following simulations are based on sending a model based feed-forward signal into a hysteretic model of the system. Both the feed-forward controller and the system model are based on the same Preisach model. The resulting simulation output represents an idealized case which does not necessarily directly reflect the actual hysteresis reduction when the feed-forward algorithm is implemented experimentally. But the output from these simulations is useful for understanding the reference to feed-forward input voltage relationship as well as for comparing the system output with parameters based on the actuator with those from the assembly.

4.5.1 Simulated Parallel Hysteresis Compensation in 0 to 10 V Range

The Classical Preisach model for assembly A taken at 10 V/s with a discrete grid of α of 1 V and β of 0.1 V has been used for the simulation of parallel hysteresis compensation in this system. Applying the block diagram scheme shown in Figure 4.16, a feed-forward compensating input voltage is generated, which is shown in the time to voltage plot in Figure 4.18. The corresponding reference input voltage and position output are shown in Figure 4.19. Unlike with Bouc-Wen based feed-forward hysteresis control, parallel Preisach based feed-forward hysteresis control does not appear to have any issues with saturation. Instead, the control signal appears to remain within the 0 to 10 volt range. Comparing the successive peak voltages of the reference (u_{ref}) to the feed-forward voltages (u_{ff}), the ascending

side of the peak of u_{ff} appears to be higher amplitude than that of u_{ref}, while the descending side of the feed-forward voltage is lower than the reference. The control signal tries to drive the system up to the linear on the ascending path and immediately downward to overcome static friction when the voltage direction changes. The major loop area for the uncompensated system is 205.11 $\mu m \cdot V$, while the displacement for 10 V input is 93.52 μm. On the other hand, the major loop area for the compensated system is 46.80 $\mu m \cdot V$, while the displacement for 10 V input is 93.03 μm. The reduction in outer loop hysteresis area is 77.18%.
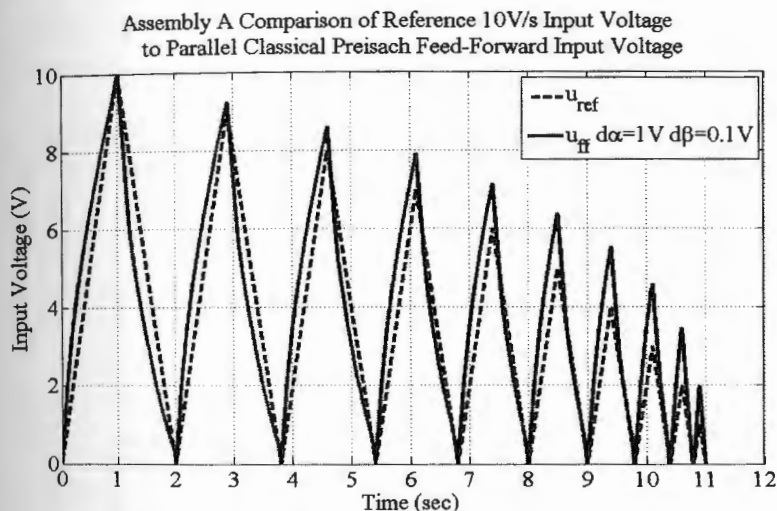
Figure 4.18. Assembly A 10 V/s Reference Input Voltage and Simulated Parallel Preisach Hysteresis Compensated Voltage for $d\alpha = 1\ V$ and $d\beta = 0.1\ V$

The same simulation was conducted with assembly B. The time to voltage plot is shown in Figure 4.20. The corresponding reference input voltage and position output are shown in Figure 4.21. The major loop area for the uncompensated system is 181.23 $\mu m \cdot V$, while the displacement for 10 V input is 100.90 μm. The major loop area for the compensated system is 38.10 $\mu m \cdot V$, and the displacement for 10 V input is 96.50 μm. The hysteresis compensation could reduce the outer loop area by 78.98%.
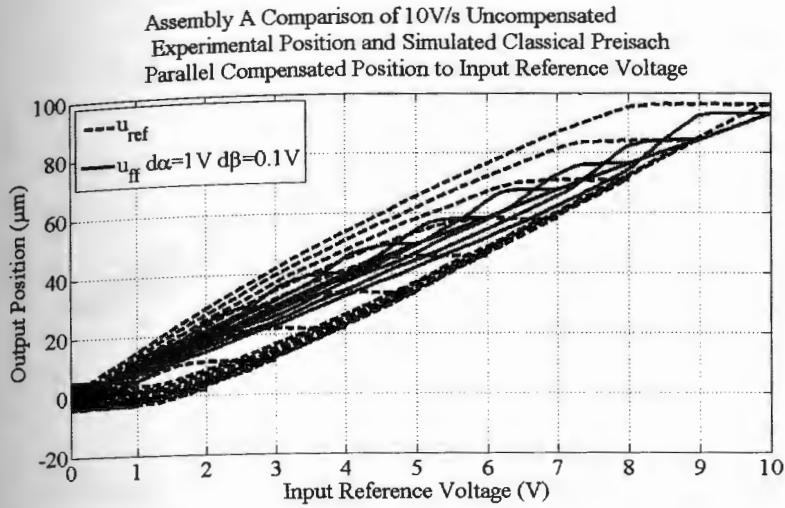
Figure 4.19. Assembly A 10 V/s Reference Voltage Input to Position Output Comparison for Simulated Parallel Preisach Hysteresis Compensated Voltage with $d\alpha = 1\ V$ and $d\beta = 0.1\ V$

Figure 4.20. Assembly B 10 V/s Reference Input Voltage and Parallel Preisach Hysteresis Compensated Voltage for $d\alpha = 1\ V$ and $d\beta = 0.1\ V$

Assembly B Comparison of 10V/s Uncompensated Experimental Position and
Parallel Classical Preisach Compensated Position to Input Reference Voltage

Figure 4.21. Assembly B 10 V/s Reference Voltage Input to Position Output Comparison for Parallel Preisach Hysteresis Compensated Voltage with $d\alpha = 1\ V$ and $d\beta = 0.1\ V$

The simulation of the Preisach parallel hysteresis compensation scheme appears to be suitable for compensating for hysteresis. In both cases, the hysteresis area could be reduced by at least 75%. There is also no significant change in displacement amplitude. The peak input voltage from each triangular-shaped input profile is higher with the feed-forward input than the reference input. The result from the input/output plot is not perfectly linear, rather it curves around the linear.

4.5.2 Simulated Series Inverse Hysteresis Compensation in 0 to 10 V Range

The Classical Preisach model for Assembly A taken at 10 V/s with a discrete grid of α of 1 V and β of 0.1 V has been also used to simulate of series inverse hysteresis compensation in Assembly A. Using the block diagram scheme shown in Figure 4.17, a feed-forward compensating input voltage is generated, which is shown in the time to voltage plot in Figure 4.22. The corresponding reference input voltage and position output are shown in Figure 4.23. Unlike with Bouc-Wen

based feed-forward hysteresis control, series inverse Preisach based feed-forward hysteresis control does not appear to have any issues with saturation. Instead, the control signal appears to remain within the 0 to 10 volt range. Comparing the successive peak voltages of the reference (u_{ref}) to the feed-forward voltages (u_{ff}), the ascending side of the peak of u_{ff} appears to be higher amplitude than that of u_{ref}, while the descending side of the feed-forward voltage is lower than the reference. The control signal tries to drive the system up to the linear on the ascending path and immediately downward to overcome static friction when the voltage direction changes. The major loop area for the uncompensated system is $205.11\mu m \cdot V$, while the displacement for 10 V input is 93.52 μm. On the other hand, the major loop area for the compensated system is 0.93 $\mu m \cdot V$, while the displacement for 10 V input is 93.03 μm. The outer loop hysteresis area reduction is 99.55%.

Assembly A Comparison of Reference 10V/s Input Voltage to
Simulation Classical Preisach Series Inverse Feed-Forward Input Voltage
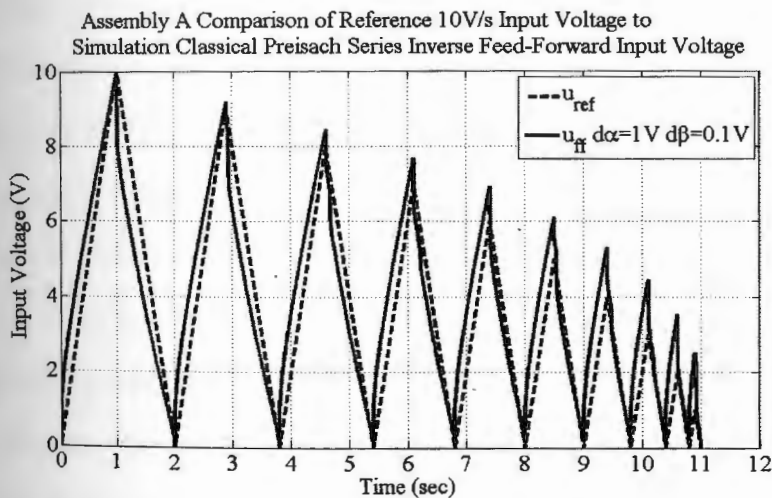
Figure 4.22. Assembly A 10 V/s Reference Input Voltage and Preisach Series Inverse Hysteresis Compensated Voltage for $d\alpha = 1\ V$ and $d\beta = 0.1\ V$

The same simulation was conducted with assembly B. The time to voltage plot is shown in Figure 4.24. The corresponding reference input voltage and position output are shown in Figure 4.25. The major loop area for the uncompensated

Assembly A Comparison of 10V/s Uncompensated Experimental
Position and Series Classical Preisach
Compensated Position to Input Reference Voltage

Figure 4.23. Assembly A 10 V/s Reference Voltage Input to Position Output Comparison for Preisach Series Inverse Hysteresis Compensated Voltage with $d\alpha = 1\ V$ and $d\beta = 0.1\ V$

system is $181.23\mu m \cdot V$, while the displacement for 10 V input is $100.90\mu m$. On the other hand, the major loop area for the compensated system is $0.96\mu m \cdot V$, while the displacement for 10 V input is $96.50\mu m$. The reduction in outer loop hysteresis area is 99.47%.

The simulated result for inverse hysteresis control appears to generally decrease the size of the hysteresis region in the input voltage to output position plot (Figure 4.25). This is especially the case for the major loop along the zero to ten and back down to zero voltage input. According to the major loop area of the controlled system, the output has been essentially linearized. The displacement for 10 V input is also essentially the same. There appears to be a discrepancy from the linear for the following descending triangular inputs. The author believes that this behavior is a numerical issue in the simulation between the generated input voltage and the modeled plant. This behavior originates from higher feed-forward voltages on the ascending branch of the input profile followed by an immediate drop in feed-forward voltage when the profile decreases, leading the plant model's
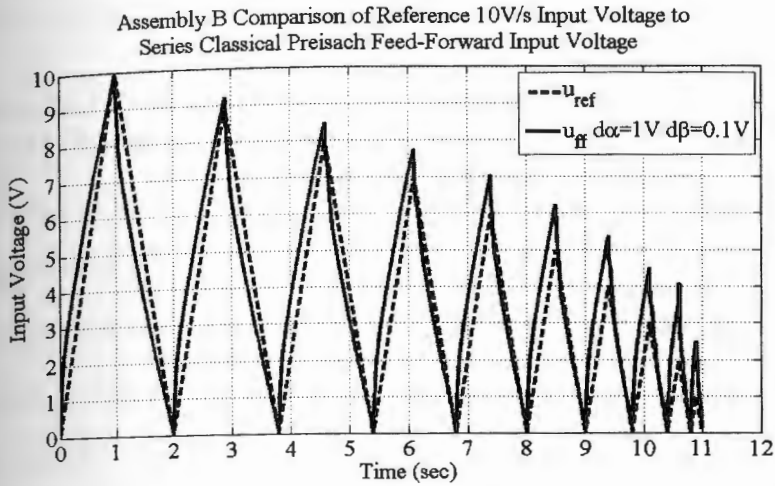
Figure 4.24. Assembly B 10 V/s Reference Input Voltage and Series Preisach Inverse Hysteresis Compensated Voltage for $d\alpha = 1\ V$ and $d\beta = 0.1\ V$

Figure 4.25. Assembly B 10 V/s Reference Voltage Input to Position Output Comparison for Series Preisach Inverse Hysteresis Compensated Voltage with $d\alpha = 1\ V$ and $d\beta = 0.1\ V$

output to deviate from a linear response. The author believes that this behavior will not occur during experimental testing.

4.5.3 Simulated Series Inverse Preisach Hysteresis Compensation in 4 to 8 V Range

The Classical Preisach model for assembly A taken at 10 V/s with an offset voltage range of 4 to 8 V, and a discrete grid of α of 1 V and β of 0.1 V has been also used to simulate of series inverse hysteresis compensation in assembly A. The time to voltage plot is depicted in Figure 4.26. The corresponding reference input voltage and position output are shown in Figure 4.27. Comparing the successive peak voltages of the reference (u_{ref}) to the feed-forward voltages (u_{ff}), the ascending side of the peak of u_{ff} appears to be higher amplitude than that of u_{ref}, while the descending side of the feed-forward voltage is lower than the reference. The control signal tries to drive the system up to the linear on the ascending path and immediately downward to overcome static friction when the voltage direction changes. The major loop area for the uncompensated system is $28.20\mu m \cdot V$, while the change in displacement for 4 to 8 V input is $20.08\mu m$. On the other hand, the major loop area for the compensated system is exactly $0\mu m \cdot V$, but the change in displacement for 4 to 8 V input is $20.04\mu m$.

Just as with the normal (0-10 V) Classical Preisach inverse compensation method, the compensation of the offset hysteresis model appears to be also effective, particularly along the major hysteresis loop. Just as with the 0 to 10 V loop data, the input to output plot likewise suggests a numerical issue in the simulation between the generated input voltage and the modeled plant. This behavior likewise originates from higher feed-forward voltages on the ascending branch of the input profile followed by an immediate drop in feed-forward voltage when the profile decreases, leading the plant model's output to deviate from a linear response. The
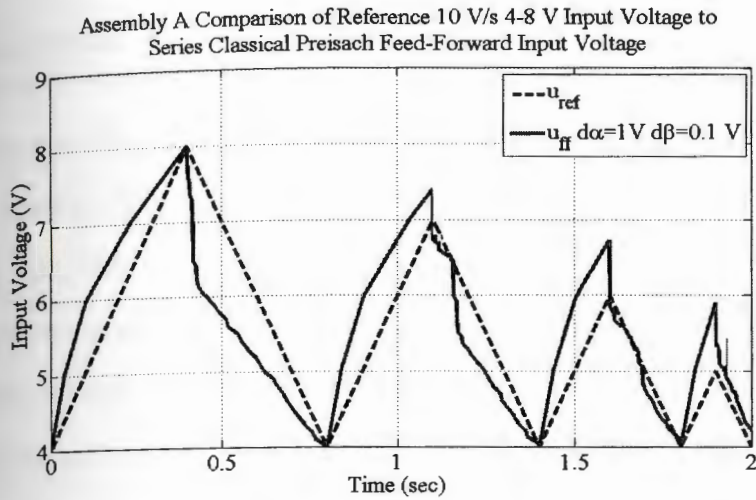
Figure 4.26. Assembly A 10 V/s Offset 4 to 8 V Reference Input Voltage and Series Preisach Inverse Hysteresis Compensated Voltage for $d\alpha = 1$ V and $d\beta = 0.1$ V
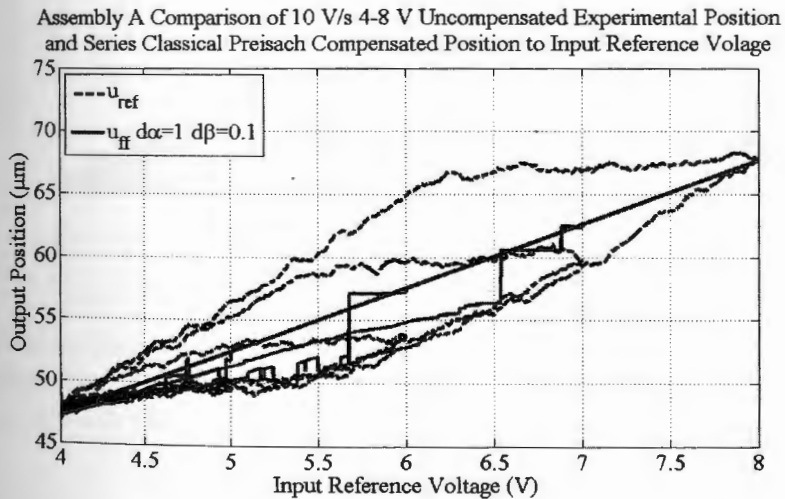
Figure 4.27. Assembly A 10 V/s Offset 4 to 8 V Reference Voltage Input to Position Output Comparison for Series Preisach Inverse Hysteresis Compensated Voltage with $d\alpha = 1$ V and $d\beta = 0.1$ V

author believes that this behavior will also not occur during experimental testing.

4.6 Experimental Parallel Hysteresis Compensation for 0 to 10 V Range for Assembly A

The Classical Preisach parallel hysteresis compensation model was tested on assembly A using profiles similar to that shown in Figure 2.3 in Chapter 2, but with slopes of 10, 100, 500, 1000 and 1500 V/s. The resulting plots of reference input voltage to output position for the uncompensated and compensated systems are shown correspondingly in Figures 4.28, 4.29, 4.30, 4.31, 4.32. A table detailing the output displacement at 10 V reference input and the area of the major hysteresis loop for both uncompensated and compensated systems are shown in Table 4.1. The average reduction in major hysteresis loop area was 66.43%.
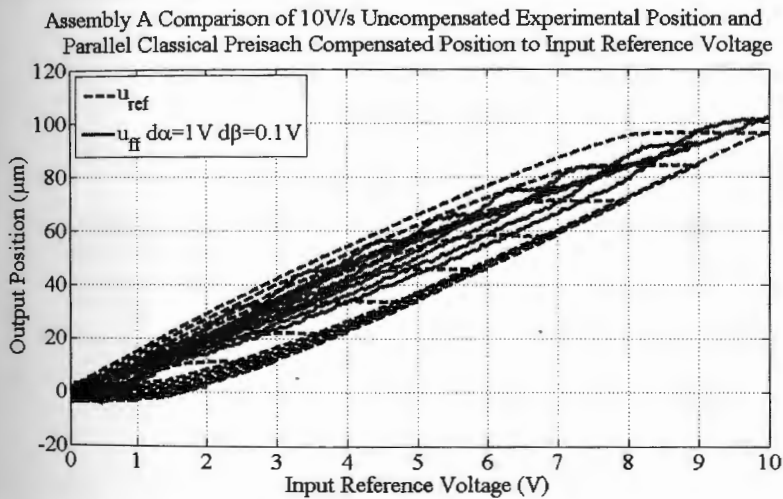
Figure 4.28. Assembly A 10 V/s Experimental Reference Voltage Input to Position Output Comparison for Parallel Preisach Hysteresis Compensated Voltage with $d\alpha = 1V$ and $d\beta = 0.1V$

There is at least a 50% reduction in major loop area for all input rates. There is also no significant change in displcaement at 10 V input. Similar to the simulated data, the hysteresis loop appears to curve around the linear and therefore the reduction in hysteresis area is good but not very significant. The decending

Assembly A Comparison of 100V/s Uncompensated Experimental Position and
Parallel Classical Preisach Compensated Position to Input Reference Voltage
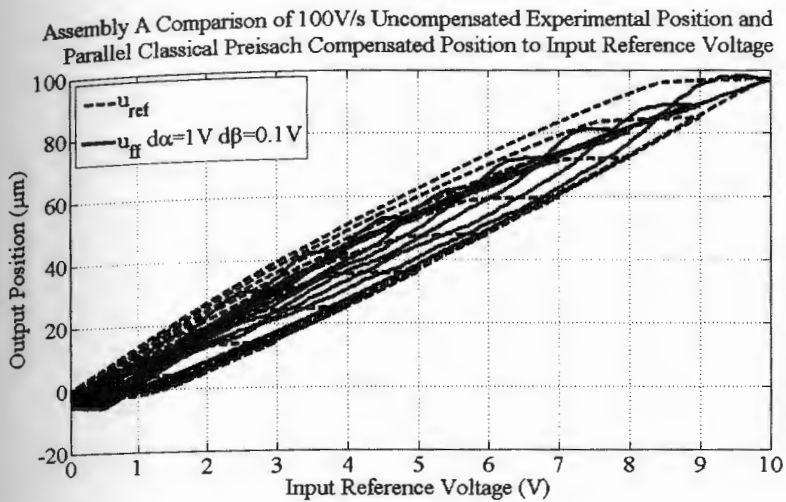
Figure 4.29. Assembly A 100 V/s Experimental Reference Voltage Input to Position Output Comparison for Parallel Preisach Hysteresis Compensated Voltage with $d\alpha = 1V$ and $d\beta = 0.1V$

Assembly A Comparison of 500V/s Uncompensated Experimental Position and
Parallel Classical Preisach Compensated Position to Input Reference Voltage

Figure 4.30. Assembly A 500 V/s Experimental Reference Voltage Input to Position Output Comparison for Parallel Preisach Hysteresis Compensated Voltage with $d\alpha = 1V$ and $d\beta = 0.1V$

Assembly A Comparison of 1000V/s Uncompensated Experimental Position and
Parallel Classical Preisach Compensated Position to Input Reference Voltage

Figure 4.31. Assembly A 1000 V/s Experimental Reference Voltage Input to Position Output Comparison for Parallel Preisach Hysteresis Compensated Voltage with $d\alpha = 1V$ and $d\beta = 0.1V$

Assembly A Comparison of 1500V/s Uncompensated Experimental Position and
Parallel Classical Preisach Compensated Position to Input Reference Voltage

Figure 4.32. Assembly A 1500 V/s Experimental Reference Voltage Input to Position Output Comparison for Parallel Preisach Hysteresis Compensated Voltage with $d\alpha = 1V$ and $d\beta = 0.1V$

Table 4.1. Assembly A Experimental Displacement at 10 V Reference Input and Major Loop Area for Uncompensated (Unc.) and Classical Preisach Parallel Compensated (Comp.) Systems

Input Rate (V/s)	10	100	500	1000	1500
Unc. Pos. at 10 V (μm)	93.52	97.14	96.76	97.22	99.25
Unc. Loop Area $(\mu m \cdot V)$	205.11	174.11	185.68	178.92	139.07
Comp. Pos. at 10 V (μm)	101.90	96.96	96.35	93.49	92.90
Comp. Loop Area $(\mu m \cdot V)$	71.17	81.50	64.39	49.75	58.79
% Red. in Maj. Loop Area	65.30	53.19	65.32	72.19	76.13

Table 4.2. Assembly A Experimental Displacement at 10 V Reference Input and Major Loop Area for Uncompensated (Unc.) and Classical Preisach Series Compensated (Comp.) Systems

Input Rate (V/s)	10	100	500	1000	1500
Unc. Pos. at 10 V (μm)	93.52	97.14	96.76	97.22	99.25
Unc. Loop Area $(\mu m \cdot V)$	205.11	174.11	185.68	178.92	139.07
Comp. Pos. at 10 V (μm)	79.75	69.44	73.99	78.51	67.50
Comp. Loop Area $(\mu m \cdot V)$	54.84	31.32	15.00	34.68	63.14
% Red. in Maj. Loop Area	73.26	82.01	91.92	80.62	54.60

hysteresis loop curving appears to be worse as the input rate increases.

4.7 Experimental Series Inverse Hysteresis Compensation for 0 to 10 V Range
4.7.1 Assembly A

In a similar manner to the previous section, the Classical Preisach series inverse hysteresis compensation model was tested on assembly A using profiles similar to that shown in Figure 2.3 in Chapter 2, but with slopes of 10, 100, 500, 1000 and 1500 V/s. The resulting plots of reference input voltage to output position for the uncompensated and compensated systems are shown correspondingly in Figures 4.33, 4.34, 4.35, 4.36, 4.37. A table detailing the output displacement at 10 V reference input and the area of the major hysteresis loop for both uncompensated and compensated systems are shown in Table 4.2. The average reduction in outer hysteresis loop area is 76.48%.

Assembly A Comparison of 10V/s Uncompensated Experimental Position and Series
Classical Inverse Preisach Compensated Position to Input Reference Voltage
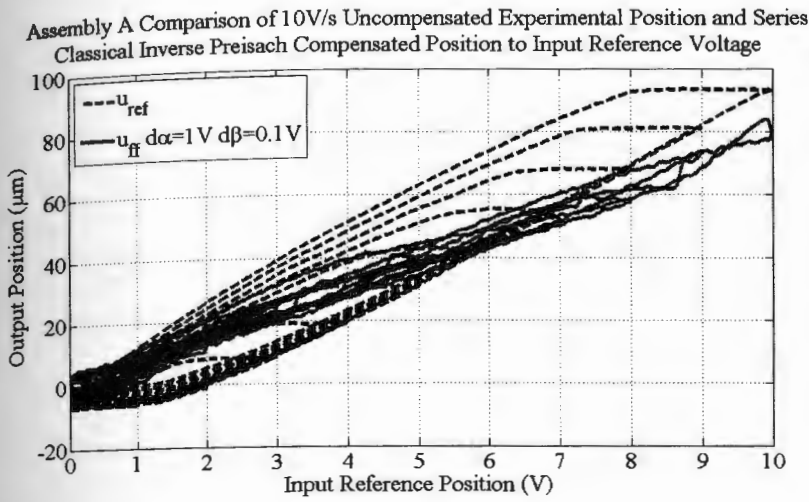
Figure 4.33. Assembly A 10 V/s Experimental Reference Voltage Input to Position
Output Comparison for Series Inverse Preisach Hysteresis Compensated Voltage
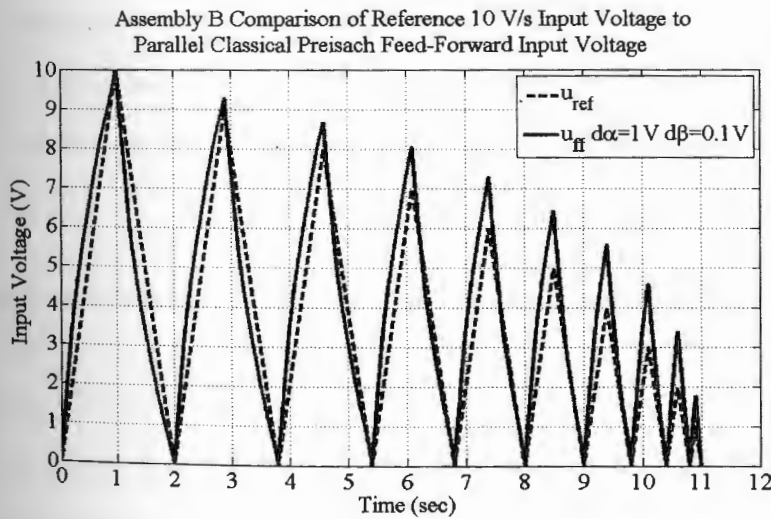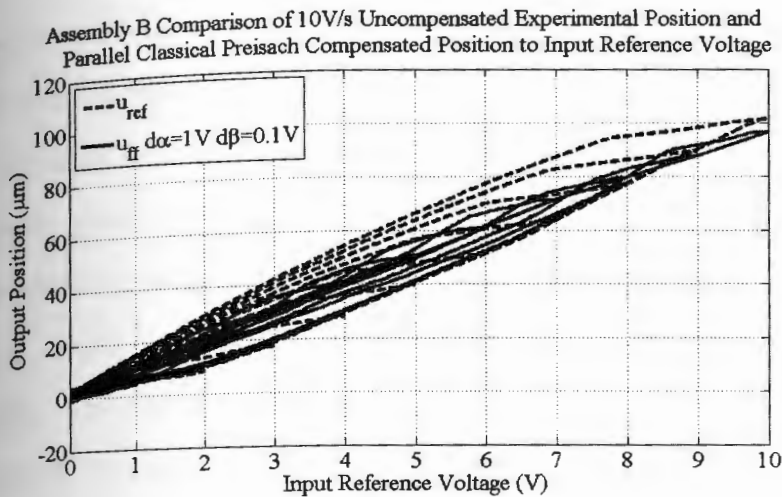with $d\alpha = 1\ V$ and $d\beta = 0.1\ V$

Assembly A Comparison of 100V/s Uncompensated Experimental Position and Series
Classical Inverse Preisach Compensated Position to Input Reference Voltage
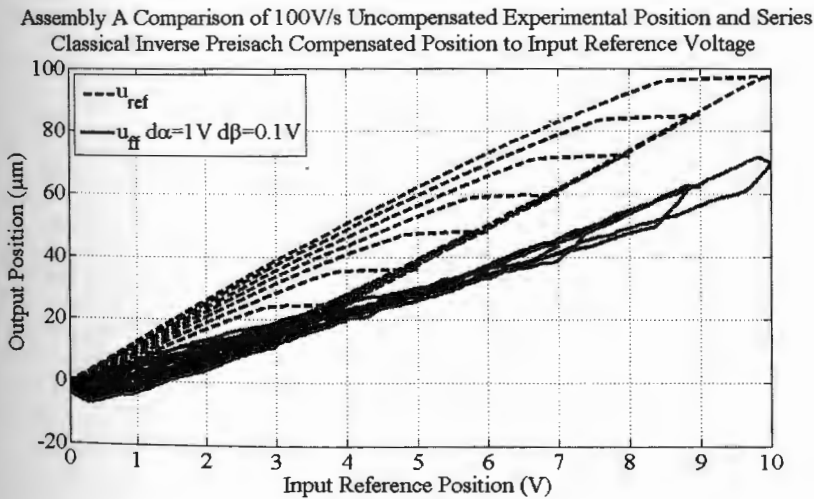
Figure 4.34. Assembly A 100 V/s Experimental Reference Voltage Input to Posi-
tion Output Comparison for Preisach Series Inverse Hysteresis Compensated Volt-
age with $d\alpha = 1\ V$ and $d\beta = 0.1\ V$

Assembly A Comparison of 500V/s Uncompensated Experimental Position and Series Classical Inverse Preisach Compensated Position to Input Reference Voltage
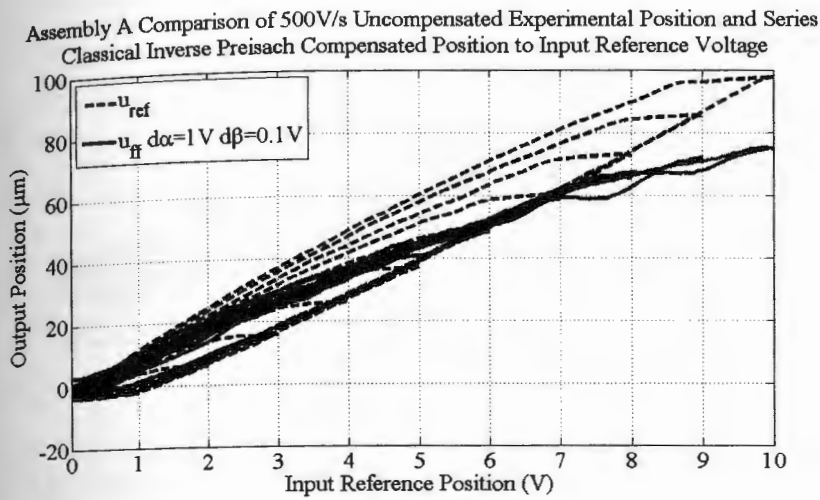
Figure 4.35. Assembly A 500 V/s Experimental Reference Voltage Input to Position Output Comparison for Preisach Series Inverse Hysteresis Compensated Voltage with $d\alpha = 1\ V$ and $d\beta = 0.1\ V$

Assembly A Comparison of 1000V/s Uncompensated Experimental Position and Series Classical Inverse Preisach Compensated Position to Input Reference Voltage
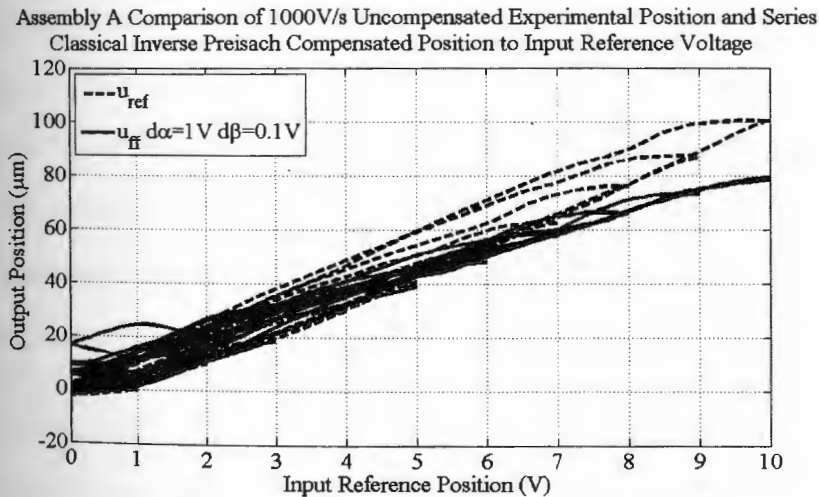
Figure 4.36. Assembly A 1000 V/s Experimental Reference Voltage Input to Position Output Comparison for Preisach Series Inverse Hysteresis Compensated Voltage with $d\alpha = 1\ V$ and $d\beta = 0.1\ V$

Assembly A Comparison of 1500V/s Uncompensated Experimental Position and Series Classical Inverse Preisach Compensated Position to Input Reference Voltage
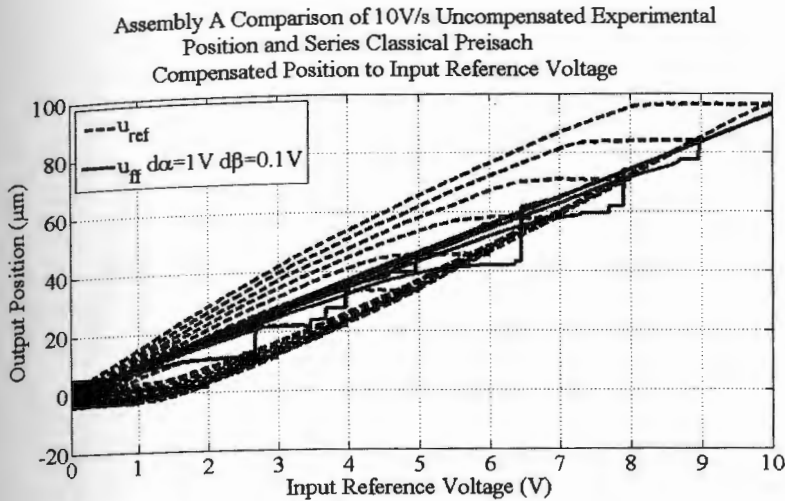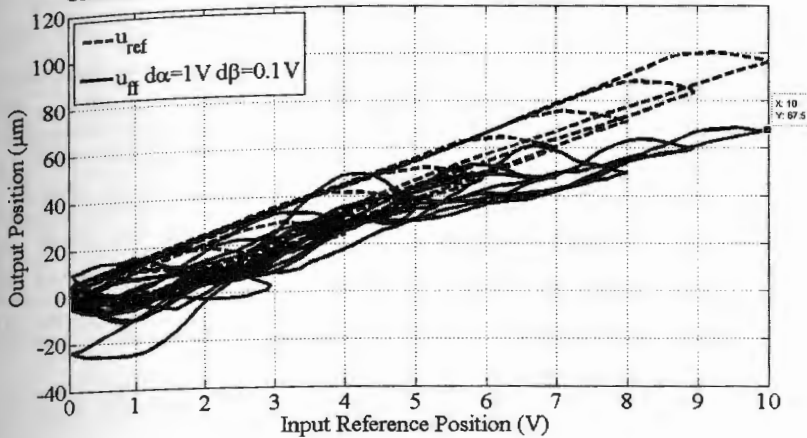
Figure 4.37. Assembly A 1500 V/s Experimental Reference Voltage Input to Position Output Comparison for Preisach Series Inverse Hysteresis Compensated Voltage with $d\alpha = 1\ V$ and $d\beta = 0.1\ V$

The hysteresis area for the series inverse feed-forward controlled system appears to be significantly reduced when compared to the parallel hysteresis compensation results. The curving effect found in the parallel Preisach compensated system does not appear to show up to any significant degree in the series inverse data. However, there appears to be a significant issue with the displacement amplitudes at 10 V voltage input. This is likely due to problem encountered in the assembly (for example, clamping to console went "out of tune" during testing) rather than an issue specific to the controller. This will be verified in the next section, when assembly B is tested with the series inverse controller.

4.7.2 Assembly B

Just as with assembly A, the Classical Preisach series inverse hysteresis compensator was tested using 10, 100, 500, 1000 and 1500 V/s descending triangle input profiles. The resulting plots of reference input voltage to output position for the uncompensated and compensated systems are shown correspondingly in Fig-

Table 4.3. Assembly B Experimental Displacement at 10 V Reference Input and Major Loop Area for Uncompensated (Unc.) and Preisach Series Compensated (Comp.) Systems

Input Rate (V/s)	10	100	500	1000	1500
Unc. Pos. at 10 V (μm)	97.90	97.55	87.20	93.91	94.47
Unc. Loop Area $(\mu m \cdot V)$	181.23	173.47	252.90	159.70	201.96
Comp. Pos. at 10 V (μm)	96.03	92.47	88.59	91.61	82.97
Comp. Loop Area $(\mu m \cdot V)$	8.75	26.52	19.55	32.07	57.62
% Red. in Maj. Loop Area	95.17	84.71	92.27	79.92	71.47

ures 4.38, 4.39, 4.40, 4.41, 4.42. Table 4.3 details the output displacement at 10 V reference input and the area of the major hysteresis loop for both uncompensated and compensated systems. The average reduction in major hysteresis loop area is 84.71%.
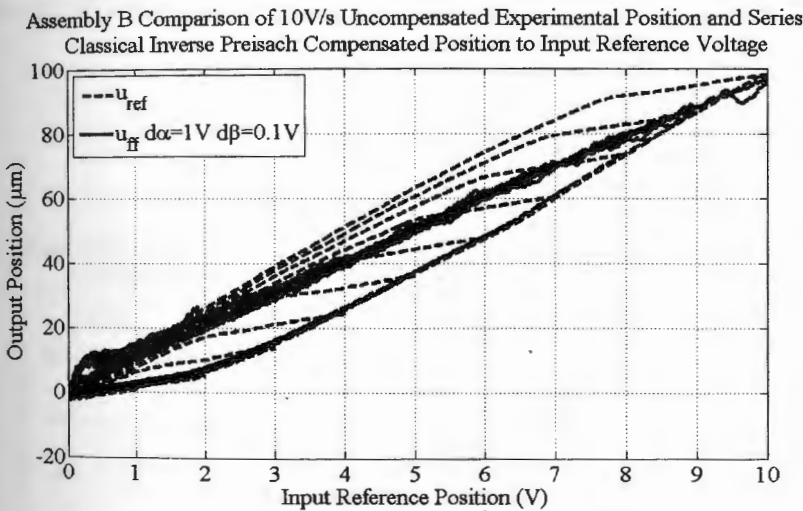
Figure 4.38. Assembly B 10 V/s Experimental Reference Voltage Input to Position Output Comparison for Series Inverse Preisach Hysteresis Compensated Voltage with $d\alpha = 1$ V and $d\beta = 0.1$ V

The series inverse controller was able to significantly reduce the hysteresis area for assembly B. It could also do this without any significant reduction in displacement at 10 V. This validates the author's hypothesis that the apparent reduction in hysteresis in found for assembly A is due to factors other than the

85

Assembly B Comparison of 100V/s Uncompensated Experimental Position and Series Classical Inverse Preisach Compensated Position to Input Reference Voltage
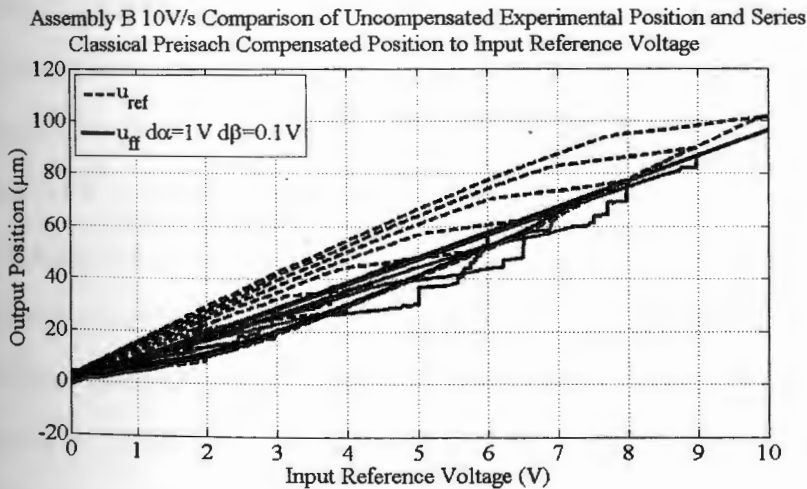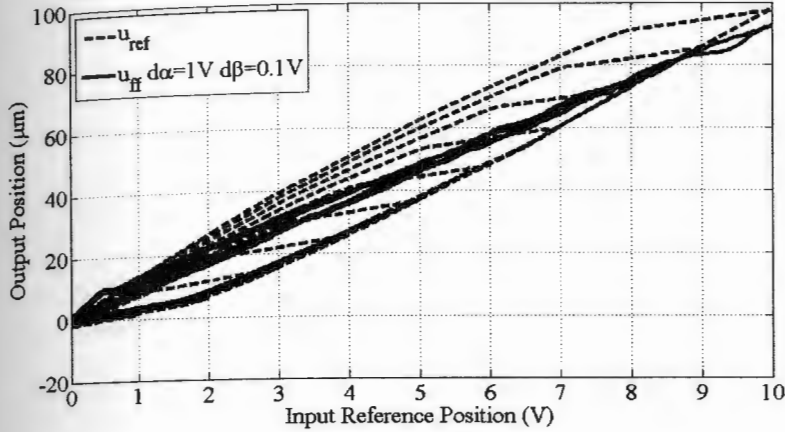
Figure 4.39. Assembly B 100 V/s Experimental Reference Voltage Input to Position Output Comparison for Preisach Series Inverse Hysteresis Compensated Voltage with $d\alpha = 1\ V$ and $d\beta = 0.1\ V$

Assembly B Comparison of 500V/s Uncompensated Experimental Position and Series Classical Inverse Preisach Compensated Position to Input Reference Voltage
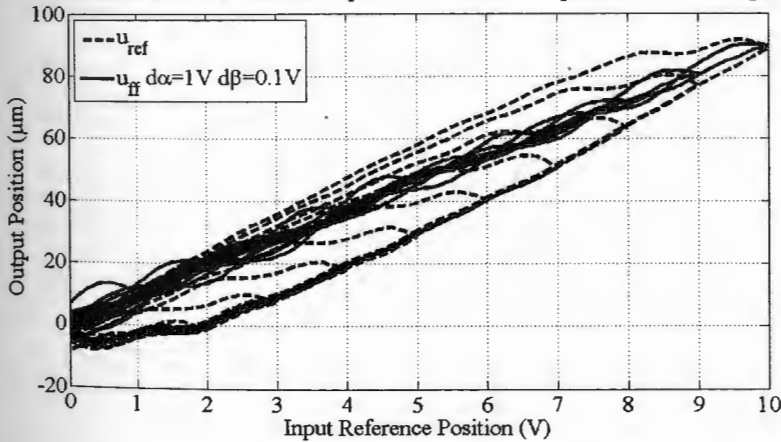
Figure 4.40. Assembly B 500 V/s Experimental Reference Voltage Input to Position Output Comparison for Preisach Series Inverse Hysteresis Compensated Voltage with $d\alpha = 1\ V$ and $d\beta = 0.1\ V$

Assembly B Comparison of 1000V/s Uncompensated Experimental Position and Series
Classical Inverse Preisach Compensated Position to Input Reference Voltage
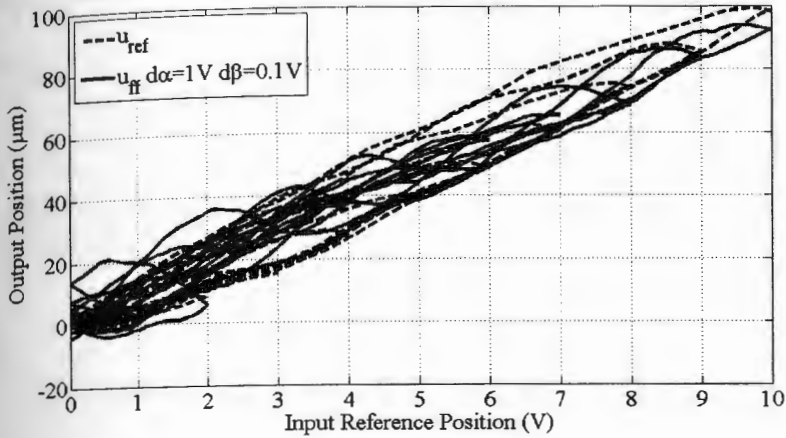
Figure 4.41. Assembly B 1000 V/s Experimental Reference Voltage Input to Position Output Comparison for Preisach Series Inverse Hysteresis Compensated Voltage with $d\alpha = 1\ V$ and $d\beta = 0.1\ V$

Assembly B Comparison of 1500V/s Uncompensated Experimental Position and Series
Classical Inverse Preisach Compensated Position to Input Reference Voltage
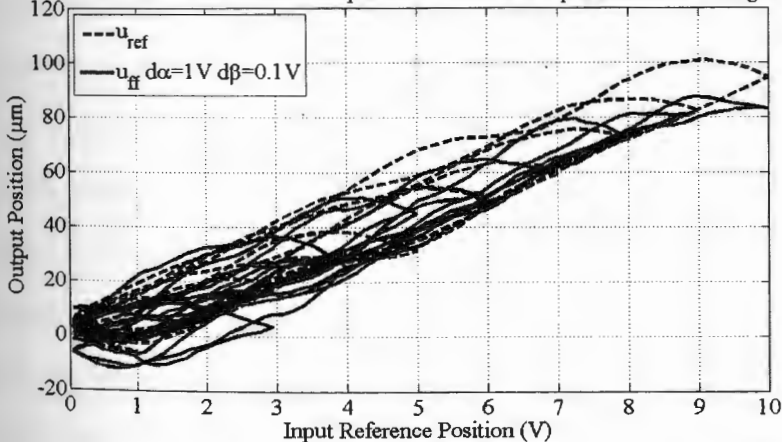
Figure 4.42. Assembly B 1500 V/s Experimental Reference Voltage Input to Position Output Comparison for Preisach Series Inverse Hysteresis Compensated Voltage with $d\alpha = 1\ V$ and $d\beta = 0.1\ V$

Table 4.4. Assembly A Experimental Displacement from 4 to 8 V Reference Input and Major Loop Area for Uncompensated (Unc.) and 4 to 8 V Offset Classical Preisach Series Inverse Compensated (Comp.) Systems

Input Rate (V/s)	10	100	500	1000
Unc. Disp. 4 - 8 V (μm)	20.20	21.49	21.77	16.96
Unc. Loop Area ($\mu m \cdot V$)	28.22	24.80	39.12	39.67
Comp. Disp. 4 - 8 V (μm)	20.98	22.27	22.07	17.99
Comp. Loop Area ($\mu m \cdot V$)	3.45	8.41	7.13	13.68
% Red. in Maj. Loop Area	95.17	66.09	81.77	65.52

control itself.

The looping behavior appears to get significantly worse at 1000 and 1500 V/s, particularly for the lower amplitude triangular input profiles. However this does not appear to be any worse than the uncompensated hysteresis curve in this region. The author decides that the series inverse implementation of Preisach hysteresis compensation is more viable, and will be pursured further.

4.8 Experimental Series Inverse Hysteresis Compensation of Assembly A for 4 to 8 V Range

Similar to the previous section the Offset 4 to 8 volt Classical Preisach series inverse hysteresis compensation model was tested on assembly A using 10, 100, 500 and 1000 V/s profiles. The assembly was also tested at 1500 V/s, but the results were not usable for this analysis. The input signal was too fast to produce any meaningful results.

The resulting plots of reference input voltage to output position for the uncompensated and compensated systems are shown correspondingly in Figures 4.43, 4.44, 4.45 and 4.46. Table 4.4 details the output displacement at 10 V reference input and the area of the major hysteresis loop for both uncompensated and compensated systems. The average major loop hysteresis reduction for this range (from 4 to 8 back to 4 volts) is 77.14%

Assembly A Comparison of 4-8 V 10V/s Uncompensated Experimental Position and Series Classical Inverse Preisach Compensated Position to Input Reference Voltage
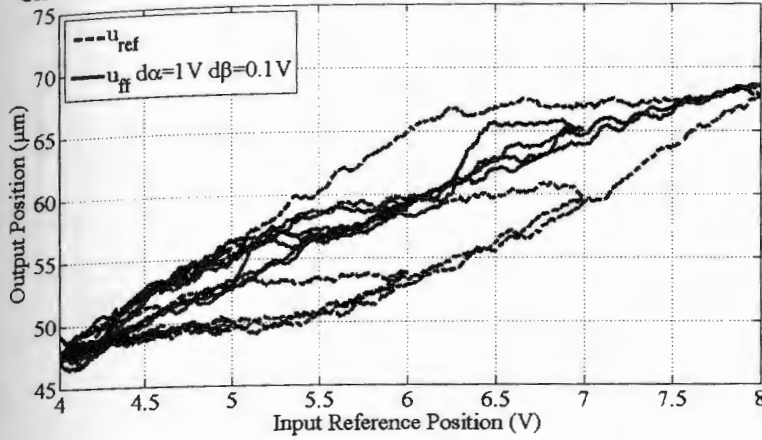
Figure 4.43. Assembly A 10 V/s between 4 and 8 V Experimental Reference Voltage Input to Position Output Comparison for Series Inverse Preisach Hysteresis Compensated Voltage with $d\alpha = 1\ V$ and $d\beta = 0.1\ V$

Assembly A Comparison of 4-8 V 100V/s Uncompensated Experimental Position and Series Classical Inverse Preisach Compensated Position to Input Reference Voltage
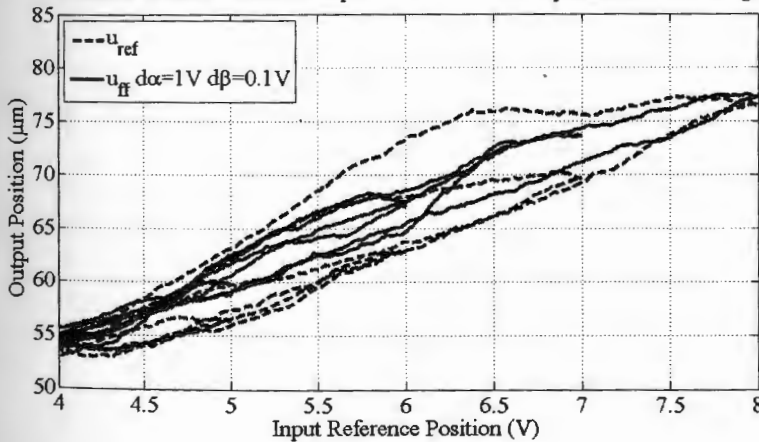
Figure 4.44. Assembly A 100 V/s between 4 and 8 V Experimental Reference Voltage Input to Position Output Comparison for Preisach Series Inverse Hysteresis Compensated Voltage with $d\alpha = 1\ V$ and $d\beta = 0.1\ V$
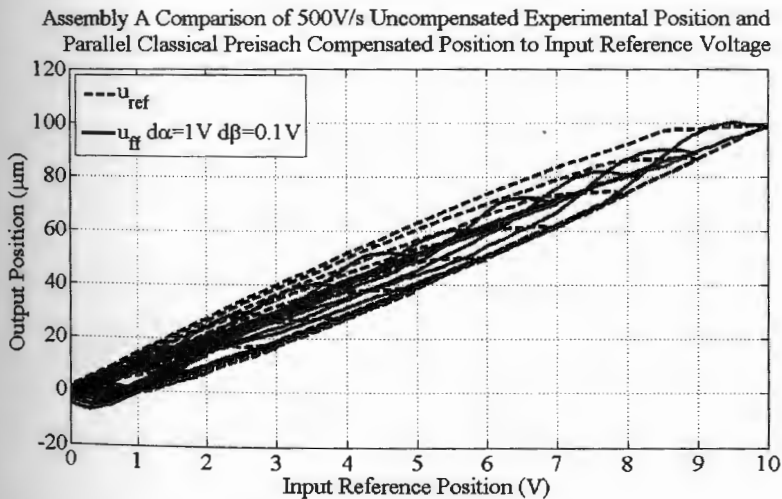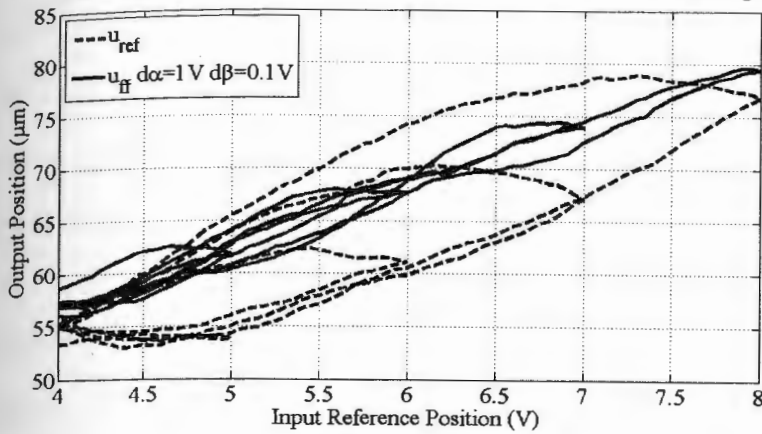
Figure 4.45. Assembly A 500 V/s between 4 and 8 V Experimental Reference Voltage Input to Position Output Comparison for Preisach Series Inverse Hysteresis Compensated Voltage with $d\alpha = 1\ V$ and $d\beta = 0.1\ V$
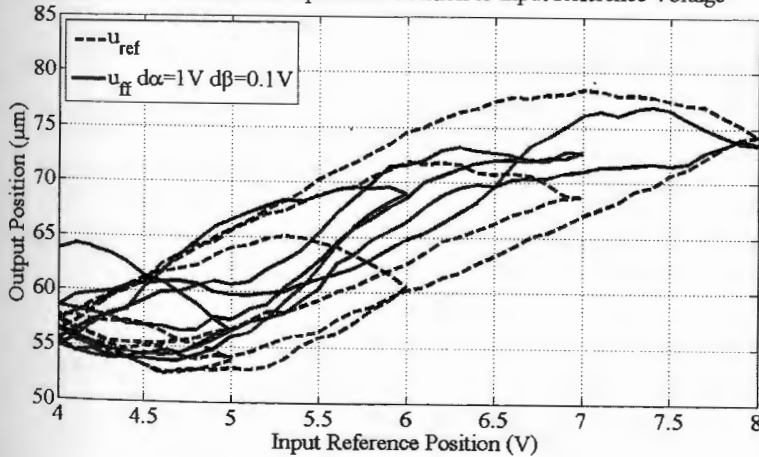
Figure 4.46. Assembly A 1000 V/s between 4 and 8 V Experimental Reference Voltage Input to Position Output Comparison for Preisach Series Inverse Hysteresis Compensated Voltage with $d\alpha = 1\ V$ and $d\beta = 0.1\ V$
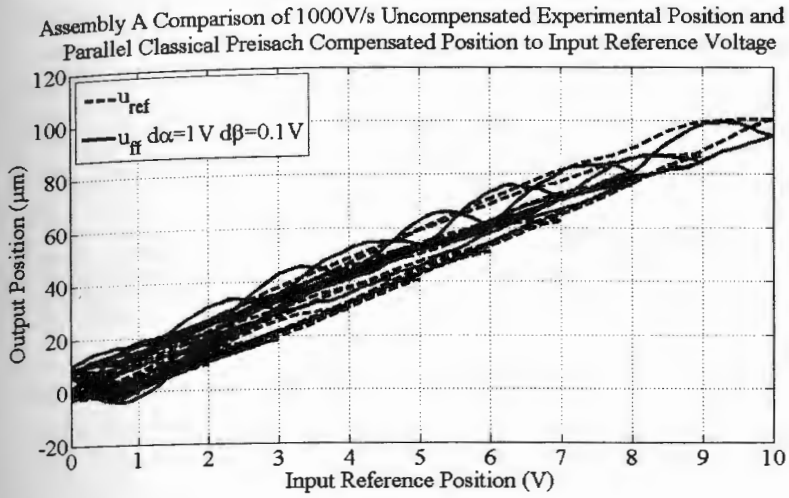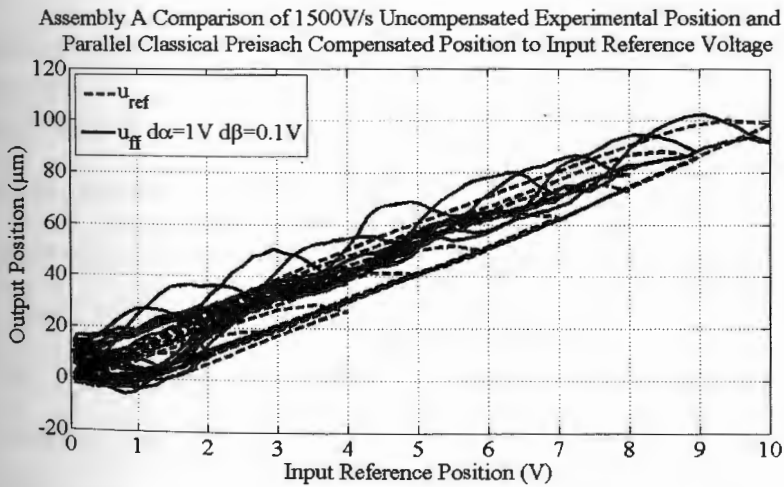
The series inverse Preisach offset hysteresis compensation algorithm is able to reduce the hysteresis area fairly significantly up to 500 V/s, although not as effectively as in the 0 to 10 V range. At 1000 V/s, the hysteresis compensation appears to have reached its limit in effectiveness, and a curved hysteresis shape appears in the controlled data. The algorithm still is able to reduce the area by two thirds, but the displacement amplitude at between 4 and 8 V is reduced when compared to lower input rates. This effect however also appears on the uncompensated data, and involve a linear phase delay due to its rounded shape.

Nevertheless, the offset series inverse Preisach compensator appears to be effective in the 4-8 input voltage range over a wide input rate. This compensator will be tested in the next section in conjunction with the filtered-X LMS algorithm to see if it can improve vibration canceling performance.

4.9 Offset Series Inverse Classical Preisach Hysteresis Compensation with Filtered-X LMS Algorithm

4.9.1 Filtered-X LMS Algorithm for Vibration and Noise Control

The Filtered-X LMS algorithm is an adaptive filter algorithm used to cancel disturbance vibration on a wood by means of superposition [33], [3]. In this case, the disturbance would originate from the machine tool. The algorithm takes the form found in Figure 4.47.

The primary path $(P(z))$ illustrates the transfer function between the disturbance (machine tool) to the sensor (accelerometer). The cancellation path $(C(z))$ represents the transfer function from the actuator to the accelerometer. These transfer functions are important for understanding the system. The filtered-X LMS algorithm requires first an identified estimate of the cancellation path $\hat{C}(z)$. Once this transfer function is determined, and if the disturbing reference signal is known, an adaptive FIR filter $(W(z))$ may be used to generate a signal along the cancellation path to counteract the output disturbance signal coming from the
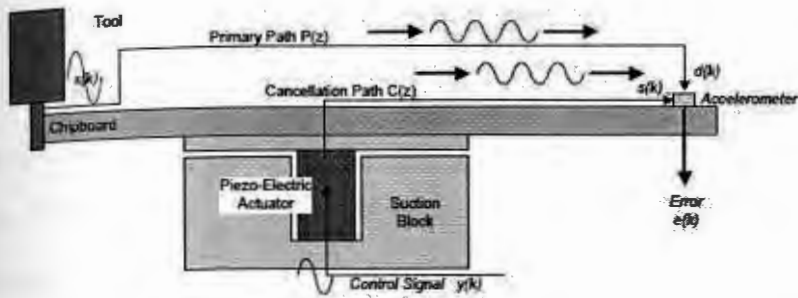
Figure 4.47. Schematic Detailing Operation of Vibration Canceling System and Illustrating Primary and Cancellation Paths (Graphic Taken from [3])

primary path. The mean square of the error signal between the output disturbance and the cancellation signal is then used by the LMS algorithm to actively adapt the coefficients of the FIR filter with the goal of minimizing this error. The block diagram for the entire algorithm is shown in Figure 4.48.
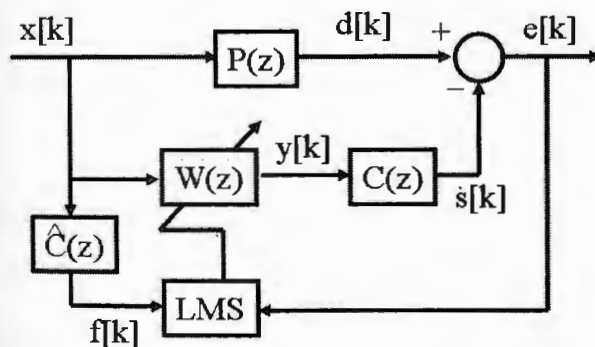
Figure 4.48. Block Diagram of Filtered-X LMS Algorithm

In this research, the cancellation path $C(z)$ includes hysteresis from the active clamp assembly. The hysteresis compensation algorithm would be integrated into the system so that the transfer function $C(z)$ is then linearized. Further detailed information regarding the theory and operation of the X-filtered LMS algorithm may be found in [33], [3].

4.9.2 Experimental Setup

A schematic of the experimental setup used for this experiment is shown in Figure 4.49. Three non-active and one active (assembly A) vacuum clamping systems are assembled to the wood machining center console. A wooden plate is placed on top of the clamps, and the vacuum is turned on. The wooden plate is also connected to an electrodynamic shaker at one corner of the wood plate. This shaker is used to simulate a disturbance input that would originate from the machine tool. An accelerometer is placed on another corner of the wooden plate.
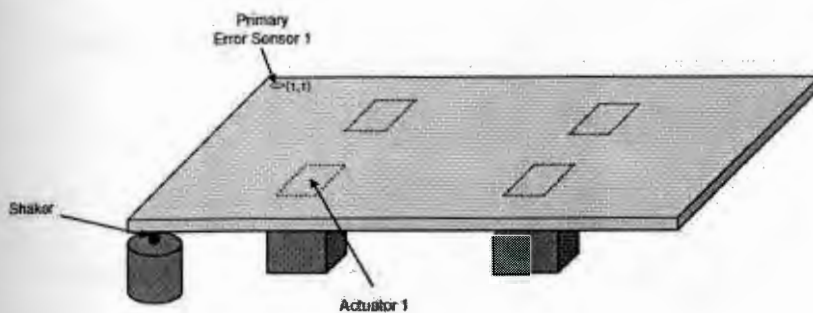
Figure 4.49. Schematic of X-Filtered LMS Experiment (Graphic Taken from [3])

The first step in implementing the feed-forward algorithm is the identification of the canceling path $C(z)$. This operation is conducted while the offset Preisach series inverse hysteresis compensator is turned off. The identified constant parameters used for FIR weighting factor determination, μ and λ, have the values $1 \cdot 10^{-4}$ and $1 \cdot 10^{-7}$ respectfully.

4.9.3 Experimental Results

The test setup was experimentally evaluated with the offset Preisach compensation off and then with it turned on. The system was given a sinusoidal disturbance from the shaker with a frequency of 300 Hz. The LMS then tries to reduce the output amplitude measured by the accelerometer. The disturbance

input has a measured amplitude output at the accelerometer of roughly $0.3m/s^2$. Figure 4.50 shows a plot of the calculated sinusoidal input voltage signal sent to the active clamp assembly to counteract the disturbance. This plot has both the uncompensated (u_{ref}, which is represented by $s[k]$ in the block diagram) and hysteresis compensated (u_{ff}, which is the resulting output of $s[k]$ filtered by the 4-8 V series inverse Classical Preisach block) results. Figure 4.51 shows the acceleration output for both cases.
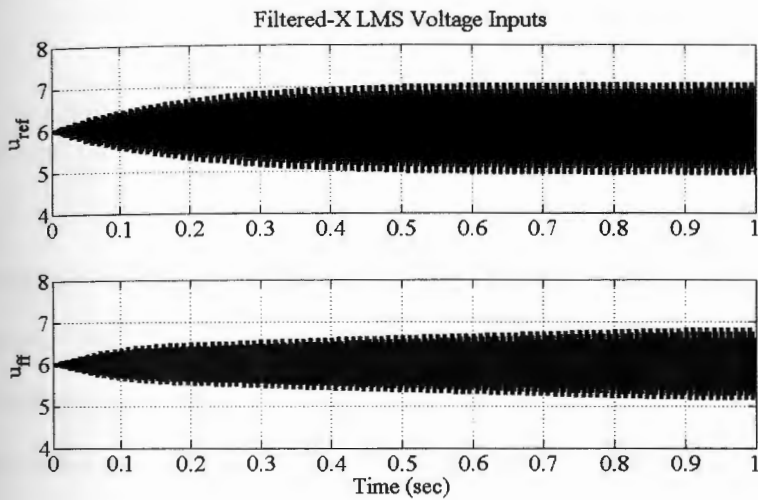
Figure 4.50. Assembly A Input Voltage from Filtered-X LMS both Uncompensated and Offset Preisach Series Inverse Compensated

The input voltage figure shows that the amplitude from the offset series inverse Preisach is less than that of the system without hysteresis compensation. From Figure 4.50, it appears that the steady-state voltage amplitude (around 1 second) by the uncompensated system is about 1 V, and the compensated amplitude is about 0.85 V. However, it appears that the hysteresis compensated system is able to reduce the acceleration amplitude to one tenth of the original value faster than the uncompensated system. The compensated system achieves an output amplitude of about $0.03m/s^2$ in about 0.24 seconds while the uncompensated system needs about 0.47 seconds. On the other hand, the compensated system does not
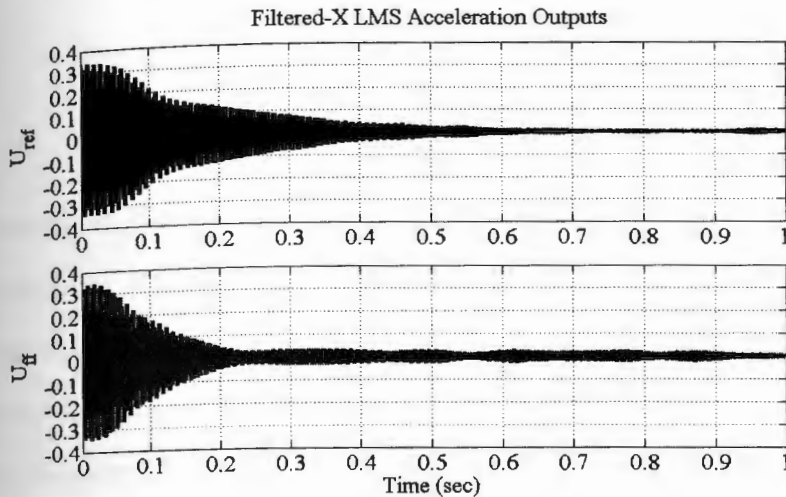
Figure 4.51. Assembly A Accelerometer Output from Filtered-X LMS both Uncompensated and Offset Preisach Series Inverse Compensated

appear to reduce the acceleration amplitude by much more than this value, but the uncompensated system is able to further reduce the amplitude into the $0.008m/s^2$ range. The author believes that since the hysteresis compensating output is based on the zeroth order ascending curve and the first order descending curve, the feed-forward output voltage does not converge to a steady state value. Instead, the output jumps around the 6 V equivalent linear output line, switching between the equivalent voltage output for the zeroth order ascending curve (when $s[k]$ is ascending) and the first order descending curve (when $s[k]$ is descending). This issue may be resolved by expanding upon the feed-forward controller to include second order ascending curve branches (Generalized Preisach) as well.

CHAPTER 5

Conclusion

5.1 Summary of Results

The assemblies' were first characterized in Chapter 2. The linear 2nd order parameters were estimated using a step response test. The hysteresis behavior was then examined for various assembly conditions as well as input signal conditions. Particularly noteworthy was the dependence of the hysteretic loop shape on the input signal voltage rate.

The assemblies' hysteresis curves were modeled using both the Bouc-Wen and Classical Preisach techniques. The Bouc-Wen hysteresis modeling was broken up into hysteresis modeling based on the unloaded actuator's parameters and parameters ascertained directly from the assembly. The actuator-based model appeared to be more suitable for feed-forward control since the level of input saturation was lower. The parameters from this model were therefore used for test. Although this control scheme appeared to work well in simulation, it was able to only partially reduce hysteretic area on descending hysteretic curves in the 0 to 10 V range for input voltage rates of 10, 100 and 500 V/s. There was no benefit for using this controller in the 1000 and 1500 V/s range. This compensation could, on average across the five input rates, reduce outer loop hysteresis by only about 30%. For this reason, the Bouc-Wen controller was deemed not suitable enough for the given application.

The Classical Preisach technique was also used for hysteresis modeling and compensation. The system was modeled in the 0 to 10 V range as well as in the offset 4 to 8 V range. This offset model would later be used for compensating the sinusoidal output from the filtered-X LMS algorithm. Compensation methods were examined which assume hysteresis effects which are in-parallel as well as in-series

96

with linear effects. It was shown that the in-series inverse Preisach compensation technique gave superior results. The parallel hysteresis compensation could reduce outer loop hysteresis on average by 66%, while the inverse series compensation could reduce hysteresis by roughly 80% in the 0 to 10 volt range. For this reason, the series inverse compensation was further investigated for application to the offset Preisach hysteresis model. The offset Preisach compensator was tested with input rates of 10, 100, 500 and 1000 V/s. The hysteresis control could also reduce the level of hysteresis in the 4 to 8 volt range by 77%.

The filtered-X LMS algorithm was tested in conjunction with the offset Classical Preisach compensator. The hysteresis compensated system was found to reduce acceleration disturbance amplitude to 10% of its original value twice as quickly as with the uncompensated system. However, the compensated system could not reduce the amplitude any further, while the uncompensated system could reduce the amplitude to less than 3% of the original disturbance value.

5.2 Recommendations for Further Research

The Classical Preisach inverse feed-forward control algorithm could reduce the level of hysteresis present in the active clamp assembly. The author believes, however, that there are several areas related to this research which could warrant further study and investigation. Some of these areas are specifically for improving the hysteresis reduction performance even further while others are more broadly based on improving the general performance and robustness of the system. These can be categorized as either control system development or hardware design related measures.

5.2.1 Recommendations for System Control

An inverse feed-forward controller based on the 4 to 8 volt offset Classical Preisach model was developed for compensating hysteresis on a 2 volt amplitude sinusoid with a 6 volt offset originating from the filtered-X LMS algorithm. This model assumes that the input voltage always cycles between 4 and some input voltage maximum. However, the amplitude from the LMS algorithm is always changing. When the input amplitude cycles back up before going down to the minimum, the output from the compensator becomes distorted. This may also help explain why the accelerometer amplitude does not reduce any further than 10%. If the offset inverse series Preisach compensation is to be used in practice, the ramifications of this distortion should be investigated in further detail.

Alternately, inverse control based on the Generalized Preisach model [1] should be investigated for this application, since theoretically it can operate along a minor hysteresis loop without any problems. However, the modeling procedure and inverse control based on the Generalized model is significantly more complex than that of the Classical Preisach model. The viability of the controller working in conjunction with the LMS algorithm would therefore need to investigated when operating in real-time (10 kHz sampling rate).

The Bouc-Wen modeling procedure was shown to effectively model the hysteresis in an unloaded actuator (Figures 3.1 and 3.2), however the modeling was less effective when applied to the assembly (Figures 3.5 and 3.6). The Bouc-Wen model is not suitable for characterizing static friction forces occurring between the horizontal and vertical wedges in the assembly. Due to the relative simplicity of identifying Bouc-Wen parameters using Matlab's Optimization Toolbox, it may be advantageous to investigate extensions of the Bouc-Wen model or other analytical models which parameterize static friction.

5.2.2 Recommendations for Hardware Design

There are many design options available for improving the active clamping system's performance. The simplest option for reducing the active's clamp hysteresis is to further investigate the use of different springs. Figure 2.8 showed that springs with lower stiffnesses can significantly reduce the level of hysteresis. The LMS algorithm should be tested with the VD-207J-01 spring with a stiffness of 3.8 N/mm to see if the system still works as expected and is able to improve performance.

Another option is to install a piezoelectric actuator with an integrated strain gage sensor. The output of this sensor can be sent to a controller integrated into the amplifier to automatically reduce hysteresis. Alternatively position sensors could be integrated into the assembly itself, and a hysteresis compensation algorithm could be developed which uses sensor feedback. Feedback control has the further benefit of automatically compensating for modeling errors and other disturbances.

The author also suggests a complete redesign of the active clamp in order to improve system performance. The assembly's nonlinear frictional characteristics present a challenge which makes hysteresis modeling difficult. An active clamp design based on a flexure stage (see Figures 5.1 and 5.2) has "negligible friction, negligible backlash, and no need for lubrication" [47]. An expansion of the actuator leads to vertical displacement of the table. While expanding, an opposing force is exerted onto the actuator which is roughly linearly dependent the stage's displacement. This assembly's hysteresis may be easier to model using Bouc-Wen technique compared to the assembly modeling results from Chapter 3.

As mentioned in Chapter 2, the active clamp is held to the wood machining center console by a screw at either end of the assembly. The assembly's displacement behavior is very dependent on both of these screw's tightening torques. Each
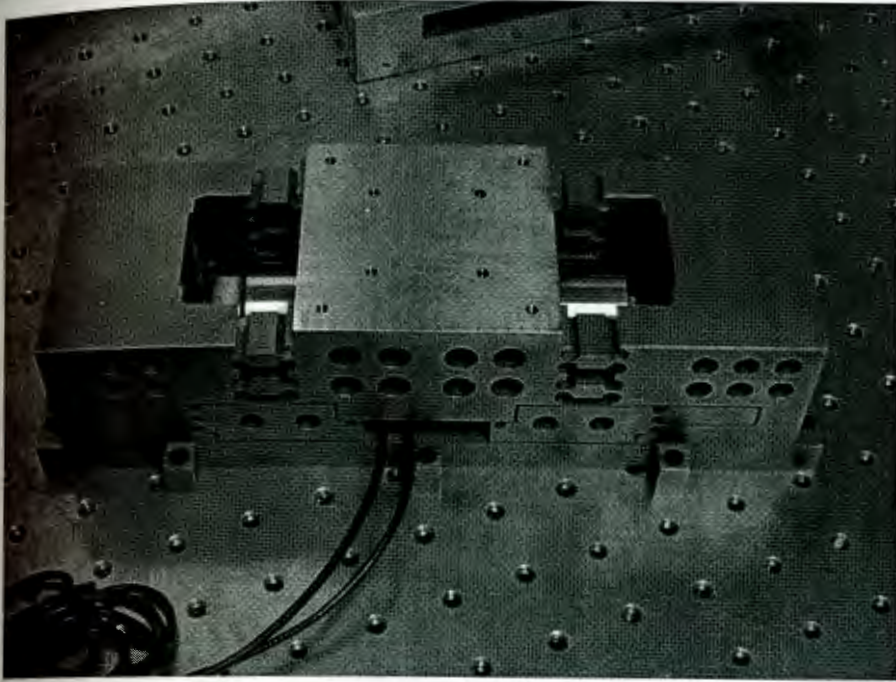
Figure 5.1. Example of Flexure Stage [4]
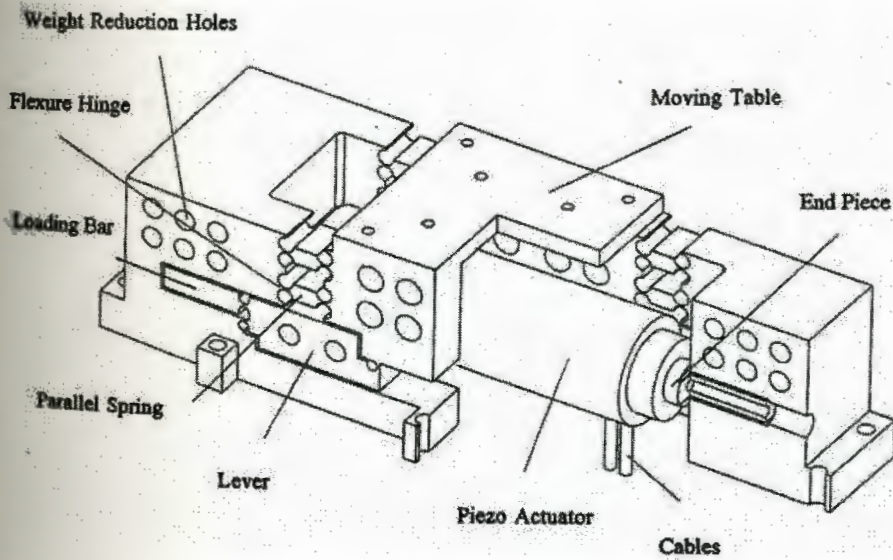
Figure 5.2. Schematic of Flexure Stage [4]

time the clamp is assembled to the console, the tightening torques needs to be properly *tuned* for optimal displacement behavior. This tightening torque is not robust and can change during testing. For this reason, it needs to be regularly inspected between experiments.

The author believes that the screws' clamping forces likely exert undesirable lateral forces directly to either end of the actuator. The degree of these forces subsequently affect the assembly's displacement for a given voltage input. The active clamp assembly should be held differently to the console to avoid exerting these lateral forces on the actuator.

A design possibility is to develop a bracket which clamps the bottom of the assembly housing in a similar manner to the vice shown in Figure 2.4. The bracket could then be assembled directly to the console. This bracket would not exert any lateral forces onto the actuator. However, the bracket should simultaneously clamp the actuator side and the suction plate side of the housing so that no lateral forces are exerted onto the actuator due to one side of the assembly hanging off of the bracket.

LIST OF REFERENCES

[1] P. Ge and M. Jouaneh, "Generalized preisach model for hysteresis nonlinearity of piezoceramic actuators," *Precision Eng*, vol. 20, 1997.

[2] P. Ge and M. Jouaneh, "Modeling of hysteresis in piezoceramic actuators," *Precision Eng*, vol. 17, 1995.

[3] T. H. Peyre, "Effective secondary path identification toward feedforward active vibration control on wood machining machine," Master's thesis, Technische Universitaet Braunschweig, 2008.

[4] Professor Jouaneh, Department of Mechanical Engineering and Applied Mechanics, University of Rhode Island. "Motion control research projects." Apr. 2009. [Online]. Available: http://www.mce.uri.edu/jouaneh/ ioncontrolprojects.htm

[5] H. Janocha, *Adaptronics and Smart Structures: Basics, Materials, Design and Applications.* Springer-Verlag Berlin Heidelberg, 2007.

[6] S. R. Moheimani and A. J. Fleming, *Piezoelectric Transducrs for Vibration Control and Damping.* Springer-Verlag London Limited, 2006.

[7] P. Ge and M. Jouaneh, "Tracking control of a piezoceramic actuators," *IEEE Transactions on Cntrol Systems Technology*, vol. 4, no. 3, 1996.

[8] G. Song, J. Zhao, X. Zhou, and J. A. D. Abreu-García, "Tracking control of a piezoceramic actuator with hysteresis compensation using inverse preisach model," *IEEE/ASME Transactions on Mechatronics*, vol. 10, no. 2, 2005.

[9] K. Kuhnen and H. Janocha, "Adaptive inverse control of piezoelectric actuators with hysteresis operators," in *Proceedings of the European Control Conference*, Karlsruhe, 1999.

[10] K. Kuhnen and H. Janocha, "Inverse feedforward controller for complex hysteretic nonlinearities in smart-material systems," *Control and Intelligent Systems*, vol. 29, 2001.

[11] U.-X. Tan, W. T. Latt, C. Y. Shee, C. Riviere, and W. T. Ang, "Modeling and control of piezoelectric actuators for active physiological tremor compensation," in *Human-Robot Interaction*, Vienna, Austria, 2005.

[12] B.-R. Lee, S.-Y. Yang, and K.-K. Ahn, "Precision control of piezoelectric actuator using inverse hysteresis model and neuro control," in *KORUS 2003: The 7th Korea-Russia International Symposium on Science and Technology*, Ulsan, Republic of Korea, 2003.

[13] C. Ru and L. Sun, "A new open-loop driving method of piezoelectric actuator for periodic reference inputs," *Ultrasonics*, vol. 44, 2006.

[14] M. Goldfarb and N. Celanovic, "A lumped parameter electromechanical model for describing the nonlinear behavior of piezoelectric actuators," *Journal of Dynamic Systems, Measurement and Control*, vol. 119, Sept. 1997.

[15] M. Goldfarb and N. Celanovic, "Modeling piezoelectric stack actuators for control of micromanipulation," *IEEE Control Systems Magazine*, vol. 17, June 1997.

[16] M. Jouaneh and H. Tian, "Accuracy enhancement of a piezoelectric actuator with hysteresis," in *ASME JAPAN/USA Symposium on Flexible Automation*, San Francisco, CA, USA, 1992.

[17] T. Low and W. Guo, "Modeling of a three-layer piezelectric bimorph beam with hysteresis," *Journal of Microelectromechanical Systems*, vol. 4, Dec. 1995.

[18] J.-L. Ha, R.-F. Fung, and C.-S. Yang, "Hysteresis identification and dynamic responses of the impact drive mechanism," *Journal of Sound and Vibration*, vol. 283, 2005.

[19] C.-J. Lin and S.-R. Yang, "Precise positioning of piezo-actuated stages using hysteresis-observer based control," *Mechatronics*, vol. 16, 2006.

[20] S.-K. Hung, E.-T. Hwu, I.-S. Hwang, and L.-C. Fu, "Postfitting control scheme for periodic piezoscanner driving," *Japanese Journal of Applied Physics*, vol. 45, no. 3B, 2006.

[21] R.-F. Fung, Y.-L. Hsu, and M.-S. Huang, "System identification of a dual-stage xy precision positioning table," *Precision Engineering*, vol. 33, 2009.

[22] J. Adriaens, W. de Koning, and R. Banning, "Design and modeling of a piezo-actuated positioning mechanism," in *Procedings of the 36th Conference on Decision and Control*, San Diego, California USA, Dec. 1997.

[23] H. J. Adriaens, W. L. de Koning, and R. Banning, "Modeling piezoelectric actuators," *IEEE/ASME Transactions on Mechatronics*, vol. 5, no. 4, Dec. 2000.

[24] R. Bouc, "Forced vibration of mechanical systems with hysteresis (abstract)," in *Proceedings for the Fourth Conference on Nonlinear Oscillation*, Prague, Cechoslovakia, 1967.

[25] Y. Wen, "Method for random vibration of hysteretic systems," *J. Eng. Mech. Div. ASCE*, vol. 102, no. 2, 1976.

[26] Y. Wen, "Equivalent linearization for hysteretic systems under random excitation," *Journal of Applied Mechanics, Transactions ASME*, vol. 47, no. 1, 1980.

[27] F. Preisach, "Über die magnetische Nachwirkung," *Zeitschrift für Physik A Hadrons und Nuclei*, vol. 94, May 1935.

[28] R. B. Mrad and H. Hu, "Dynamic modeling of hysteresis in piezoceramics," in *IEEE/ASME International Conference on Advanced Intelligent Mechatronics Proceedings*, Como, Italy, 2001.

[29] Y. Yu, Z. Xiao, N. G. Naganathan, and R. V. Dukkipati, "Dynamic preisach modelling of hysteresis for the piezoceramic actuator system," *Mechanism and Machine Theory*, vol. 37, 2002.

[30] R. B. Mrad and H. Hu, "A model for voltage-to-displacement dynamics in piezoceramic actuators subject to dynamic-voltage excitations," *IEEE/ASME Transactions on Mechatronics*, vol. 7, no. 4, 2002.

[31] H. Hu, H. Zhang, and R. B. Mrad, "Preisach based dynamic hysteresis model," in *International Conference on Intelligent Mechatronics and Automation*, Chengdu, China, 2004.

[32] H. Hu, H. Georgiou, and R. Ben-Mrad, "Enhancement of tracking ability in piezoceramic actuators subject to dynamic excitation conditions," *IEEE/ASME Transactions on Mechatronics*, vol. 10, no. 2, 2005.

[33] H.-W. Hoffmeister, B.-C. Schuller, and K. Loeis, "Active vibration reduction on clamping systems for stationary machining centers," in *Adaptronic Congress*, Göttingen, Germany, 2007.

[34] Physik Instrumente GmbH & Co. KG. "P-212, p-216 pica^{TM} power piezo stack actuators." Apr. 2009. [Online]. Available: http://www.physikinstrumente. com/en/pdf/P212_P216_Datasheet.pdf

[35] Physik Instrumente GmbH & Co. KG. "E-481 pica^{TM} piezo high-powered amplifier/controller." Apr. 2009. [Online]. Available: http://www.physikinstrumente.com/en/pdf/E481_Datasheet.pdf

[36] dSPACE GmbH. "Ds1006 processor board." Apr. 2009. [Online]. Available: http://www.dspace.de/shared/data/pdf/catalog2009/DS1006-ProcessorBoard%_dSPACE_Catalog_2009.pdf

[37] dSPACE GmbH. "Ds2004 high-speed a/d board." Apr. 2009. [Online]. Available: http://www.dspace.de/shared/data/pdf/catalog2009/DS2004-HighSpeed-AD-Board_dSPACE_Catalog_2009.pdff

[38] dSPACE GmbH. "Ds2101/ds2102/ds2103 d/a boards." Apr. 2009. [Online]. Available: http://www.dspace.de/shared/data/pdf/catalog2009/DS2101-DS2102-DS2103-DA-Boards_dSPACE_Catalog_2009.pdf

[39] dSPACE GmbH. "Targetlink 3.0." Apr. 2009. [Online]. Available: http://www.dspace.de/shared/data/pdf/flyer2009/dspace_2009_targetlink30_en_pi823.pdf

[40] dSPACE GmbH. "Control desk." Apr. 2009. [Online]. Available: http://www.dspace.de/shared/data/pdf/catalog2009/ControlDesk_dSPACE_Catalog_2009.pdf

[41] Micro-Epsilon Messtechnik GmbH & Co. KG. "optoncdt 1607." Apr. 2009. [Online]. Available: http://www.micro-epsilon.com/download/products/dat--optoNCDT-1607--en.pdf

[42] Physik Instrumente GmbH & Co. KG. "Piezo-university: Fundamentals of piezoelectric actuators." Apr. 2009. [Online]. Available: http://www.physikinstrumente.com/en/products/prdetail.php?sortnr=400600.40

[43] W. J. Palm, *System Dynamics.* McGraw-Hill, 2005.

[44] Physik Instrumente GmbH & Co. KG. "Piezo-university: Dynamic operation fundamentals." Apr. 2009. [Online]. Available: http://www.physikinstrumente.com/en/products/prdetail.php?sortnr=400600.60

[45] R. V. Iyer and X. Tan, "Control of hysteretic systems through inverse compensation," *IEEE Control Systems Magazine*, vol. 29, Feb. 2009.

[46] The MathWorks, Inc. "Optimization toolbox 4 - user's guide." Apr. 2009. [Online]. Available: http://www.mathworks.com/access/helpdesk/help/pdf_doc/optim/optim_tb.pdf

[47] R. Yang, M. Jouaneh, and R. Schweizer, "Design and characterization of a low-profile micropositioning stage," *Precision Eng*, vol. 18, 1996.

APPENDIX

Matlab Scripts and Simulink Block Diagrams

A.1 Bouc-Wen Identification Code
A.1.1 runboucwenid.m

This is the main program used to identify Bouc-Wen parameters using Matlab's Optimization Toolbox. In this script, the parameter search bounds as well as initial search values are supplied by the user. This function then calls the function to be minimized boucoptm.m using the function "fmincon".

```
ct=cputime;
% declaration of global variables
global m c k
global U Udot x_exp t_exp y_t U_0 F_sp_0 x_num_state
global a b g d x0 X1 X2 H X1dot X2dot Hdot Tsamp t_num
global x_num i x_num_sp
%
% initialize experimental result data .
U=ub_10v;
t_exp=tb_10v;
x_exp=xb_10v*1e6;
%
% U=assy_a_desc_1vs .Y(1 ,4) . Data;          % D/A (0-10 V)
% x_exp=assy_a_desc_1vs .Y(1 ,3) . Data;   % real data (m)
% t_exp=assy_a_desc_1vs .X. Data;             % time (s)
% % zero measurement position to first value
% x_exp=x_exp-x_exp(1);
% %
```

```
% % sampling time for test
% Tsamp=t_exp(2)-t_exp(1);
TL=max(t_exp);
TL=round(TL*10000)/10000;
Tsamp=0.01;
%
% initialize constants to be optimized for best fit to data
v0(1)=1;              % alpha
v0(2)=0.5;           % beta
v0(3)=0.5;           % gamma
v0(4)=10;    % voltage-displacement constant (m/V)
%
% initialize lower and upper bounds for data
vlb(1)=0;            %alpha
vlb(2)=0;             % beta
vlb(3)=-2;       % gamma
vlb(4)=9; % voltage-displacement constant (m/V)
%
vub(1)=5;         % alpha
vub(2)=5;         % beta
vub(3)=5;         % gamma
vub(4)=14; % voltage-displacement constant (m/V)
%
% Constrained optimization with upper and lower bounds
% Minimizes difference between numerical and experimental
% data using least squares best fit method
```

```
%
% set options for fmincon
options=optimset ;
options=optimset(options ,'Display','iter');
options=optimset(options ,'LargeScale','off');
%options=optimset(options ,'Display','final');
options=optimset(options ,'MaxFunEvals',3000);
%
% fmincon finds minimum of constrained
% nonlinear multivariable function
% x is solution array
% fval is value of objective function at solution x
% @bouc_optm is link to objective function
% x0 is array of initial values
% x_lb , x_ub are lower bounds and
% upper bounds of x solution
[v,Jv]=fmincon(@bouc_optm ,v0 ,[] ,[] ,[] ,[] ,
.. vlb ,vub ,[[] ,[]] , options );
%
% best fit bouc—wen parameters
a=v(1)
b=v(2)
g=v(3)
d=v(4)
% time to compute
ct=cputime−ct
```

A.1.2 boucoptm.m

This is continuously called by runboucwenid.m, until a minimum of the cost function is found. This function calls the Simulink block diagram simphystID-digsim4 to simulate the response for a given parameter set. The function uses the RMS cost function J between the identified simulation and the experimental data. This function also plots both the time and input/output hysteresis curve.

The block diagram depiction of simphystIDdigsim4 is shown in Figure A.1.
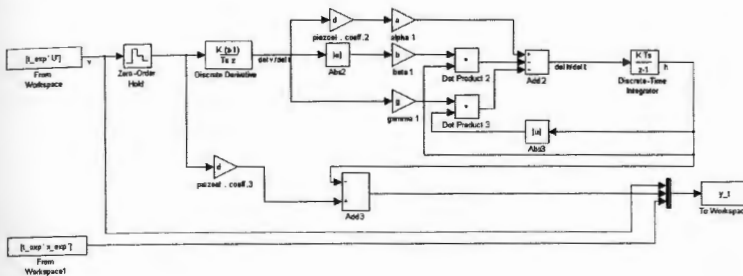
Figure A.1. Simulink Model of Digitized Bouc-Wen Model for Identification Routine

```
function [J]=bouc_optm(v)
% declaration of global variables
global m c k
global U Udot x_exp t_exp t_num x_num x_num_sp U_0
global F_sp_0 x_num_state
global a b g d x0 X1 X2 H X1dot X2dot Hdot Tsamp i y_t
%
% initialize variables every time optimization is run
a=v(1); % alpha
b=v(2); % beta
g=v(3); % gamma
d=v(4); % voltage−strain constant
```

```matlab
%
% % initialization vector for y
x0=[x_exp(1);0;0];
% %
% % solve nonlinear state equations using ODE
% [t_num,x_num_state]=ode113('bouc_state',t_exp,x0);
% x_num=x_num_state(:,1);
% %
% %
% %
% solve nonlinear system using Simulink
sim('simp_hyst_ID_dig_sim4');
% scale output to m
x_num=y_t.signals.values(:,2);
t_num=y_t.time;
U_num=y_t.signals.values(:,1);
x_sim_exp=y_t.signals.values(:,3);
%
% cost function to minimize (RMS)
J=norm(x_sim_exp-x_num,2)/sqrt(length(x_num));
%
% resulting timeseries response and hysteresis plots
figure(1)
clf;
plot(t_exp,x_exp,t_num,x_num)
xlabel('Test time (sec)')
```

```
ylabel('Displacement Output (m)')
legend('Exp. Data','Bouc-Wen Sim')
title(['Hysteresis Actuator A Sp. DF-2440 8 cNm
..  Inner Loop 1V/s, d='
.., num2str(d),' \mu m/V, \alpha=',num2str(a),',
..\beta=',num2str(b),', \gamma=',num2str(g)])
figure(2)
clf;
plot(U,x_exp,U_num,x_num)
xlabel('Voltage Input (V)')
ylabel('Displacement Output (m)')
legend('Exp. Data','Bouc-Wen Sim')
title(['Hysteresis Actuator A Sp. DF-2440 8 cNm Inner
..Loop 1V/s, d='
.., num2str(d),' \mu m/V, \alpha=',num2str(a),', \beta=',
..num2str(b), ', \gamma=',num2str(g)])
return;
```

A.2 Classical Preisach Code
A.2.1 clpreisid.m

This script is used to determine and save the data points for the Classical Preisach model. In this script, one can set the range of α and β as well as $d\alpha$ and $d\beta$. The data points will then be saved in the Matlab array cl_pr_lu_tb.

```
% Script for classical Preisach identification
% from descending hysteresis tests. Uses data from
% first order reversal curves to build lookup table
%
```

```
% load data as workspace variables
  clear cl_pr_lu_tb U_n U_n2 x_exp_n x_exp_n2 U x_exp t_exp;
% U=assy_a_desc_1vs.Y(1,4).Data;            % D/A (0-10 V)
% x_exp=assy_a_desc_1vs.Y(1,3).Data;   % real data (m)
% t_exp=assy_a_desc_1vs.X.Data;            % time (s)
% U=actc_8cnm_dn_10_0_st1_sl1_0_001.Y(1,4).Data;
% x_exp=actc_8cnm_dn_10_0_st1_sl1_0_001.Y(1,3).Data;
% t_exp=actc_8cnm_dn_10_0_st1_sl1_0_001.X.Data;
U=u1_dsp_n;              % D/A (0-10 V)
x_exp=x_las_n2*1e6;   % experimental data (m)
t_exp=t_dsp_n;              % time (s)
%
% smooth x_exp data over 50 data points
%x_exp=smooth(x_exp,50);
%
% sampling time for test
Ts=t_exp(2)-t_exp(1);
% input minimum sample location for analysis
% (preferably after first major
% loop ( try >> figure,plot(U) to find this location)
%samp_min=1.887e4;
%samp_min=20006;
samp_min=1;
%
% zero data
 x_exp=x_exp-x_exp(samp_min);
```

```
%
% cut data at sample data location
U_n=U(samp_min:length(U));
x_exp_n=x_exp(samp_min:length(x_exp));
% x_exp_n=xs_exp(samp_min:length(xs_exp));
%
% constants for determining Preisach
% triangle density for lookup table
% This data should be determined from the plot of U_n
% alpha maximum voltage
al_max=10;
% alpha minimum voltage
al_min=0;
% alpha step voltage
al_s=1;
% beta maximum voltage
be_max=al_max;
% beta minimum voltage
be_min=al_min;
% beta step voltage
be_s=0.1;
%
% create header in cl_pr_lu_tb with alpha and
% beta max, min and step sizes
cl_pr_lu_tb=[al_max be_max -1 -1 -1 -1;
             al_min be_min -1 -1 -1 -1;
```

```
           al_s      be_s      -1 -1 -1 -1;
           -1        -1        -1 -1 -1 -1];

%
% initialize lookup table position
i=4;
%% zero data
% [trash, al_loc_s]=min(abs(U_n-al_min));
% U_n=U_n(al_loc_s:length(U_n));
% x_exp_n=x_exp_n-x_exp_n(al_loc_s);
% x_exp_n=x_exp_n(al_loc_s:length(x_exp_n));
%
[trash, samp_max1]=min(abs(U_n-al_max));
U_n1=U_n(1:samp_max1);
x_exp_n1=x_exp_n(1:samp_max1);
% insert zeroth order ascending hysteresis curve data
for al_loc=[al_min:al_s:al_max]
    i=i+1;
    % find data point location and cut data here
    [trash, al_loc_s]=min(abs(U_n1-al_loc));
    samp_min=al_loc_s;
    U_n1=U_n1(samp_min:length(U_n1));
    x_exp_n1=x_exp_n1(samp_min:length(x_exp_n1));
    %
    % alpha and beta are same on zeroth order
    % ascending hysteresis
    be_loc=al_loc;
```

```matlab
    % determine Xalpha
    Xalpha=x_exp_n1(1);
    % determine Xbeta=Xalpha
    Xbeta=Xalpha;
    % determine change in displacement from alpha
    % to beta
    dXalphabeta=Xalpha-Xbeta;
    dBeta=al_loc-be_loc;
    cl_pr_lu_tb(i,:)=[al_loc be_loc Xalpha Xbeta
    ..dXalphabeta dBeta]
end
%
minXalpha=cl_pr_lu_tb(5,3);
for j=5:length(cl_pr_lu_tb)
    if cl_pr_lu_tb(j,3)<minXalpha
        cl_pr_lu_tb(j,3)=minXalpha;
    end
end
maxXalpha=cl_pr_lu_tb(length(cl_pr_lu_tb),3);
%
% insert -1's for zeroth order /
% first order hysteresis separation
i=i+1;
cl_pr_lu_tb(i,:)=[-1 -1 -1 -1 -1 -1];
%
U_n=U_n(samp_max1:length(U_n));
```

```matlab
dUdt=(U_n(1)-U_n(2))/Ts;
x_exp_n=x_exp_n(samp_max1:length(x_exp_n));
% loop for creating lookup table from
% 1st order reversal curves
for al_loc=[al_max:-al_s:al_min]
    % find peak of alpha in data
    [trash,al_loc_s]=min(abs(U_n-al_loc));
    % enter into lookup table first point on reversal curve
    % for alpha=beta
    be_max=al_loc;
    be_stop=round((be_max-be_min)/(dUdt*Ts))+1;
    %
    samp_min=round(al_loc_s);
    U_n=U_n(samp_min:length(U_n));
    U_n2=U_n(1:be_stop);
    x_exp_n=x_exp_n(samp_min:length(x_exp_n));
    x_exp_n2=x_exp_n(1:be_stop);
    % data table organized as follows:
    % [alpha(i) beta(i) Xalpha(i)
    % ..Xalphabeta(i) dXalphabeta(i)]
    for be_loc=[be_max:-be_s:be_min]
        % lookup table location
        i=i+1;
        [trash,be_loc_s]=min(abs(U_n2-be_loc));
        % determine Xalpha
        Xalpha=x_exp_n2(1);
```

```
% correct data
if Xalpha<minXalpha

    Xalpha=minXalpha;

end
if Xalpha>maxXalpha

    Xalpha=maxXalpha;

end
% determine Xbeta
Xbeta=x_exp_n2( be_loc_s );
% correct data
if Xbeta<minXalpha

    Xbeta=minXalpha;

end
if Xbeta>Xalpha

    Xbeta=Xalpha;

end
% determine change in displacement
% from alpha to beta
dXalphabeta=Xalpha-Xbeta;
dBeta=al_loc-be_loc;
% enter data into lookup table
cl_pr_lu_tb(i,:)=[al_loc be_loc Xalpha
        ..Xbeta dXalphabeta dBeta];
end
% make X(beta=be_min)=xmin(alpha=al_min)
if Xbeta~=cl_pr_lu_tb(5,3)
```

```
        Xbeta=cl_pr_lu_tb(5,3);

        dXalphabeta=Xalpha-Xbeta;

        cl_pr_lu_tb(i,:)=[al_loc  be_loc  Xalpha

                ..Xbeta  dXalphabeta  dBeta];

    end

    % after looping through all beta values for particular

    % alpha, cut data at last beta

    samp_min=be_loc_s;

    U_n=U_n(samp_min:length(U_n));

    x_exp_n=x_exp_n(samp_min:length(x_exp_n));

end
```

A.2.2 clpreissim.m

This script may be used independently from clpreisid.m. One must only
have the array cl_pr_lu_tb in the Matlab workspace with the Classical Preisach
data points. The block diagram of this set up is shown in Figure

```
% Simulation of system hysteresis using
% Classical Preisach method
%
% extract data from combined lookup table array variable
% determined from cl_preis_id.m script
%
% mesh range and density constants
al_max=cl_pr_lu_tb(1,1);
be_max=cl_pr_lu_tb(1,2);
al_min=cl_pr_lu_tb(2,1);
```

```matlab
be_min=cl_pr_lu_tb(2,2);
al_s=cl_pr_lu_tb(3,1);
be_s=cl_pr_lu_tb(3,2);
% calculate max # beta for given alpha
% dummy beta and dX based on max # beta for given alpha
beta_in=ones(1,length(be_min:be_s:be_max))*-1e6;
dX_in=ones(1,length(be_min:be_s:be_max))*-1e6;
%
% zeroth order hysteresis
zeroth=flipud(cl_pr_lu_tb(5:(5+(al_max-al_min)/al_s),:));
%
% first order hysteresis (order flipped with flipud)
first=cl_pr_lu_tb((7+(al_max-al_min)/al_s):
..length(cl_pr_lu_tb),:);
%
zeroth_X0=zeroth(length(zeroth(:,1)),3);
%
zeroth_XM=zeroth(1,3);
% min voltage
zeroth_U0=zeroth(length(zeroth(:,1)),1);
% max voltage
zeroth_UM=zeroth(1,1);
% strain constant
d=(zeroth(1,3)-zeroth(length(zeroth(:,1)),3))/(zeroth(1,1)
..-zeroth(length(zeroth(:,1)),1))*1e-6;
```

A.2.3 preisachsim.mdl

This block diagram simulates the rate-independent hysteretic output of the system from the zeroth order descending curve and first order ascending curves given by the script clpreissim.m. The block diagram for this Simulink model is shown in Figure A.2.
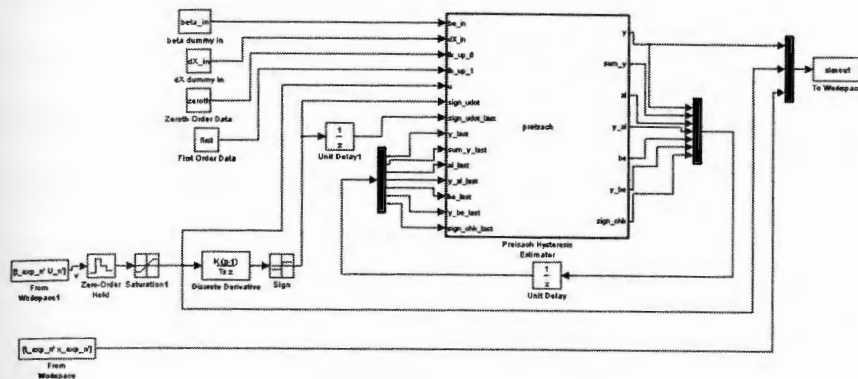
Figure A.2. Simulink Model for Classical Preisach Hysteresis

The Embedded Matlab source code for the *Preisach Hysteresis Estimator* block is shown below:

```
function [y,sum_y,al,y_al·,be,y_be,sign_chk] =
..preisach(be_in,dX_in,lk_up_0,lk_up_1,u,sign_udot,
..sign_udot_last,y_last,sum_y_last,al_last,y_al_last,
..be_last,y_be_last,sign_chk_last)
% This block supports the Embedded MATLAB subset.
% See the help menu for details.
%
% determine the voltage input case
if sign_udot==1 && (sign_udot_last==0 || sign_udot_last==1)
    in_case=1;
```

120

```matlab
elseif sign_udot==1 && sign_udot_last==-1
    in_case=2;
elseif sign_udot==-1 && (sign_udot_last==0 ||
.. sign_udot_last==-1)
    in_case=3;
elseif sign_udot==-1 && sign_udot_last==1
    in_case=4;
else % sign_udot==0
    in_case=5;
end


switch in_case
%
    case 1
        % sign_udot==1 && (last_sign_udot==0 ||
        % .. last_sign_udot==1)
        % case positive voltage rate - use increasing
        % hysteresis curve data "zeroth"
        %
        al=u;
        be=be_last;
        % if u in index of alpha, set f(index)=1
        f=lk_up_0(:,1)==u;
        %
        y_u=-1e6;
        % loop through elements
```

```matlab
for q=1:numel(lk_up_0(:,1))
    % if f(element)==1, then current
    % u found in alpha
    if f(q)==1
        % y(u,beta_(k)') = Xab(alpha)
        y_u=lk_up_0(q,3);
    end
end
% check if y_u is dummy output
% (u not in lookup table)
if y_u==-1e6
    % locate lower bound index of alpha
    [trash,m]=max(lk_up_0(:,1)<=u);
    %m=m-1;
    % locate upper bound index of alpha
    [trash,n]=min(lk_up_0(:,1)>u);
    n=n-1;
    y_u=interpolate_ln_al_be(al,lk_up_0(m,1),
        ..lk_up_0(m,3),lk_up_0(n,1),
        ..lk_up_0(n,3));
end
% sum_y stays same since no change in
% voltage rate direction
if sign_chk_last==1 || sign_chk_last==0
    sum_y=sum_y_last;
else % sign_chk_last==-1
```

```matlab
        sum_y=y_last;
    end
    sign_chk=1;
    % add new position to sum_y
    y=sum_y+(y_u-y_be_last);
    % y=sum_y+y_u;
    % lower, beta position from path stays constant
    y_be=y_be_last;
    % alpha position gets updated for current position
    y_al=y;
%

    case 2
        % sign_udot==1 && sign_udot_last==-1
        % case positive voltage rate - use increasing
        % hysteresis curve data "zeroth"
        %
        al=u;
        be=be_last;
        % if u in index of alpha, set f(index)=1
        f2=lk_up_0(:,1)==u;
        %
        y_u=-1e6;
        % loop through elements
        for q=1:numel(lk_up_0(:,1))
            % if f(element)==1, then current
            % u found in alpha
```

```matlab
    if  f2(q)==1
        % y(u,beta_(k)') = Xab(alpha)
        y_u=lk_up_0(q,3);
    end
end
% check if y_u is dummy output
% (u not in lookup table)
if y_u==-1e6
    % locate lower bound index of alpha
    [trash,m]=max(lk_up_0(:,1)<=u);
    %m=m-1;
    % locate upper bound index of alpha
    [trash,n]=min(lk_up_0(:,1)>u);
    n=n-1;
    y_u=interpolate_ln_al_be(al,lk_up_0(m,1)
        ..,lk_up_0(m,3),lk_up_0(n,1),
        ..lk_up_0(n,3));
end
% sum_y adds first order reversal curve
% between alpha and beta for change in
% voltage rate direction
sum_y=y_last;
sign_chk=1;
% add new position to sum_y
y=sum_y+(y_u-y_be_last);
% lower, beta position from path stays constant
```

```matlab
        y_be=y_last;
        % alpha position gets updated for current position
        y_al=y;

    case 3
        % sign_udot==-1 &&
        % ..( sign_udot_last==0 || sign_udot_last==-1)
        % case positive voltage rate - use decreasing
        % hysteresis curve data "first"
        %
        al=al_last;
        be=u;
        % if last alpha in lookup table, set f(index)=1
        f3=lk_up_1(:,1)== al_last;
        %
        % initialize beta_temp and dX_temp for coming loop
        % since EML doesnot support dynamically sized
        % arrays. Either can not have morethan 11 elements
        % (beta range 10->0 V)
        beta_temp=be_in;
        dX_temp=dX_in;
        y_u=-1e6;
        % loop through elements
        k=0;
        for q=1:numel(lk_up_1(:,1))
            % if f(element)==1, then last
```

```matlab
        % alpha in lookup table
        if f3(q)==1
            k=k+1;
            beta_temp(k)=lk_up_1(q,2);
            dX_temp(k)=lk_up_1(q,5);
        end
    end
%
% now look up u in beta column of lk_up_1_temp
if beta_temp(1)~=-1e6
    f3_1=beta_temp(:)==u;

    for p=1:numel(beta_temp)
        % if f(element)==1, then
        % current u found in alpha
        if f3_1(p)==1
            % y(u,beta_(k)') = Xab(alpha)
            y_u=dX_temp(p);
        end
    end
end
% check if y_u produced no output
if y_u==-1e6
    [al0,be0,dX0,al1,be1,dX1,al2,be2,
    ..dX2,al3,be3,dX3]=findverticies(u,al_last,
    ..lk_up_0,lk_up_1,beta_temp,dX_temp);
```

```
    if dX1==-1e6 && al3==al0

        y_u=interpolate_ln_al_be

                ..( be , be0 ,dX0, be3 ,dX3 );

    elseif dX1==-1e6 && al3~=al0

        y_u=interpolate_tr_al_be ( al ,be ,

        .. al0 , be0 ,dX0, al2 , be2 ,dX2, al3 , be3 ,dX3 );

    elseif dX1~=-1e6 && al3==al0

        y_u=interpolate_ln_al_be ( be , be0 ,

        .. dX0, be3 ,dX3 );

    else

        y_u=interpolate_sq_al_be ( al , be , al0 , be0 ,

.. dX0, al1 , be1 ,dX1, al2 , be2 ,dX2, al3 , be3 ,dX3 );

    end

end

%

% sum_y adds first order reversal curve

% between alpha and beta for change in

% voltage rate direction

if sign_chk_last==-1 || sign_chk_last==0

    sum_y=sum_y_last ;

else % sign_chk_last==1

    sum_y=sum_y_last+( y_al_last -y_be_last );

end

sign_chk=-1;

% add new position to sum_y

y=sum_y-y_u ;
```

```
        % lower, beta position from path stays constant
        y_al=y_al_last;
        % alpha position gets updated for current position
        y_be=y;

%

    case 4
        % sign_udot==-1 && sign_udot_last==1
        % case positive voltage rate - use decreasing
        % hysteresis curve data "first"
        %
        al=al_last;
        be=u;
        % if last alpha in lookup table, set f(index)=1
        f4=lk_up_1(:,1)== al_last;
        %
        % initialize beta_temp and dX_temp for coming loop
        % since EML does not support dynamically sized
        % arrays. Either can not have more than 11
        % elements (beta range 10->0 V)
        beta_temp=be_in;
        dX_temp=dX_in;
        % loop through elements
        k=0;
        y_u=-1e6;
        for q=1:numel(lk_up_1(:,1))
            % if f(element)==1, then last
```

```matlab
        % alpha in lookup table
        if f4(q)==1
            k=k+1;
            beta_temp(k)=lk_up_1(q,2);
            dX_temp(k)=lk_up_1(q,5);
        end
    end
    %
    % now look up u in beta column of lk_up_1_temp
    if beta_temp(1)~=-1e6
        %% resize beta_temp and dX_temp to right size
        f4_1=beta_temp(:)==u;
        for p=1:numel(beta_temp(:,1))
            % if f(element)==1, then
            % current u found in alpha
            if f4_1(p)==1
                % y(u,beta_(k)') = Xab(alpha)
                y_u=dX_temp(p);
            end
        end
    end
    % check if y_u produced no output
    if y_u==-1e6
        [al0,be0,dX0,al1,be1,dX1,al2,be2,
    ..dX2,al3,be3,dX3]=findverticies(u,al_last,lk_up_0,
    ..lk_up_1,beta_temp,dX_temp);
```

```
        if  dX1==-1e6 &&  al3==al0

            y_u=interpolate_ln_al_be(be,be0,

            ..dX0,be3,dX3);

        elseif  dX1==-1e6 &&  al3~=al0

            y_u=interpolate_tr_al_be(al,be,al0,

            ..be0,dX0,al2,

            ..be2,dX2,al3,be3,dX3);

        elseif  dX1~=-1e6 &&  al3==al0

            y_u=interpolate_ln_al_be(be,be0,

            ..dX0,be3,dX3);

        else

            y_u=interpolate_sq_al_be(al,be,al0,

    ..be0,dX0,al1,be1,dX1,al2,be2,dX2,al3,be3,dX3);

        end

    end

%

% sum_y adds first order reversal curve between

% alpha and beta for change in

% voltage rate direction

sum_y=sum_y_last+(y_al_last-y_be_last);

sign_chk=-1;

% add new position to sum_y

y=sum_y-y_u;

% lower, beta position from path stays constant

y_al=y_al_last;

% alpha position gets updated for current position
```

130

```
        y_be=y;
%

    otherwise
        % case zero voltage rate − keep output same
        sum_y=sum_y_last;
        y_al=y_al_last;
        y_be=y_be_last;
        y=y_last;
        al=al_last;
        be=be_last;
        sign_chk=sign_chk_last;

end


%
%
function [al0,be0,dX0,al1,be1,dX1,al2,be2,dX2,al3,be3,dX3]=
.. findverticies(u,a_last,lk_up_0,lk_up_1,bt,dXt)
% determination of vertex locations for first order curves
% determines if alpha/beta in square or triangle
%
al_lo=−1e6;
%al_hi=−1e6;
f=lk_up_0(:,1)==a_last;
% loop through elements
for q=1:numel(lk_up_0(:,1))
    % if f(element)==1, then last alpha in lookup table
```

```matlab
        if  f(q)==1
            al_lo=lk_up_0(q,1);
        end
    end
    %
    if al_lo==-1e6
        % find lower bound of alpha corresponding to last alpha
        [trash,m]=max(lk_up_0(:,1)<a_last);
        %m=m-1;
        al_lo=lk_up_0(m,1);
        % find upper bound of alpha corresponding to last alpha
        [trash,n]=min(lk_up_0(:,1)>a_last);
        n=n-1;
        al_hi=lk_up_0(n,1);
    else
        al_hi=al_lo;
    end
    %
    f_al_lo=lk_up_1(:,1)==al_lo;
    f_al_hi=lk_up_1(:,1)==al_hi;
    % loop through elements
    k=0;
    %lk_up_1_al_lo=ones(1,11)*1e-6;
    be_al_lo_temp=bt;
    dX_al_lo_temp=dXt;
    for q=1:numel(lk_up_1(:,1))
```

```matlab
        % if f(element)==1, then last alpha in lookup table
        if f_al_lo(q)==1
            k=k+1;
            %lk_up_1_al_lo(k,:)=lk_up_1(q,:);
            be_al_lo_temp(k)=lk_up_1(q,2);
            dX_al_lo_temp(k)=lk_up_1(q,5);
        end
    end
% resize
%lk_up_1_al_lo=lk_up_1_al_lo(1:k);
k=0;
%lk_up_1_al_hi=ones(1,11)*1e-6;
be_al_hi_temp=bt;
dX_al_hi_temp=dXt;

for q=1:numel(lk_up_1(:,1))
    % if f(element)==1, then last alpha in lookup table
    if f_al_hi(q)==1
        k=k+1;
        %lk_up_1_al_hi(k,:)=lk_up_1(q,:);
        be_al_hi_temp(k)=lk_up_1(q,2);
        dX_al_hi_temp(k)=lk_up_1(q,5);
    end
end
%lk_up_1_al_hi=lk_up_1_al_hi(1:k);
%
```

```matlab
% find (alpha_low ,beta_low) corresponding to last alpha
% and current input
[trash ,m]=max( be_al_lo_temp<=u);
%m=m-1;
be_lo_al_lo=be_al_lo_temp(m);
dX_be_lo_al_lo=dX_al_lo_temp(m);
%
% find (alpha_hi ,beta_low) corresponding to last alpha
% and current input
[trash ,m1]=max( be_al_hi_temp<=u);
%m1=m1-1;
be_lo_al_hi=be_al_hi_temp(m1);
dX_be_lo_al_hi=dX_al_hi_temp(m1);
% find (alpha_hi ,beta_hi) corresponding to last alpha
% and current input
[trash ,n1]=min( be_al_hi_temp>u);
n1=n1-1;
be_hi_al_hi=be_al_hi_temp(n1);
dX_be_hi_al_hi=dX_al_hi_temp(n1);
%
% before finding (alpha_lo ,beta_hi) need to determine
% if in square or triangle grid
if be_lo_al_lo==max( be_al_lo_temp)
    % IN A TRIANGLE!!!
    % within triangle grid!
    % grid location 0
```

```
    al0=al_lo ;

    be0=be_lo_al_lo ;

    dX0=dX_be_lo_al_lo ;

    % grid  location  2

    al2=al_hi ;

    be2=be_lo_al_hi ;

    dX2=dX_be_lo_al_hi ;

    % grid  location  3

    al3=al_hi ;

    be3=be_hi_al_hi ;

    dX3=dX_be_hi_al_hi ;

    % grid  location  2 − nonexistent !!

    al1=−1e6 ;

    be1=−1e6 ;

    dX1=−1e6 ;

else

    % IN  A  SQUARE !!!

    % find ( alpha_lo , beta_hi ) corresponding  to  last

    % alpha  and  current  input

    [ trash , n]=min( be_al_lo_temp >u );

    n=n−1;

    be_hi_al_lo=be_al_lo_temp(n);

    dX_be_hi_al_lo=dX_al_lo_temp(n);

    %

    % grid  location  0

    al0=al_lo ;
```

```matlab
        be0=be_lo_al_lo;
      dX0=dX_be_lo_al_lo;
      % grid location 1
      al1=al_lo;
      be1=be_hi_al_lo;
      dX1=dX_be_hi_al_lo;
      % grid location 2
      al2=al_hi;
      be2=be_lo_al_hi;
      dX2=dX_be_lo_al_hi;
      % grid location 3
      al3=al_hi;
      be3=be_hi_al_hi;
      dX3=dX_be_hi_al_hi;
end


%
function xab=interpolate_sq_al_be(alp,bep,al0,be0,dX0,
..al1,be1,dX1,al2,be2,dX2,al3,be3,dX3)
% function to calculate X value for square verticies
% xab=dX0/((al3-al0)*(be3-be0))*(al3-alp)*(be3-bep)...
%      +dX1/((al3-al0)*(be3-be0))*(alp-al2)*(be2-bep)...
%      +dX2/((al3-al0)*(be3-be0))*(al1-alp)*(bep-be1)...
%      +dX3/((al3-al0)*(be3-be0))*(alp-al0)*(bep-be0);
dX_lo=(be1-bep)/(be1-be0)*dX0+(bep-be0)/(be1-be0)*dX1;
dX_hi=(be3-bep)/(be3-be2)*dX2+(bep-be2)/(be3-be2)*dX3;
```

```
xab=(al3-alp)/(al3-al0)*dX_lo+(alp-al0)/(al3-al0)*dX_hi;
%
function xab=interpolate_tr_al_be(alp,bep,al0,be0,dX0,
..al2,be2,dX2,al3,be3,dX3)
% function to calculate X value for triangle verticies
% xab=dX0/(al_be_para(3)*al_be_para(6))*((be3*al2-be2*al3)
%..+(al3-al2)*bep+(be2-be3)*alp)...
%      +dX2/(al_be_para(3)*al_be_para(6))*((be2*al0-be3*al0)
%..+(al0-al3)*bep+(be3-be0)*alp)...
%      +dX3/(al_be_para(3)*al_be_para(6))*((be2*al3-be0*al2)
%..+(al2-al0)*bep+(be0-be2)*alp);
dX_le=dX0-((dX0-dX2)*(al0-alp)/(al0-al2));
dX_ri=dX0-((dX0-dX3)*(al0-alp)/(al0-al3));
be_le=(alp-al0)*(be2-be0)/(al2-al0)+be0;
be_ri=(alp-al0)*(be3-be0)/(al3-al0)+be0;
xab=dX_ri-((dX_ri-dX_le)*(be_ri-bep)/(be_ri-be_le));
%
%
function xab=interpolate_ln_al_be(alp,al0,dX0,al3,dX3)
% function to calculate X value for triangle verticies
xab=1/(al3-al0)*((al3-alp)*dX0+(alp-al0)*dX3);
```

This code was directly used for the estimation of parallel hysteresis for compensation. The block diagram showing this parallel hysteresis estimation being used for controlling another classical Preisach model is shown in Figure A.3.
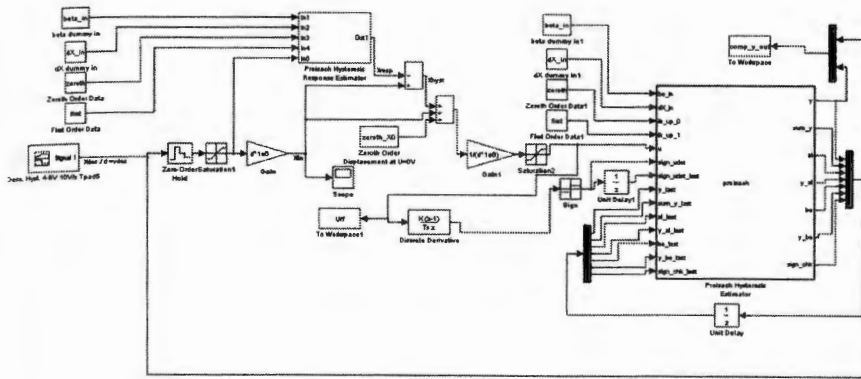
Figure A.3. Simulink Model for Classical Preisach Hysteresis Parallel Feed-forward Estimation

A.2.4   preisachinvfeedforward.mdl

The model for simulating Classical Preisach series inverse hysteresis feedforward control is shown in Figure A.4.
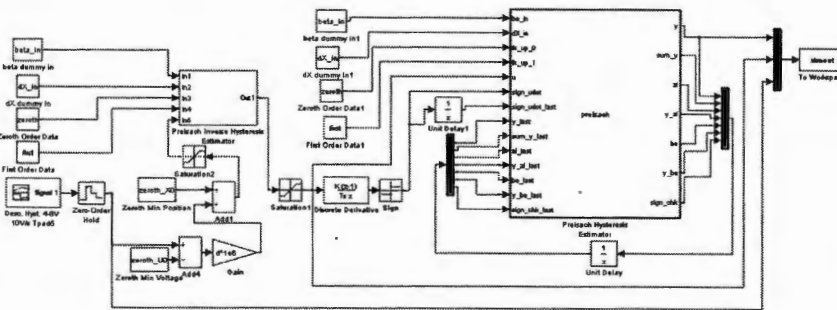
Figure A.4. Simulink Model for Classical Preisach Series Inverse Hysteresis Feedforward Estimation

On the left hand side of this model, the Preisach Inverse Hysteresis Estimator determines the inverse model of the Classical Preisach Hysteresis. The code for this block is shown below:

```
function  [u,sum_u,al ,y_al ,be,y_be,sign_chk]
..=  invpreisach(be_in ,dX_in ,lk_up_0 ,lk_up_1 ,y,
```

138

```matlab
.. sign_ydot , sign_ydot_last
.. , u_last , sum_u_last , al_last , y_al_last , be_last
.. , y_be_last , sign_chk_last )
% This block supports the Embedded MATLAB subset.
% See the help menu for details.
%
% determine the voltage input case
if sign_ydot==1 && (sign_ydot_last==0 || sign_ydot_last==1)
    in_case=1;
elseif sign_ydot==1 && sign_ydot_last==-1
    in_case=2;
elseif sign_ydot==-1 && (sign_ydot_last==0 ||
 .. sign_ydot_last==-1)
    in_case=3;
elseif sign_ydot==-1 && sign_ydot_last==1
    in_case=4;
else % sign_ydot==0
    in_case=5;
end

switch in_case
%

    case 1
        % sign_ydot==1 && (last_sign_ydot==0 ||
        .. last_sign_ydot==1)
        % case positive voltage rate - use increasing
```

```matlab
% hysteresis curve data "zeroth"
%
y_al=y;
y_be=y_be_last;
% if u in index of alpha, set f(index)=1
f=lk_up_0(:,3)==y;
%
u_y=-1e6;
u_lin=-1e6;
u_sq=-1e6;
u_tr=-1e6;
% loop through elements
for q=1:numel(lk_up_0(:,3))
    % if f(element)==1, then current
    % u found in alpha
    if f(q)==1
        % y(u,beta_(k)') = Xab(alpha)
        u_y=lk_up_0(q,1);
        u_lin=0;
        u_sq=0;
        u_tr=0;
    end
end
% check if y_u is dummy output
% (u not in lookup table)
if u_y==-1e6
```

```matlab
    % locate lower bound index of alpha
    [trash ,m]=max(lk_up_0(:,3)<=y);
    %m=m-1;
    % locate upper bound index of alpha
    [trash ,n]=min(lk_up_0(:,3)>y);
    n=n-1;
    u_y=interpolate_ln_al_be(y_al ,lk_up_0(m,3),
        ..lk_up_0(m,1),lk_up_0(n,3),lk_up_0(n,1));
    u_lin=u_y;
    u_sq=0;
    u_tr=0;
end
% sum_y stays same since no change in voltage
% rate direction
if sign_chk_last==1 || sign_chk_last==0
    sum_u=sum_u_last;
else % sign_chk_last==-1
    sum_u=u_last;
end
sign_chk=1;
% add new position to sum_y
u=sum_u+(u_y-be_last);
% lower , beta position from path stays constant
be=be_last;
% alpha position gets updated for current position
al=u;
```

```matlab
        y_al0=0;
        be0=0;
        dX0=0;
        y_al1=0;
        be1=0;
        dX1=0;
        y_al2=0;
        be2=0;
        dX2=0;
        y_al3=0;
        be3=0;
        dX3=0;
    %
    case 2
        % sign_ydot==1 && sign_ydot_last==-1
        % case positive position rate - use increasing
        % hysteresis curve data "zeroth"
        y_al=y;
        y_be=y_be_last;
        % if u in index of alpha, set f(index)=1
        f2=lk_up_0(:,3)==y;
        %
        u_y=-1e6;
        u_lin=-1e6;
        u_sq=-1e6;
        u_tr=-1e6;
```

```matlab
% loop through elements
for q=1:numel(lk_up_0(:,3))
    % if f(element)==1, then current
    % u found in alpha
    if f2(q)==1
        % y(u,beta_(k)') = Xab(alpha)
        u_y=lk_up_0(q,1);
        u_lin=0;
        u_sq=0;
        u_tr=0;
    end
end
% check if y_u is dummy output
% (u not in lookup table)
if u_y==-1e6
    % locate lower bound index of alpha
    [trash,m]=max(lk_up_0(:,3)<=y);
    %m=m-1;
    % locate upper bound index of alpha
    [trash,n]=min(lk_up_0(:,3)>y);
    n=n-1;
    u_y=interpolate_ln_al_be(y_al,lk_up_0(m,3),
        ..lk_up_0(m,1),lk_up_0(n,3),lk_up_0(n,1));
    u_lin=u_y;
    u_sq=0;
    u_tr=0;
```

```
end
% sum_u adds first order reversal curve between
% alpha and beta for change in
% position rate direction
% sum_y=y_be_last;
sum_u=u_last;
sign_chk=1;
% sum_y=sum_y_last+y_be_last;
% add new position to sum_y
u=sum_u+(u_y-be_last);
% lower, beta position from path stays constant
be=u_last;
% alpha position gets updated for current position
al=u;
y_al0=0;
be0=0;
dX0=0;
y_al1=0;
be1=0;
dX1=0;
y_al2=0;
be2=0;
dX2=0;
y_al3=0;
be3=0;
dX3=0;
```

%

```
case 3
    % sign_ydot==-1 && (sign_ydot_last==0
    % || sign_ydot_last==-1)
    % case negative position rate - use decreasing
    % hysteresis curve data "first"
    %
    y_al=y_al_last;
    y_be=y;
    % if last alpha in lookup table, set f(index)=1
    f3=lk_up_1(:,3)==y_al_last;
    %
    % initialize beta_temp and dX_temp for coming loop
    % since EML does not support dynamically sized
    % arrays.   Either can not have more
    % than 11 elements (beta range 10->0 V)
    beta_temp=be_in;
    dX_temp=dX_in;
    u_y=-1e6;
    u_lin=-1e6;
    u_sq=-1e6;
    u_tr=-1e6;
    y_al0=0;
    be0=0;
    dX0=0;
    y_al1=0;
```

```matlab
be1=0;
dX1=0;
y_al2=0;
be2=0;
dX2=0;
y_al3=0;
be3=0;
dX3=0;
% loop through elements
k=0;
for q=1:numel(lk_up_1(:,3))
    % if f(element)==1, then last
    % alpha in lookup table
    if f3(q)==1
        k=k+1;
        beta_temp(k)=lk_up_1(q,6);
        dX_temp(k)=lk_up_1(q,4);
    end
end
%
% now look up u in beta column of lk_up_1_temp
if dX_temp(1)~=-1e6
    f3_1=dX_temp(:)==y;

    for p=1:numel(dX_temp)
        % if f(element)==1, then current
```

146

```
% u found in alpha
    if  f3_1(p)==1
        % y(u, beta_(k)') = Xab(alpha)
        u_y=beta_temp(p);
        u_lin=0;
        u_sq=0;
        u_tr=0;
    end

    end

end

% check if y_u produced no output
if u_y==-1e6
    [y_al0 , be0 , dX0, y_al1 , be1 , dX1,
        .. y_al2 , be2 , dX2, y_al3 , be3 , dX3]
        ..= findverticies(y, y_al_last , lk_up_0 ,
        .. lk_up_1 , beta_temp , dX_temp);
    if be1==-1e6 && y_al3==y_al0
        u_y=interpolate_ln_al_be(y_be , dX0,
        .. be0 , dX3, be3);
        u_lin=u_y;
        u_sq=0;
        u_tr=0;
    elseif be1==-1e6 && y_al3~=y_al0
        u_y=interpolate_tr_al_be(y_al , y_be , y_al0 ,
        .. be0 , dX0, y_al2 , be2 , dX2, y_al3 , be3 , dX3);
        u_lin=0;
```

```
        u_sq=0;

        u_tr=u_y;

    elseif be1~=-1e6 && y_al3==y_al0

        u_y=interpolate_ln_al_be(y_be,dX0,

        ..be0,dX3,be3);

        u_lin=u_y;

        u_sq=0;

        u_tr=0;

    else

        u_y=interpolate_sq_al_be(y_al,y_be,y_al0,

        ..be0,dX0,y_al1,be1,dX1,y_al2,be2,dX2,

        ..y_al3,be3,dX3);

        u_lin=0;

        u_sq=u_y;

        u_tr=0;

    end

end

%

% sum_y adds first order reversal curve between

% alpha and beta for change

% in voltage rate direction

if sign_chk_last==-1 || sign_chk_last==0

    sum_u=sum_u_last;

else % sign_chk_last==1

    sum_u=sum_u_last+(al_last-be_last);

end
```

148

```
        sign_chk=-1;
        % add new position to sum_y
        u=sum_u-u_y;
        % lower, beta position from path stays constant
        al=al_last;
        % alpha position gets updated for current position
        be=u;
%

    case 4
        % sign_ydot==-1 && sign_ydot_last==1
        % case positive position rate - use decreasing
        % hysteresis curve data "first"
        %
        y_al=y_al_last;
        y_be=y;
        % if last alpha in lookup table, set f(index)=1
        f4=lk_up_1(:,3)==y_al_last;    .
        %
        % initialize beta_temp and dX_temp for coming loop
        % since EML does not support dynamically sized
        % arrays. Either can not have more
        % than 11 elements # (beta range 10->0 V)
        beta_temp=be_in;
        dX_temp=dX_in;
        % loop through elements
        k=0;
```

```
u_y=-1e6;

u_lin=-1e6;

u_sq=-1e6;

u_tr=-1e6;

y_al0=0;

be0=0;

dX0=0;

y_al1=0;

be1=0;

dX1=0;

y_al2=0;

be2=0;

dX2=0;

y_al3=0;

be3=0;

dX3=0;

for  q=1:numel(lk_up_1(:,3))
    % if  f(element)==1, then last
    % alpha  in  lookup  table
    if  f4(q)==1
        k=k+1;
        beta_temp(k)=lk_up_1(q,6);
        dX_temp(k)=lk_up_1(q,4);
    end
end
%
```

```
% now look up u in beta column of lk_up_1_temp
if dX_temp(1)~=-1e6

    %% resize beta_temp and dX_temp to right size
    f4_1=dX_temp(:)==y;

    for p=1:numel(dX_temp(:,1))

        % if f(element)==1, then current
        % u found in alpha
        if f4_1(p)==1

            % y(u,beta_(k)') = Xab(alpha)
            u_y=beta_temp(p);
            u_lin=0;
            u_sq=0;
            u_tr=0;

        end

    end

end
% check if u_y produced no output
if u_y==-1e6

    [y_al0,be0,dX0,y_al1,be1,dX1,y_al2,be2,dX2,
    ..y_al3,be3,dX3]=
    ..findverticies(y,y_al_last,lk_up_0,lk_up_1,
    ..beta_temp,dX_temp);
    if be1==-1e6 && y_al3==y_al0

        u_y=interpolate_ln_al_be(y_be,dX0,
        ..be0,dX3,be3);
        u_lin=u_y;
```

151

```
        u_sq=0;

        u_tr=0;

    elseif be1==-1e6 && y_al3~=y_al0

        u_y=interpolate_tr_al_be(y_al,y_be,y_al0,

        ..be0,dX0,y_al2,be2,dX2,y_al3,be3,dX3);

        u_lin=0;

        u_sq=0;

        u_tr=u_y;

    elseif be1~=-1e6 && y_al3==y_al0

        u_y=interpolate_ln_al_be(y_be,dX0,

        ..be0,dX3,be3);

        u_lin=u_y;

        u_sq=0;

        u_tr=0;

    else

        u_y=interpolate_sq_al_be(y_al,y_be,y_al0,

        ..be0,dX0,y_al1,be1,dX1,y_al2,be2,dX2,

        ..y_al3,be3,dX3);

        u_lin=0;

        u_sq=u_y;

        u_tr=0;

    end

 end

%

% sum_y adds first order reversal curve between

% alpha and beta for change in
```

152

```
        % voltage rate direction
        sum_u=sum_u_last+(al_last-be_last);
        sign_chk=-1;
        % add new position to sum_y
        u=sum_u-u_y;
        % lower, beta position from path stays constant
        al=al_last;
        % alpha position gets updated for current position
        be=u;
%
    otherwise
        % case zero voltage rate - keep output same
        sum_u=sum_u_last;
        y_al=y_al_last;
        y_be=y_be_last;
        u=u_last;
        al=al_last;
        be=be_last;
        sign_chk=sign_chk_last;
        u_y=0;
        u_lin=0;
        u_sq=0;
        u_tr=0;
        y_al0=0;
        be0=0;
        dX0=0;
```

```
            y_al1=0;
            be1=0;
            dX1=0;
            y_al2=0;
            be2=0;
            dX2=0;
            y_al3=0;
            be3=0;
            dX3=0;
    end


%
%
function [y_al0, be0, dX0, y_al1, be1, dX1,
.. y_al2, be2, dX2, y_al3, be3, dX3]
..=findverticies(y, y_a_last, lk_up_0, lk_up_1, bt, dXt)
% determination of vertex locations for first order curves
% determines if alpha/beta in square or triangle
%
y_al_lo=-1e3;
%al_hi=-1e6;
f=lk_up_1(:,3)==y_a_last;
% loop through elements
for q=1:numel(lk_up_1(:,3))
    % if f(element)==1, then last alpha in lookup table
    if f(q)==1
```

```matlab
            y_al_lo=lk_up_1(q,3);
        end
    end
%
    if  y_al_lo==-1e3
        % find lower bound of alpha corresponding to last alpha
        [trash ,m]=max(lk_up_1(:,3)<y_a_last);
        %m=m-1;
        y_al_lo=lk_up_1(m,3);
        % find upper bound of alpha corresponding to last alpha
        [trash ,n]=min(lk_up_1(:,3)>y_a_last);
        n=n-1;
        y_al_hi=lk_up_1(n,3);
    else
        y_al_hi=y_al_lo;
    end
%
    f_al_lo=lk_up_1(:,3)==y_al_lo;
    f_al_hi=lk_up_1(:,3)==y_al_hi;
    % loop through elements
    k=0;
    be_al_lo_temp=bt;
    al_al_lo_temp=bt;
    dX_al_lo_temp=dXt;
    for  q=1:numel(lk_up_1(:,3))
        % if f(element)==1, then last alpha in lookup table
```

```
    if  f_al_lo(q)==1

        k=k+1;
        % get  alpha  for  later  check  that  not  multiple
        % values  of  alpha  in  table
        al_al_lo_temp(k)=lk_up_1(q,1);
        % dX_al_lo_temp(k)=lk_up_1(q,5);

    end

end
% get  last  (lowest  value  of  alpha  in  al_al_lo_temp)
al_lotemp=al_al_lo_temp(k);
f_al_al_lo=lk_up_1(:,1)==al_lotemp;
%
k=0;
for  q=1:numel(lk_up_1(:,3))
    % if  f(element)==1,  then  last  alpha  in  lookup  table
    if  f_al_al_lo(q)==1

        k=k+1;
        be_al_lo_temp(k)=lk_up_1(q,6);
        dX_al_lo_temp(k)=lk_up_1(q,4);

    end

end


% resize
k=0;
be_al_hi_temp=bt;
dX_al_hi_temp=dXt;
```

```
for q=1:numel(lk_up_1(:,3))
    % if f(element)==1, then last alpha in lookup table
    if f_al_hi(q)==1
        k=k+1;
        be_al_hi_temp(k)=lk_up_1(q,6);
        dX_al_hi_temp(k)=lk_up_1(q,4);
    end
end
%
% find (alpha_low,beta_low) corresponding to last alpha
% and current input
%[trash,m]=max(dX_al_hi_temp<=y);
[trash,m]=max(dX_al_lo_temp<=y);
%m=m-1;
be_lo_al_lo=be_al_lo_temp(m);
dX_be_lo_al_lo=dX_al_lo_temp(m);
%
% find (alpha_hi,beta_low) corresponding to last alpha
% and current input
%[trash,m1]=max(dX_al_hi_temp<=y);
[trash,m1]=max(dX_al_hi_temp<=y);
%m1=m1-1
be_lo_al_hi=be_al_hi_temp(m1);
dX_be_lo_al_hi=dX_al_hi_temp(m1);
% find (alpha_hi,beta_hi) corresponding to last alpha
```

```
% and current input
[trash,n1]=min(dX_al_hi_temp>y);
n1=n1-1;
be_hi_al_hi=be_al_hi_temp(n1);
dX_be_hi_al_hi=dX_al_hi_temp(n1);
%
% before finding (alpha_lo,beta_hi) need to determine
% if in square or triangle grid
if  dX_be_lo_al_lo==max(dX_al_lo_temp)
    % IN A TRIANGLE!!!
    % within triangle grid!
    % grid location 0
    y_al0=y_al_lo;
    be0=be_lo_al_lo;
    dX0=dX_be_lo_al_lo;
    % grid location 2
    y_al2=y_al_hi;
    be2=be_lo_al_hi;
    dX2=dX_be_lo_al_hi;
    % grid location 3
    y_al3=y_al_hi;
    be3=be_hi_al_hi;
    dX3=dX_be_hi_al_hi;
    % grid location 2 - nonexistent!!
    y_al1=-1e6;
    be1=-1e6;
```

```
        dX1=−1e6 ;

else
        % IN A SQUARE!!!
        % find (alpha_lo ,beta_hi) corresponding to last alpha
        % and current input
        [trash ,n]=min(dX_al_lo_temp>y);
        n=n−1;
        be_hi_al_lo=be_al_lo_temp(n);
        dX_be_hi_al_lo=dX_al_lo_temp(n);
        %
        % grid location 0
        y_al0=y_al_lo ;
        be0=be_lo_al_lo ;
        dX0=dX_be_lo_al_lo ;
        % grid location 1
        y_al1=y_al_lo ;
        be1=be_hi_al_lo ;
        dX1=dX_be_hi_al_lo ; ·
        % grid location 2
        y_al2=y_al_hi ;
        be2=be_lo_al_hi ;
        dX2=dX_be_lo_al_hi ;
        % grid location 3
        y_al3=y_al_hi ;
        be3=be_hi_al_hi ;
        dX3=dX_be_hi_al_hi ;
```

```
end

%

function uab=interpolate_sq_al_be(y_alp,y_bep,y_al0,
..be0,dX0,y_al1,be1,dX1,y_al2,be2,dX2,y_al3,be3,dX3)
be_al_lo=(dX1-y_bep)/(dX1-dX0)*be0+
..(y_bep-dX0)/(dX1-dX0)*be1;
be_al_hi=(dX3-y_bep)/(dX3-dX2)*be2+
..(y_bep-dX2)/(dX3-dX2)*be3;
uab=(y_al3-y_alp)/(y_al3-y_al0)*be_al_lo+
..(y_alp-y_al0)/(y_al3-y_al0)*be_al_hi;
%

function uab=interpolate_tr_al_be(y_alp,y_bep,y_al0,be0,dX0
..,y_al2,be2,dX2,y_al3,be3,dX3)
be_le=be0-((be0-be2)*(y_al0-y_alp)/(y_al0-y_al2));
be_ri=be0-((be0-be3)*(y_al0-y_alp)/(y_al0-y_al3));
dX_le=(y_alp-y_al0)*(dX2-dX0)/(y_al2-y_al0)+dX0;
dX_ri=(y_alp-y_al0)*(dX3-dX0)/(y_al3-y_al0)+dX0;
uab=be_ri-((be_ri-be_le)*(dX_ri-y_bep)/(dX_ri-dX_le));
%

function uab=interpolate_ln_al_be(y_alp,y_al0,be0,
..y_al3,be3)
% function to calculate X value for triangle verticies
uab=1/(y_al3-y_al0)*((y_al3-y_alp)*be0+(y_alp-y_al0)*be3);
```

BIBLIOGRAPHY

Adriaens, H. J., de Koning, W. L., and Banning, R., "Modeling piezoelectric actuators," *IEEE/ASME Transactions on Mechatronics*, vol. 5, no. 4, Dec. 2000.

Adriaens, J., de Koning, W., and Banning, R., "Design and modeling of a piezo-actuated positioning mechanism," in *Procedings of the 36th Conference on Decision and Control*, San Diego, California USA, Dec. 1997.

Bouc, R., "Forced vibration of mechanical systems with hysteresis (abstract)," in *Proceedings for the Fourth Conference on Nonlinear Oscillation*, Prague, Czechoslovakia, 1967.

dSPACE GmbH. "Control desk." Apr. 2009. [Online]. Available: http://www.dspace.de/shared/data/pdf/catalog2009/ControlDesk_dSPACE_Catalog_2009.pdf

dSPACE GmbH. "Ds1006 processor board." Apr. 2009. [Online]. Available: http://www.dspace.de/shared/data/pdf/catalog2009/DS1006-ProcessorBoard%_dSPACE_Catalog_2009.pdf

dSPACE GmbH. "Ds2004 high-speed a/d board." Apr. 2009. [Online]. Available: http://www.dspace.de/shared/data/pdf/catalog2009/DS2004-HighSpeed-AD-Board_dSPACE_Catalog_2009.pdff

dSPACE GmbH. "Ds2101/ds2102/ds2103 d/a boards." Apr. 2009. [Online]. Available: http://www.dspace.de/shared/data/pdf/catalog2009/DS2101-DS2102-DS2103-DA-Boards_dSPACE_Catalog_2009.pdf

dSPACE GmbH. "Targetlink 3.0." Apr. 2009. [Online]. Available: http://www.dspace.de/shared/data/pdf/flyer2009/dspace_2009_targetlink30_en_pi823.pdf

Fung, R.-F., Hsu, Y.-L., and Huang, M.-S., "System identification of a dual-stage xy precision positioning table," *Precision Engineering*, vol. 33, 2009.

Ge, P. and Jouaneh, M., "Modeling of hysteresis in piezoceramic actuators," *Precision Eng*, vol. 17, 1995.

Ge, P. and Jouaneh, M., "Tracking control of a piezoceramic actuators," *IEEE Transactions on Cntrol Systems Technology*, vol. 4, no. 3, 1996.

Ge, P. and Jouaneh, M., "Generalized preisach model for hysteresis nonlinearity of piezoceramic actuators," *Precision Eng*, vol. 20, 1997.

Goldfarb, M. and Celanovic, N., "A lumped parameter electromechanical model for describing the nonlinear behavior of piezoelectric actuators," *Journal of Dynamic Systems, Measurement and Control*, vol. 119, Sept. 1997.

Goldfarb, M. and Celanovic, N., "Modeling piezoelectric stack actuators for control of micromanipulation," *IEEE Control Systems Magazine*, vol. 17, June 1997.

Ha, J.-L., Fung, R.-F., and Yang, C.-S., "Hysteresis identification and dynamic responses of the impact drive mechanism," *Journal of Sound and Vibration*, vol. 283, 2005.

Hoffmeister, H.-W., Schuller, B.-C., and Loeis, K., "Active vibration reduction on clamping systems for stationary machining centers," in *Adaptronic Congress*, Göttingen, Germany, 2007.

Hu, H., Georgiou, H., and Ben-Mrad, R., "Enhancement of tracking ability in piezoceramic actuators subject to dynamic excitation conditions," *IEEE/ASME Transactions on Mechatronics*, vol. 10, no. 2, 2005.

Hu, H., Zhang, H., and Mrad, R. B., "Preisach based dynamic hysteresis model," in *International Conference on Intelligent Mechatronics and Automation*, Chengdu, China, 2004.

Hung, S.-K., Hwu, E.-T., Hwang, I.-S., and Fu, L.-C., "Postfitting control scheme for periodic piezoscanner driving," *Japanese Journal of Applied Physics*, vol. 45, no. 3B, 2006.

Iyer, R. V. and Tan, X., "Control of hysteretic systems through inverse compensation," *IEEE Control Systems Magazine*, vol. 29, Feb. 2009.

Janocha, H., *Adaptronics and Smart Structures: Basics, Materials, Design and Applications*. Springer-Verlag Berlin Heidelberg, 2007.

Jouaneh, M. and Tian, H., "Accuracy enhancement of a piezoelectric actuator with hysteresis," in *ASME JAPAN/USA Symposium on Flexible Automation*, San Francisco, CA, USA, 1992.

Kuhnen, K. and Janocha, H., "Adaptive inverse control of piezoelectric actuators with hysteresis operators," in *Proceedings of the European Control Conference*, Karlsruhe, 1999.

Kuhnen, K. and Janocha, H., "Inverse feedforward controller for complex hysteretic nonlinearities in smart-material systems," *Control and Intelligent Systems*, vol. 29, 2001.

Lee, B.-R., Yang, S.-Y., and Ahn, K.-K., "Precision control of piezoelectric actuator using inverse hysteresis model and neuro control," in *KORUS 2003: The 7th Korea-Russia International Symposium on Science and Technology*, Ulsan, Republic of Korea, 2003.

Lin, C.-J. and Yang, S.-R., "Precise positioning of piezo-actuated stages using hysteresis-observer based control," *Mechatronics*, vol. 16, 2006.

Low, T. and Guo, W., "Modeling of a three-layer piezoelectric bimorph beam with hysteresis," *Journal of Microelectromechanical Systems*, vol. 4, Dec. 1995.

The MathWorks, Inc. "Optimization toolbox 4 - user's guide." Apr. 2009. [Online]. Available: http://www.mathworks.com/access/helpdesk/ help/pdf_doc/optim/optim_tb.pdf

Micro-Epsilon Messtechnik GmbH & Co. KG. "optoncdt 1607." Apr. 2009. [Online]. Available: http://www.micro-epsilon.com/download/products/ dat--optoNCDT-1607--en.pdf

Moheimani, S. R. and Fleming, A. J., *Piezoelectric Transducrs for Vibration Control and Damping.* Springer-Verlag London Limited, 2006.

Mrad, R. B. and Hu, H., "Dynamic modeling of hysteresis in piezoceramics," in *IEEE/ASME International Conference on Advanced Intelligent Mechatronics Proceedings*, Como, Italy, 2001.

Mrad, R. B. and Hu, H., "A model for voltage-to-displacement dynamics in piezoceramic actuators subject to dynamic-voltage excitations," *IEEE/ASME Transactions on Mechatronics*, vol. 7, no. 4, 2002.

Palm, W. J., *System Dynamics.* McGraw-Hill, 2005.

Peyre, T. H., "Effective secondary path identification toward feedforward active vibration control on wood machining machine," Master's thesis, Technische Universitaet Braunschweig, 2008.

Physik Instrumente GmbH & Co. KG. "E-481 pica™ piezo high-powered amplifier/controller." Apr. 2009. [Online]. Available: http: //www.physikinstrumente.com/en/pdf/E481_Datasheet.pdf

Physik Instrumente GmbH & Co. KG. "P-212, p-216 pica™ power piezo stack actuators." Apr. 2009. [Online]. Available: http://www.physikinstrumente. com/en/pdf/P212_P216_Datasheet.pdf

Physik Instrumente GmbH & Co. KG. "Piezo-university: Dynamic operation fundamentals." Apr. 2009. [Online]. Available: http: //www.physikinstrumente.com/en/products/prdetail.php?sortnr=400600.60

Physik Instrumente GmbH & Co. KG. "Piezo-university: Fundamentals of piezoelectric actuators." Apr. 2009. [Online]. Available: http://www. physikinstrumente.com/en/products/prdetail.php?sortnr=400600.40

Preisach, F., "Über die magnetische Nachwirkung," *Zeitschrift für Physik A Hadrons und Nuclei*, vol. 94, May 1935.

Professor Jouaneh, Department of Mechanical Engineering and Applied Mechanics, University of Rhode Island. "Motion control research projects." Apr. 2009. [Online]. Available: http://www.mce.uri.edu/jouaneh/motioncontrolprojects. htm

Ru, C. and Sun, L., "A new open-loop driving method of piezoelectric actuator for periodic reference inputs," *Ultrasonics*, vol. 44, 2006.

Song, G., Zhao, J., Zhou, X., and Abreu-García, J. A. D., "Tracking control of a piezoceramic actuator with hysteresis compensation using inverse preisach model," *IEEE/ASME Transactions on Mechatronics*, vol. 10, no. 2, 2005.

Tan, U.-X., Latt, W. T., Shee, C. Y., Riviere, C., and Ang, W. T., "Modeling and control of piezoelectric actuators for active physiological tremor compensation," in *Human-Robot Interaction*, Vienna, Austria, 2005.

Wen, Y., "Method for random vibration of hysteretic systems," *J. Eng. Mech. Div. ASCE*, vol. 102, no. 2, 1976.

Wen, Y., "Equivalent linearization for hysteretic systems under random excitation," *Journal of Applied Mechanics, Transactions ASME*, vol. 47, no. 1, 1980.

Yang, R., Jouaneh, M., and Schweizer, R., "Design and characterization of a low-profile micropositioning stage," *Precision Eng*, vol. 18, 1996.

Yu, Y., Xiao, Z., Naganathan, N. G., and Dukkipati, R. V., "Dynamic preisach modelling of hysteresis for the piezoceramic actuator system," *Mechanism and Machine Theory*, vol. 37, 2002.